1-1-2012

Probing the dynamics of radical reactions with polyatomic hydrocarbons by crossed-beam dc slice imaging

Armando Dura Estillore
Wayne State University,

PROBING THE DYNAMICS OF RADICAL REACTIONS WITH POLYATOMIC HYDROCARBONS BY CROSSED-BEAM DC SLICE IMAGING

by

ARMANDO D. ESTILLORE

DISSERTATION

Submitted to the Graduate School

of Wayne State University,

Detroit, Michigan

in partial fulfillment of the requirements

for the degree of

DOCTOR OF PHILOSOPHY

2012

MAJOR: CHEMISTRY (Physical)

Approved by:

_____

Advisor Date

_____

_____

_____

_____

DEDICATION

This dissertation is dedicated to

my father: Carlos Sr;

my brother: Carlos Jr;

my sisters: Rebecca and Liza, the princesses of our lives.

ACKNOWLEDGEMENTS

Grad school is exciting but at times it can be "unfriendly at its best, cruel at its worst." This section is my way of immortalizing my heartfelt gratitude to individuals who have helped me towards completing my PhD degree.

On top of my list is my family. To my father who always reminds me that I am not only a student of Wayne State but also to the University of Life. My older brother, Carlos with his family and to my younger sisters: Rebecca and Liza, for all the love and support while I am at the other half part of the world chasing after my dream.

I am forever grateful to my advisor, Prof. Arthur G. Suits. It is truly an honor to be mentored by one of the best scientists in the field of chemical dynamics. I searched for the right terms but my words can never do justice in detailing how great a mentor and a great person he is. His never-ending passion in science is very contagious. I will depart from his lab equipped with the right tools to become an independent scientist. Thank you very much boss!

I am privileged to be a part of a team dedicated to doing crossed-beam experiments in the Suits Lab. These experiments proved to be very challenging but thanks to a former postdoc, Dr. Cunshun Huang for providing me the ABCs of performing these tasks. When he left, I was fortunate to have worked with smart and brilliant students: Laura M. Visger-Kiefer and Tarek Abdul Ghani. To the intelligent international people of the Suits Lab working on their respective cutting-edge experiments. Thanks to all, past and present, whom I have associated since I joined Suits lab namely: Dr. Sridhar Lahankar, Dr. Lei Shen, Dr. Ruchira Silva, Dr. Wilson Gichuhi, Nuradhika Herath, Lu Yan, Bernadette Broderick, Fadia Cudry, Chamara Abeysekera, Yuanyuan Shi, Richard Van Camp, Ravin Fernando, Michael

B. Doyle, Dr. Joalland Baptiste, Dr. James Oldham, and Dr. Prashant Chandra Singh. The atmosphere in the lab fosters friendship, teamwork, and intellectual exchange of ideas.

I thank the members of my committee: Prof. H. Bernhard Schlegel, Prof. Matthew J. Allen, and Prof. Simon Ng for their expert insights and suggestions in completing this dissertation. To the staff of the Chemistry Department for taking care of all the necessary logistics in the duration of my PhD studies. I thank Sharon Kelly, Melissa Barton, Erin Bachert, Deborah McCreless, Diane Kudla, Nestor Ocampo, Bernadette Miesik and Mary Wood. I thank Dr. Kopin Liu of the Institute of Atomic and Molecular Sciences, Academia Sinica, Taiwan for hosting my one-week visit in his lab.

I am indebted to the kindness and generosity of my friends: Janir Datukan and Aileen Angcajas for all their help in getting myself acquainted to the new environment during my first year in grad school. To Ellen Inutan and Rollie Inutan, Joel Garcia, Dr. Janeth Presores of Georgetown University for being an amazing friends. When homesickness bugs bite, these are the people I talk to in person or online.

Not to be discounted are my friends who, during my vacations and trips, have opened their homes that allows me to write papers and part of this dissertation in the comfort of their place. I thank Joe Obedencio, DVM and Ruan Presores-Obedencio, DVM for their hospitality during my sojourn in Bukidnon, Philippines. To Conmar Malmis, for being not too busy to assist me during my one-week visit in the Academia Sinica in Taiwan. I also acknowledge Analyn Galo-Gultiano and Kirstin Rhys Pueblos for their generous help.

To my Chemistry family in Iligan Institute of Technology of the Mindanao State University and to all my friends back home not named here, my heartfelt thanks to all of you!

PREFACE

This dissertation is based closely on the following refereed publications:

Chapter 3: A. D. Estillore, L. M. Visger, and A. G. Suits. "Crossed-beam dc slice imaging of chlorine atom reactions with pentane isomers." *Journal of Chemical Physics*, **132**, 164313 (2010). DOI: 10.1063/1.3414353.

Chapter 4: A. D. Estillore, L. M. Visger-Kiefer, T. A. Ghani, and A. G. Suits. "Dynamics of H and D abstraction in the reaction of Cl atom with butane-1,1,1,4,4,4-d_6." *Physical Chemistry Chemical Physics*, **13**, 8433 (2011). DOI: 10.1039/c1cp20137a.

Chapter 5: A. D. Estillore, L. M. Visger, and A. G. Suits. "Imaging the dynamics of chlorine atom reactions with alkenes." *Journal of Chemical Physics*, **133**, 074306 (2010). DOI: 10.1063/1.3473049.

Chapter 6: A. D. Estillore, L. M. Visger-Kiefer, and A. G. Suits. "Reaction dynamics of Cl + butanol isomers by crossed-beam sliced ion imaging." *Faraday Discussions*, **157**, xxxx (2012) (In press). DOI: 10.1039/C2FD20059G.

Chapter 7: C. Huang, W. Li, A. D. Estillore, and A. G. Suits. "Dynamics of CN + alkane reactions by crossed-beam dc slice imaging." *Journal of Chemical Physics*, **129**, 074301 (2008). DOI: 10.1063/1.2968547.

Chapter 8: A. D. Estillore, L. M. Visger, R. I. Kaiser, and A. G. Suits. "Crossed-Beam Imaging of the H Abstraction Channel in the Reaction of CN with 1-Pentene." *Journal of Physical Chemistry Letters*, **1**, 2417 (2010). DOI: 10.1021/jz100861t.

The author of this dissertation performed the experiments, analyzed the data, and wrote the papers above. Calculations are done by Laura M. Visger-Kiefer. The advisor: Prof. Arthur G. Suits conceived and designed the experiments.

TABLE OF CONTENTS

LIST OF TABLES

LIST OF FIGURES

Chapter 1

Introduction

Most of the observables in our immediate environment such as color changes, evolution of gas, and chemical transformation can be fully understood only by looking at the elementary steps that make up the whole process. These steps could represent a broad range of successful reactive collisions or energy transfer collisions depending on the forces acting on the participants of the reaction, and they often involve transient radicals or excited states. For over a century, kinetic methods have been central to efforts to explain the complicated chemistry in numerous bimolecular reactions. However, thermal rate methods are not incisive enough to provide a concrete explanation of the individual encounters because they measure the average of myriads of random collisions of atoms, molecules, radicals, or ions. Notwithstanding, this averaging gave rise to many chemical insights and set the stage for fundamental experiments geared towards detailing the dynamics of the reaction.

The field of reaction dynamics has become a solid platform in understanding the intimate details of chemical reactions that are otherwise obscured when studied by conventional techniques that average over thermal conditions and report only end-products. This field made a revolutionary impact when in 1986; Herschbach [1], Lee [2], and Polanyi [3] shared the Nobel Prize in Chemistry for their work concerning the dynamics of elementary chemical processes. The dynamics of atom-diatom type reactions have been understood at the molecular level through the collaborative efforts in theory, experiments, and computations. However, most of the reactions ubiquitous in nature involve collisions of atoms or radicals with polyatomic

molecules. Polyatomic molecules collectively present several experimental and theoretical challenges that can deliver insights beyond what is learned from an atom-diatom systems. Now, these pioneering efforts are being extended to systems beyond the atom + diatom type reactions, to include now complex polyatomic systems, radical-radical reactions, transition metal reactions, and reactions involving electronically excited species. The practical application covers many broadly important chemical territories such as combustion, marine, terrestrial and atmospheric environments [4–7]. Reaction dynamics, in its purist sense, aims to look at the individual collisions of atoms, molecules, radicals, or ions. These experiments are performed by crossing two collimated molecular beams usually at 90°, with the scattered products probed by a variety of detection technique such as the universal mass-spectrometric detection [8], H-atom Rydberg tagging [9, 10], resonance enhanced multiphoton ionization (REMPI) [11], laser-induced fluorescence (LIF) spectroscopy [12], and ion imaging [13]. DC slice or 3-D ion imaging provides the velocity flux contour map directly as the product of the experiment [14, 15]. Furthermore, the reaction differential cross section and the product translational energy distribution can be deduced directly from the image of the product to elucidate the details of the reaction dynamics.

The crossed molecular beam approach is an ideal method that permits visualization of the microscopic details of chemical reactions. The experiments involve, first, defining the initial conditions of the reactants such as velocities, approach angle, and internal quantum state (electronic, vibrational, and rotational) and then measuring the velocity and angular distribution of the products. The product velocity distributions supply the necessary information on how the total available reaction energy is partitioned into translation, rotation, or internal excitation of the products. The product angular distributions serve as a primary diagnostic tool in understanding the details of the mechanism of the reaction. It also contains information on the lifetime of the collision complex. The distinct form of product angular distributions, $I(\theta)$, in the center-of-mass frame contains information on how the reaction products scatter relative to the direction of approach of the reactants. Elementary

reactions can be grouped into two main categories namely: direct reactions and complex-forming reactions. For direct reactions $I(\theta)$ exhibits marked forward-backward asymmetry with respect to the incoming reactants, suggesting rapid separation of the products ($\sim 10^{-13}$ s or less). For lingering or complex-forming reactions, $I(\theta)$ has forward-backward symmetry, indicating that an intermediate complex forms that survives long enough to execute at least a few full rotations ($\sim 5 \times 10^{-12}$ or longer) [16]. Meticulous measurements of the final product states provide insights into the many forces within and between reactants that influence their interaction in the transition state region.

To provide an accurate model in predicting the behaviors of different systems towards chemical reactions, it is essential to perform studies under single-collision conditions and detect the products before they undergo secondary collisions. Two important reactions in nature include: chlorine atom reactions with hydrocarbons, represented by reaction (1.1a), and cyano (CN) radical reactions with polyatomic hydrocarbons, represented by reaction (1.2a).

$$\mathrm{Cl + RH \rightarrow \quad R\cdot + HCl}\ (v,\ J) \tag{1.1a}$$

$$\mathrm{CN + RH \rightarrow \quad R\cdot + HCN} \tag{1.2a}$$

These reactions offer several points of dynamical interest as well as challenges to the experimentalists and theoreticians. For Cl + RH reactions, crossed molecular beam studies of these systems allow systematic investigation of its dynamics with the possibility of investigating the products of the reaction, see reaction (1.1a), using single photon ionization and resonance enhanced multiphoton ionization (REMPI) techniques as a product probe for the hydrocarbon radical and HCl (v, J) products, respectively. These are fast reactions affording good signal-to-noise ratio in challenging scattering studies. The reaction energetics lie in the intermediate regime, i. e., some are endoergic, others thermoneutral or exoergic, and with modest barrier or no barrier at all. In addition, there are different abstraction sites and the possibility to investigate the associated reactivity. Finally, the H abstraction process leads

to the diatomic product HCl, which can be detected with quantum state specificity and good sensitivity using REMPI techniques.

Extensive efforts have been dedicated to understanding the chemistry of Cl + methane (and its isotopologues) reactions, as well as some small hydrocarbons. The *photoloc* technique is the most celebrated method in studying the nascent HCl (v, J) product of the reaction. Experimental outcomes with theoretical confirmations showed a cold rotational-state distribution in the nascent HCl/DCl (v, J) and is ascribed to a collinear C-H(D)-Cl transition state. In fact, cold HCl rotational distributions have turned out to be a universal signature of Cl + alkanes reactions. In the case of Cl atom reactions with alcohol, the measured nascent HCl(v, J) distribution was observed to have a larger degree of rotational excitation than that of Cl + alkanes [11].

Dynamical investigations involving more complex systems such as polyatomic hydrocarbons are made more interesting, and more challenging, owing to the high dimensionality and complexity of the potential energy surfaces of these systems [17]. Some of these issues include molecular structure and stereochemistry, polarity, degree of unsaturation, conformational isomerism, and competing reactive sites. This is the intriguing set of questions investigated in the series of dynamical studies of Cl + RH reactions using crossed-beam imaging methods. The results are compiled in this dissertation with emphasis on detecting the hydrocarbon radical products generated from reactions (1.1a) and (1.2a) using single photon ionization as a product probe.

This dissertation is structured as follows: Chapter 2 highlights the experimental techniques used in the study. Here, the concepts of crossed molecular beam and ion imaging techniques will be discussed. Chapter 3 shows the results of the experiments in the crossed-beam reactions of atomic chlorine with the three isomers of pentane: n-pentane, isopentane, and neopentane. These are interesting target molecules because of the different type of hydrogens subject to abstraction. Neopentane for example, has only primary H-atoms while n-pentane and isopentane carry primary, secondary, and tertiary hydrogen atoms. Chapter

4 reports the sensitive approach to studying abstraction of primary and secondary hydrogen atom using deuterated butane as the target system at relatively high collision energy. Chapter 5 marks the first in the field to probe the dynamics of chlorine atom reactions with monounsaturated hydrocarbons coupled with *ab initio* calculations in determining the associated reaction enthalpies. Decades of kinetics investigations have been devoted to establish the mechanisms of these reactions. Alkenes, because of the presence of double bond, are susceptible to several reaction pathways such as addition to the double bond, addition-elimination, and direct abstraction. These competing pathways often change as a function of temperature and pressure. A collision energy dependence studies were performed to a different set of alkene molecules. Efforts in studying the reaction dynamics of ground state chlorine atom with butanol isomers: n-butanol, sec-butanol, iso-butanol, and tert-butanol are presented in Chapter 6. Butanol is now prominent among the prototype renewable biofuels. Oxidation studies of a variety of butanol isomers were investigated under single collision conditions using chlorine atom as the oxidizing agent to gain detailed insight into the energetics and dynamics of these reactions.

In addition to Cl + RH reactions, the CN radical reactions are specifically prevalent in atmospheric environment, on earth and in particular in planetary atmospheres. It is reactive with saturated hydrocarbons but less so with methane and towards unsaturated hydrocarbons without barriers to reaction. Chapter 7 deals with experiments on H-atom abstraction of CN radicals from alkanes. The reaction of CN with unsaturated hydrocarbons is one way of producing long chain hydrocarbons and complex organic compounds with several competing pathways. In addition to addition and addition-elimination routes, hydrogen abstraction to produce HCN and resonantly-stabilized allyl radical is also possible for larger alkenes. However, this channel has not been widely examined in kinetics studies. With improved experimental sensitivity, the associated dynamics of CN reactions with 1-pentene is reported in Chapter 8. Translational energy release and angular distributions reveal details of the reactions that were not observed previously.

Chapter 2

Methods

2.1 Ion imaging

Ion imaging was developed by Chandler and Houston in 1987 to investigate the photodissociation dynamics of methyl iodide, CH_3I [18]. This pioneering work on imaging involves photolysis of CH_3I molecules at 266 nm wavelength to generate CH_3 radicals and I atoms. The CH_3 products are ionized by (2 + 1) resonance enhanced multiphoton ionization (REMPI) methods and the recoiling ions are accelerated in a Wiley-McLaren [19] time-of-flight mass spectrometer and projected onto an imaging detector. The apparatus consists of a repeller electrode, grid, ion shutter, and a microchannel plate (MCP) coupled to a phosphor screen detector. In general principle, ion imaging uses a photolysis laser to effect bond fission and a probe laser to ionize the neutral products following a photodissociation event after which the three-dimensional (3D) ion cloud is projected onto a two-dimensional (2D) MCP detector coupled with a charge-coupled device (CCD) camera. To extract meaningful chemical information from the 2D projected image, a tedious mathematical inversion method such as the inverse Abel transformation is often employed to reconstruct the 3D distribution. These snapshots measure simultaneously the product velocity distribution and angular distribution of the photofragment of interest. One major limitation of the technique, however, was the poor resolution of the images obtained, which was limited by the dimensions of the ionization region. The use of grids also perturbs the trajectories of the ions as they traverse

through the grid wires. The details of ion-imaging are pictorially represented in Fig. 2.1.

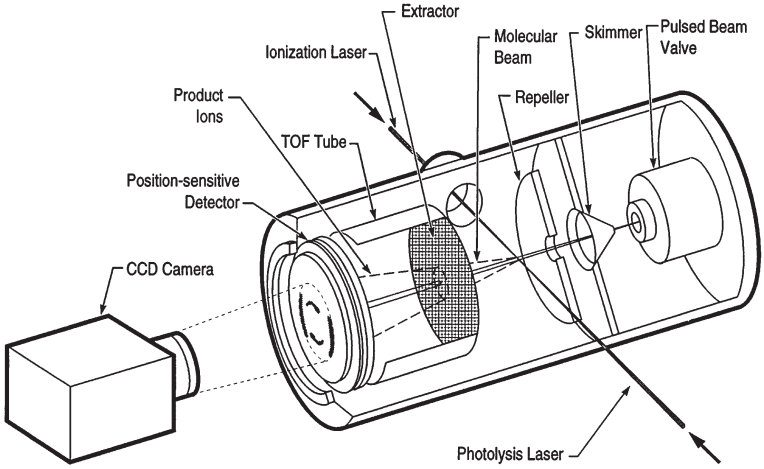

Figure 2.1: Schematic diagram of a conventional photofragment ion imaging apparatus. Adapted with permission from McDonnell et al, *J. Mass Spectrom.* **33**: 415. John Wiley and Sons. Copyright 1998.

This problem was circumvented by the introduction of velocity map imaging (VMI) by Eppink and Parker [20]. The VMI technique works without the disadvantage of spatial blurring of the images. This was achieved by the use of ion lenses in place of grids allowing particles with the same velocity vector in the plane perpendicular to the flight axis to hit the detector on the same point, irrespective of their point of origin. The replacement of conventional grid electrodes with lens improved the energy resolution on the order of 1% or better. However, the projection-reconstruction method remained. The inversion process brings noise in the symmetry axis of the recovered image compromising experimental resolution. The VMI method also requires the system to have cylindrical symmetry to recover the 3D distribution of the 2D velocity projections. The latter poses limitations, particularly in two-color experiments where the polarizations of the photolysis and probe lasers are desired to be orthogonal. Such is a pre-requisite in studies involving vector correlations in the angular momentum alignment and/or orientation in unimolecular dissociation events. It is therefore desirable to develop a method that directly analyzes the 3D distribution of the

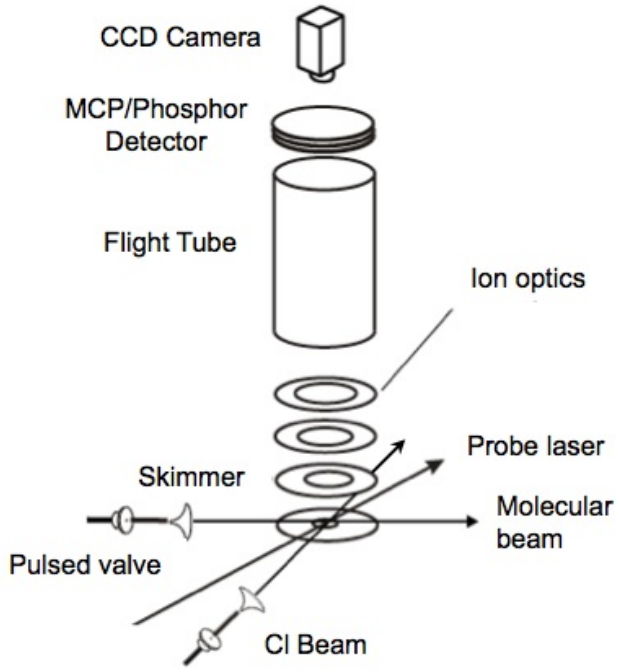

Figure 2.2: DC slice imaging ion optics set-up used in the crossed molecular beam ion imaging apparatus.

non-cylindrical image without the need for projection-reconstruction.

Further refinement of the imaging technique was achieved when the slice imaging strategy was introduced. The idea is to stretch the ion cloud to several hundred of nanoseconds to allow only the central slice of the ion cloud to be imaged directly, simply by using narrow time gate at the detector. Direct current (DC) slice imaging [14] is one of the variants to the VMI method developed by the Suits group to address the issues associated with the previous methods while preserving all the inherent advantages of the conventional and velocity map imaging. The use of low fields in the extraction region and additional two focusing lenses adequately stretches the ion packet increasing the arrival width onto the detector. This is especially important to allow the central slice of the ion cloud to be imaged directly onto the MCP detector. The main advantage of DC slicing is the ability to decode the total translational energy and angular distribution directly from the equatorial slice without

utilizing inversion methods. In this method, a spread of ion cloud is obtained by using a very low repeller voltage. The optimum focusing is achieved by maintaining the precise voltage ratio applied to the repeller and extractor lenses, and an additional lens element. This technique eliminates the use of grids or pulsed electric fields, which distort the ion cloud. DC slicing has become the standard experimental tool employed in all the imaging machines in the Suits lab both in unimolecular and bimolecular scattering experiments, and is widely used by other groups around the world. It is in principle equivalent to the "3-D" imaging approach developed independently by Kopin Liu, and published in the same issue of the *Review of Scientific Instruments* [15]. The features of DC slice imaging are illustrated in Figure 2.2.

2.2 Crossed molecular beams

Atomic and molecular beams are proven effective experimental probe in investigating molecular structures and chemical reactivity in research areas beyond the mix and stir methods [21]. Molecular beam is defined as the collection of molecules moving in the same direction under a collisionless environment in an evacuated vessel. These are produced by coexpanding, from a high-pressure region, a dilute mixture of a molecule seeded with a rare gas such as helium through a small nozzle and collimated by a skimmer into a vacuum. As the gas expands, the molecules are accelerated to many times their thermal velocity leading to a supersonic beam of internally cold molecules, converting the enthalpy of the gas to bulk translational energy [22]. The translational energy peak at higher energies and markedly narrowed compared to the Maxwell-Boltzmann distribution, depicted in black curve, as shown in Figure 2.3, for example in the case of ammonia seeded in xenon undergoing supersonic expansion [23]. During expansion, molecular vibrations and rotations are cooled. Collisions within the beam are therefore avoided that may otherwise distort the direction of motion, kinetic energy, or internal state of the molecule [24]. The terminal velocity of ammonia molecules will be similar to that of xenon.

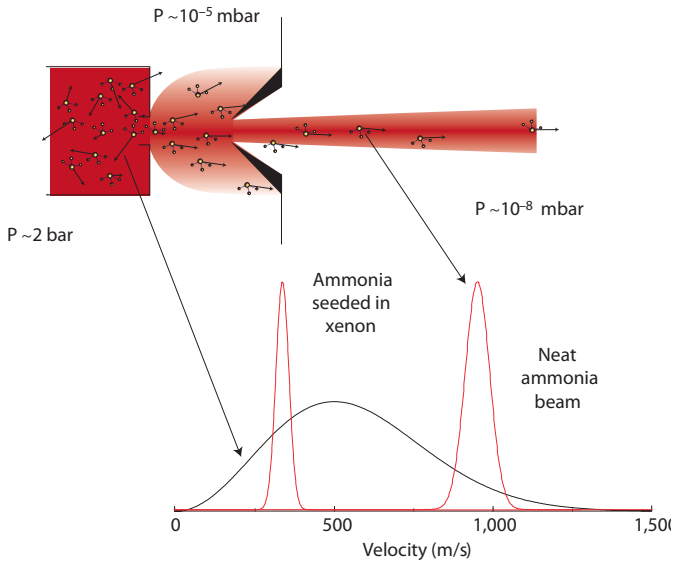

Figure 2.3: Schematic view of a supersonic expansion. Adapted with permission from van de Meerakker et al., *Nature Physics* **4**: 595. Macmillan Publishers Ltd. Copyright 2008.

One of the most appealing consequences of molecular beam methods in chemical dynamics experiments is that it affords means for single collision studies. This enables measurement of the product information before secondary collisions can occur [25]. For this reason, it is imperative that the mean free path of the gas must be greater than the distance from the collision region to the detector. The experiments presented here make use of a crossed-beam imaging apparatus shown in Figure 2.4. The machine is partitioned into two source chambers fixed at 90° and a main scattering chamber. The pressures are maintained at $\sim 10^{-7}$ Torr (base) and $\sim 10^{-5}$ Torr (operational) by turbomolecular pumps under each source chamber and in the main scattering chamber to provide efficient differential pumping conditions. The atomic and molecular beams are isolated in separate source chambers. This condition allows collisions in a localized region at specified collision energy. In addition, build up of pre-reaction products prior to collision are avoided. The low background pressure, the absence of collisions within the beam and prior to collision, and the long mean free path inside vacuum chambers ensure that only single and well-defined collision events are observed.

The experiments presented here are characterized by two main stages: characterization

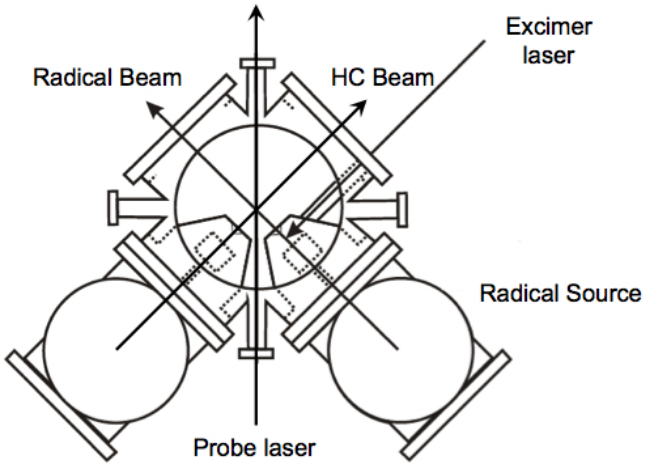

Figure 2.4: Top view of the schematic diagram of a crossed molecular beam ion imaging apparatus.

and optimization of molecular (atomic) beams and imaging the product of the reaction. The fusion of crossed molecular beam, Fig. 2.4, with the sophisticated dc slice imaging technique, Fig. 2.2, offers molecular snapshots to decode the underlying dynamics in several complicated bimolecular reactions. The applicability of this method stands to help considerably in enhancing our understanding of chemical reactions. The experimental details specific for each investigation compiled here are discussed in each chapter.

Chapter 3

Crossed-beam dc slice imaging of chlorine atom reactions with pentane isomers

3.1 Introduction

Crossed-beam studies of the dynamics of the gas-phase atom-diatom reaction have provided deep insight into elementary chemical reaction with systems such as H + H_2 [26–29], F + H_2 [30–33], Cl + H_2 [34–37], and O + H_2 [38–40] serving as benchmarks that have shaped our understanding. These are particularly important from a theoretical perspective since for these reactions it is possible to construct complete and accurate *ab initio* potential energy surfaces [41, 42] as well as perform full quantum scattering calculations [43, 44]. Now, one key goal for dynamics studies is to extend these insights to polyatomic reactions. Polyatomic systems possess different conformations, polarities, and structures that may alter the course of reaction and thus, the dynamics [45]. The reaction may proceed via multiple or competing pathways or through unusual dynamics. Reactions may occur at a central or terminal location of the molecule, with varying energy and angular momentum release. As the number of atoms and degrees of freedom in the reaction increase, the chemistry becomes much more complicated and new issues and new insights may emerge.

The reaction of chlorine atoms with hydrocarbons (RH) has been an important touchstone in exploring the dynamics in polyatomic systems. Literature on these and some related

systems through 2004 was summarized in a comprehensive review by Murray and Orr-Ewing [11]. Cl + hydrocarbon reactions are also of practical importance in combustion [46, 47], marine [48], and atmospheric environments [49, 50]. Extensive information on the kinetics of these reactions has been published elsewhere [51–53]. Literature data indicate that these reactions exhibit non-Arrhenius temperature dependencies so that activation energy is difficult to specify. Flynn and co-workers [54] were the first to report state-to-state reaction dynamics information on these systems, for the reaction of Cl with c-C_6D_{12}. They used diode laser absorption spectroscopy to measure the nascent DCl($v = 0$, J) product. The rotational-state distribution in the observed DCl($v = 0$, J) was found to be cold and they ascribed this result to a collinear C-D-Cl transition state as Cl atoms abstract D atom from c-C_6D_{12}. In fact, cold HCl rotational distributions have turned out to be a universal feature of Cl + RH reactions, with hotter rotational distributions seen in reactions with alcohols, for example [55–57]. The dynamics underlying the rotational distributions in these reactions were examined in detail by Murray and Orr-Ewing [11, 58].

Related work on the reaction of Cl(^{2}P) with RH was carried out by several groups. Interestingly, in the Cl + RH reaction series, only methane exhibits a significant activation barrier height, 2.83 kcal/mol, and is the only endothermic reaction, $\Delta H_{298} = +1.82$ kcal/mol. This reaction establishes a foundation in our understanding of the dynamics of other Cl + polyatom reactions. The use of the *photoloc* [59] method has been proven fruitful in detailing the dynamics of this reaction and other photoinitiated bimolecular reactions [55, 60–64]. Investigations of the nascent HCl($v = 0$) products using REMPI detection for the reaction Cl + CH_4 showed that the product HCl($v = 0$) is formed with cold rotational-state distribution and is strongly backscattered. The product state and angular distributions for the ground-state reaction are consistent with line-of-centers model, in which the cone of acceptance is only narrowly open [55]. Simpson *et al.* [60, 61] also investigated the vibrationally excited reaction Cl + $CH_4(v_3 = 1)$. The analysis of the results gave an extraordinarily detailed picture of the dynamics.

The dynamics of Cl + $C_2H_6 \rightarrow C_2H_5$ + HCl has also received attention from Kandel *et al.* [62], Bass *et al.* [64], using *photoloc*, and Huang *et al.* [65, 66] using slice imaging, in independent studies of the reaction. Kandel [62] reported that the C_2H_5 product exhibits broad scattering that peaks sideways and that the C_2H_5 fragment acts largely as a spectator. Bass *et al.* [64], however, found the angular distribution to be forward peaking and that 22% of the available energy was channeled into internal excitation of the ethyl coproducts. Further study on the effects of vibrational excitation of $C_2H_6(v_5 = 1)$ found a reaction cross section enhanced by only 5-10% in contrast to a tenfold enhancement for the Cl + $CH_4(v_3 = 1)$ reaction. Huang *et al.* [65, 66] provided the first state-resolved crossed-beam scattering results for Cl + C_2H_6, employing the dc sliced ion imaging technique to probe HCl($v = 0$, $j = 0$ - 5) with (2 + 1) REMPI detection. Analyses of the HCl images revealed center-of-mass translational energy and angular distributions are strongly coupled. The backscattered products, principally for $J = 2$, showed a bimodal translational energy distribution, one with 15% of the total energy partitioned to C_2H_5 internal energy, and the other with 66%. The forward scattered product showed only the fast peak. The fast peak was ascribed to direct reaction, while the slow peak was attributed to chattering-type collisions.

The crossed molecular beam ion imaging [18, 20] method has brought our understanding of reaction dynamics to an unprecedented level of detail. DC slice [14] or three-dimensional [15] imaging methods provide the velocity flux contour map directly as the product of the experiment. Because of the enhanced detection efficiency and resolution, it is now possible to pursue state-resolved scattering experiments to greater effect than ever before [67–69]. While the (2 + 1) REMPI detection offers the advantage of state-resolved experiments, it suffers from lower detection sensitivity due to small probe volumes associated with multiphoton ionization, and does not necessarily offer a global picture of the dynamics. Universal studies using mass spectrometric detection have many advantages, and this approach was applied to Cl + alkane reactions by Blank *et al.* [70] and Hemmi and Suits [71] with single photoion ionization detection of the alkyl radical using a tunable synchrotron source. Laboratory

angular distributions and time-of-flight spectra of the alkyl product were used to obtain the center-of-mass translational energy and angular distributions. The results showed that the translational and angular distributions are strongly coupled, with the formation of cold forward scattered alkyl products and internally excited backscattered radicals, leaving more energy in the internal excitation in the products. The backscattered product, particularly in the Cl + n-pentane reaction, revealed evidence of considerable internal excitation in the alkyl product, in contrast to investigations involving smaller alkanes, where the alkyl radical was treated as a spectator [54, 61] in the reaction. Recently, the Suits group has been successful in using a F_2 excimer probe [72, 73] in crossed molecular beam imaging studies. This combination has been proven effective in studying the underlying dynamics of a variety of polyatomic bimolecular reactions such as $O(^3P)$ + alkanes [74–76], $Cl(^2P)$ + alcohols [77, 78], and CN ($X\ ^2\Sigma^+$) + alkanes [79]. This universal imaging approach has some compelling advantages over crossed-beam scattering with mass spectrometric detection: There are no kinematic limitations for imaging; one measures the product in the center-of-mass frame directly; in the slice imaging case, the contour maps are the primary form of the data and no tedious analysis or fitting is necessary. A disadvantage has been background arising from interference from dissociation of the parent beam. As a consequence, in some of the previous work, scattering in the forward direction was deemed unreliable and unreported. In the present studies, improvement in detection efficiency and in the Cl beam source now allows us to determine the double differential cross sections over the full center-of-mass angular range. Moreover, these enhancements allow us to obtain these experimental results fairly quickly, motivating now a systematic investigation of H abstraction by Cl atoms over a broad range of target molecules. Here, the first of the series of studies is presented, for the

following reactions: $Cl(^2P_{3/2})$ + n-pentane:

$$Cl + \text{n-}C_5H_{12} \rightarrow \quad HCl + CH_2CH_2CH_2CH_2CH_3 \qquad \Delta_r H = -2.0\text{kcal/mol} \qquad (3.1a)$$

$$Cl + \text{n-}C_5H_{12} \rightarrow \quad HCl + CH_3CHCH_2CH_2CH_3 \qquad \Delta_r H = -5.3\text{kcal/mol} \qquad (3.1b)$$

$$Cl + \text{n-}C_5H_{12} \rightarrow \quad HCl + CH_3CH_2CHCH_2CH_3 \qquad \Delta_r H = -5.3\text{kcal/mol} \qquad (3.1c)$$

$Cl(^2P_{3/2})$ + isopentane:

$$Cl + CH_3CH_2CH(CH_3)_2 \rightarrow \quad HCl + CH_2CH_2CH(CH_3)_2 \quad \Delta_r H = -2.0\text{kcal/mol} \quad (3.2a)$$

$$Cl + CH_3CH_2CH(CH_3)_2 \rightarrow \quad HCl + CH_3CHCH(CH_3)_2 \quad \Delta_r H = -5.3\text{kcal/mol} \quad (3.2b)$$

$$Cl + CH_3CH_2CH(CH_3)_2 \rightarrow \quad HCl + CH_3CH_2C(CH_3)_2 \quad \Delta_r H = -8.2\text{kcal/mol} \quad (3.2c)$$

$Cl(^2P_{3/2})$ + neopentane:

$$Cl + C(CH_3)_4 \rightarrow \quad HCl + CH_2C(CH_3)_3 \qquad \Delta_r H = -2.10\text{kcal/mol} \qquad (3.3a)$$

These 298 K reaction enthalpies are taken from Ref. [71] for reaction (1) and the values for reactions (3.1a) and (3.1b) are used for reactions (3.2a) and (3.2b); the values for reactions (3.2c) and (3.3a) are from Ref. [80].

There are a number of key questions we can hope to address with such detailed and systematic dynamical studies: Are there different dynamics for primary, secondary, and tertiary H abstraction? What is the fraction of energy appearing in translation, vibration, or rotation of the two products, and what factors govern this disposition of energy? How do these issues change with collision energy or temperature? What effect do structural or stereochemical influences have on the dynamics? As seen in the preceding paragraphs, these questions have been examined with varying degrees of success in the many studies reported over the years. However, inconsistencies persist and many open questions remain. Slice imaging experiments promise some new insights into some of these open questions.

3.2 Experiment

The experiments were performed in a crossed-beam imaging apparatus described elsewhere [66, 78]. A molecular beam of oxalyl chloride, $(ClCO)_2$, was produced by passing helium through a bubbler containing $(ClCO)_2$ held at 0°C. The Cl atom beam was then generated by photodissociation of the oxalyl chloride, $(ClCO)_2$, using the 193 nm output of an ArF excimer laser (60 mJ, 10 Hz) at the nozzle of a piezoelectric pulsed valve. This results in a very intense Cl atom beam owing to the very large absorption cross section of oxalyl chloride at 193 nm and the fact that two Cl atoms are produced for each photon absorbed. The chlorine atom has two spin-orbit states ($^2P_{3/2}$ and $^2P_{1/2}$) with a separation of 882 cm^{-1}. Ahmed *et al.* reported state-selected imaging of the photodissociation of $(ClCO)_2$ and found Cl, $Cl^*(^2P_{1/2})$, and CO as products of the photodissociation process [81]. Hemmi and Suits extended this to 193 nm [82]. The excited spin-orbit $Cl(^2P_{1/2})$ produced at 230 nm is also anticipated at 193 nm. However, after entrainment in the supersonic expansion, most of the $Cl(^2P_{1/2})$ are likely to be quenched to the ground state [23]. Moreover, quenching studies of $Cl(^2P_{1/2})$ by various atmospheric gases showed that relaxation by helium is usually fast [83]. The Cl beam was skimmed before entering the main chamber where the scattering took place.

The alkane (n-pentane, isopentane, and neopentane), seeded ∼5% in He or H_2, was expanded from a total pressure of 4 bars through another pulsed valve, collimated by a single skimmer, and crossed the Cl beam at 90 in the interaction region. The alkyl radical products with m/z = 71 were detected by single photon ionization at 157 nm using a F_2 excimer laser (GAM EX-10, 0.5 mJ, 10 Hz) focused loosely using a MgF_2 lens (f = 135 cm) into the interaction region of the two crossed molecular beams. The product ions were accelerated via a four-electrode dc slice ion optics assembly [14] to impact on a 75 mm diameter dual microchannel plate (MCP) detector coupled to a fast phosphor screen held at 5 kV (Photonis/Burle, Sturbridge, MA). The front of the MCP assembly was held at ground

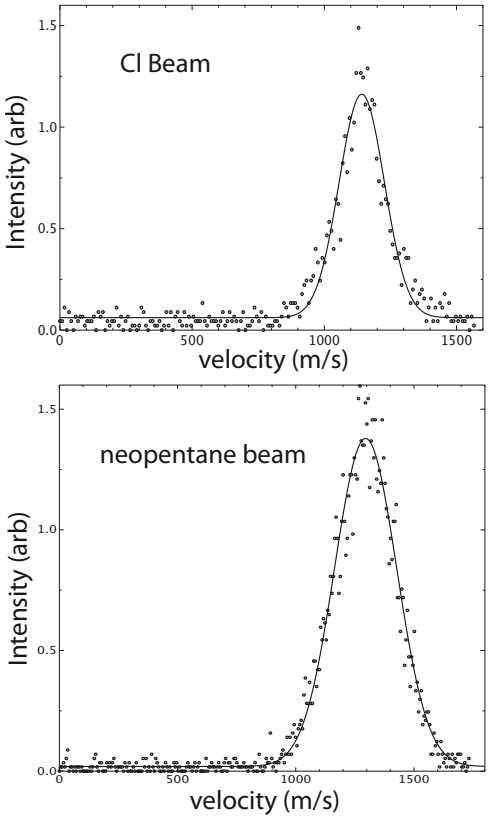

Figure 3.1: Sample beam profiles. Top: Cl beam detected using nonresonant ionization at 157 nm. Bottom: neopentane beam detected at 157 nm.

potential and the back plate was pulsed to gate the central slice of the reaction products at a specific mass by application of a high voltage pulse (2.2/1 kV bias, 70 ns width) using a commercial pulser (DEI PVX-4140, Fort Collins, CO). The timing of the pulsed molecular beam nozzles, firing of the photolysis and probe lasers, and detector gate pulse were controlled using a delay generator (BNC 555, San Rafael, CA). The resulting image was recorded using a charged coupled device camera (Mintron 2821e, 512 × 480 pixels, Taipei, Taiwan). The dc slice imaging detection scheme and megapixel acquisition program IMACQ were used to accumulate the raw images containing centroided data [84]. Image accumulation to reach a satisfactory signal-to-noise ratio took 1-3 hours. Background images obtained with the 193 nm laser off were also recorded and subtracted (after converting to signed integer data) before analysis. In previous studies [75, 77–79], background arising from photodissociation of the parent hydrocarbon to give the radical mass precluded reliable measurements in the

vicinity of the alkane beam. Here, owing to the intense Cl beam and the loose focusing of the probe laser, this background has been greatly reduced relative to the signal. Reliable measurements in the forward direction are now a routine, as will be seen in the data below.

The Cl atom beam velocity was measured using both direct probe via 2+1 REMPI ionization around 235 nm, as well as nonresonant multiphoton ionization at 157 nm. The results agreed well so the 157 nm detection was adopted for routine measurements. For the alkane beam, 157 nm ionization of the parent was also used for beam velocity determination. Typical measured beam velocity distributions are shown in Figure 3.1. These give speed ratios $\sim$4 for the pentane beam and $\sim$4.5 for the Cl beam, for an overall spread in collision energy of $\sim$30% full width at half maximum. Spots also appear in both beams at the detected radical mass (m/z = 71) with 157 nm detection, but it was found after extensive investigation that these do not accurately reflect the reactant beam velocities. The spot associated with the pentane beam that appears at the radical mass is faster than the beam itself, and appears only on one side of the relative velocity vector. This contribution is thus excluded in determining the angular distributions. Calibration of the velocity scale was performed using imaging of CO($J = 50$) from photodissociation of carbonyl sulfide, OCS. The velocity origin was determined first by recording a series of product masses in each beam at varying delay times and tracing the beam velocities back to the crossing point, and by monitoring background masses in the absence of the molecular beams. These approaches gave values in reasonable agreement.

The product dc sliced images embody the product scattering distributions directly containing the full dynamics of the reaction. However, the raw images must be corrected for the fact that the slower fragments, arising from scattering events that take place before the probe laser fires, are detected with greater likelihood than fast fragments (density-flux correction). This modest correction is readily achieved by scaling each pixel intensity by a value $(\alpha + v)$, where v is the laboratory frame velocity (simply proportional to the distance from the origin) and α is an empirically determined parameter that accounts for the finite size of the inter-

action volume and prevents the signal at low laboratory velocities from vanishing [65]. Once fixed, α is not varied for any of the data presented; in any case, the distributions extracted from the data are not very sensitive to this parameter. The conditions of the experiment are illustrated in an accompanying video online. The video shows the live reactive scattering signal with the principal Newton diagram superimposed. This raw video is uncorrected for the density-flux detection, and showed that the correction is not a large one. For the images shown below, the live video is centroided in real time and the centroided data are accumulated. Analogous images are recorded with the Cl laser off and these are subtracted from the signal images before analysis. Although the centroided data can be interpolated to subpixel precision, for these studies the spread in the collision energy is such that this additional resolution is not warranted. The analysis is thus performed at the native 512 $\times$ 480 pixel resolution. The magnitude of the background subtraction and the density-to-flux correction are shown in Figure 3.2. Figure 3.2a shows a raw image without background subtraction or density-to-flux correction. All of the features of the final result, shown in Fig. 3.2b, are present in the original image, but there is some asymmetry across the relative velocity vector owing to the enhanced sensitivity for products that are slow in the laboratory frame. To provide a sense of the inherent uncertainty in the data, total translational energy [Fig. 3.2c] and angular distributions [Fig. 3.2d] are generated from a series of Cl + n-pentane reactions at the indicated collision energies, each obtained several days apart. The reproducibility is excellent.

3.3 Results

The H abstraction reaction, Cl + $C_5H_{12} \rightarrow$ HCl + C_5H_{11}, for the three target pentane isomers is studied at two different collision energies $\sim$5 and $\sim$9 kcal/mol. In the case of neopentane, data obtained at low collision energy is not reported due to the very weak signal in that case. One question that immediately arises is the isomeric identity of the detected pentyl radical product. For n-pentane, for example, abstraction of a terminal

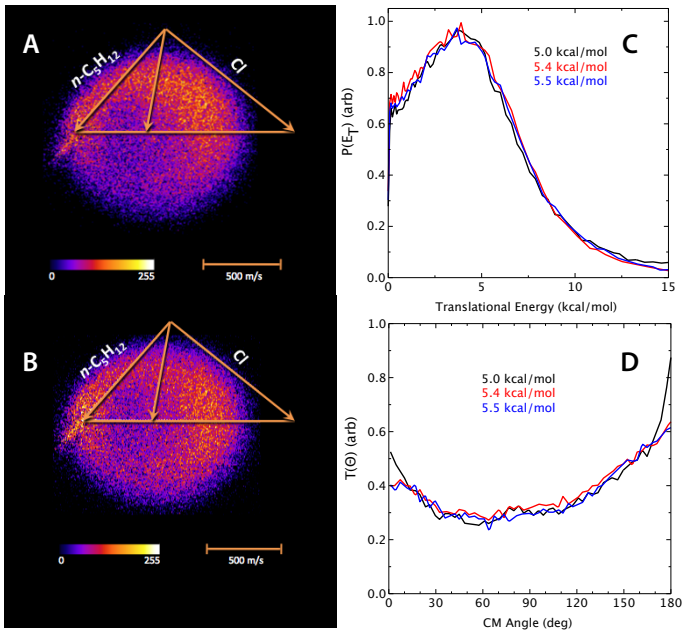

Figure 3.2: (a) Accumulated centroided data for Cl + n-pentane reaction at 5 kcal/mol collision energy without background subtraction or density-to-flux correction. (b) Same image as (a) after background subtraction and density-to-flux correction. (c) Translational energy and (d) angular distributions obtained for a series of Cl + n-pentane experiments at indicated collision energies.

primary H atom gives the 1-pentyl radical, while abstraction of a secondary H atom can give 2-pentyl or 3-pentyl radicals. The latter have reported ionization energies significantly lower than the 1-pentyl radical. If the detection is substantially biased in favor of the 2- and 3-pentyl radicals, then the current results may not be representative of the overall dynamics. However, a recent study of relative ionization efficiency for products of heptane isomer photodissociation at 157 nm [85] showed surprisingly little (less than 20%) variation in detection efficiency for the various radical products. This variation is thus neglected in the current study.

Figure 3.3 shows the dc sliced images of the alkyl radical products for all subject reactions with the nominal Newton diagrams superimposed on the images. These are after background subtraction and density-to-flux correction as described in Sec. 2.2. Figure 3.4 shows the total translational energy distributions, integrated over all angles, and the center-of-mass angular distributions, integrated over all recoil speeds, derived from the images. The translational

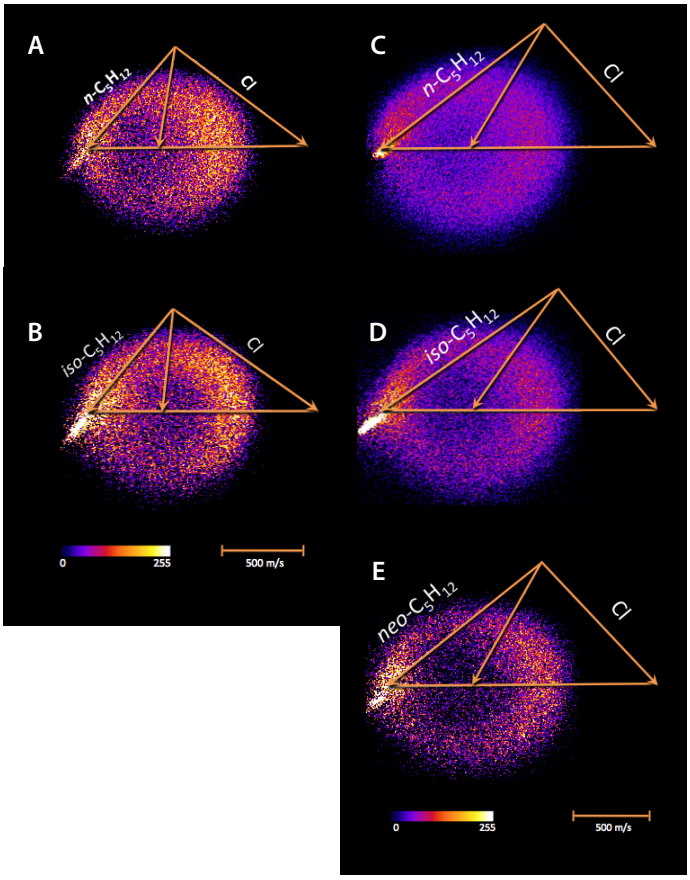

Figure 3.3: DC sliced images for pentyl radical product from Cl atom reaction with indicated pentane isomer and superimposed Newton diagrams. (A) n-pentane, collision energy 5.4 kcal/mol; (B) isopentane, collision energy 5.3 kcal/mol; (C) n-pentane, collision energy 8.4 kcal/mol; (D) isopentane, collision energy 9.5 kcal/mol; (E) neopentane 8.0 kcal/mol.

energy distributions at low collision energy for n-pentane and isopentane both show a peak around 3-4 kcal/mol and extend beyond 10 kcal/mol. At high collision energy, these distributions are shifted to slightly higher energies, but show strong similarities. The angular distributions at low E_C show flux in all directions, with modestly enhanced scattering in the backward direction with respect to the alkane beam. As the collision energy increases, the stronger scattering shifts to the forward direction for all cases.

The integrated data for average translational energy release, fraction forward scattered, and forward-to-backward peak height ratio are compiled in Table 1. At low collision energy, the backward peak drops off around 120° and the forward peak begins around 60°. Increasing

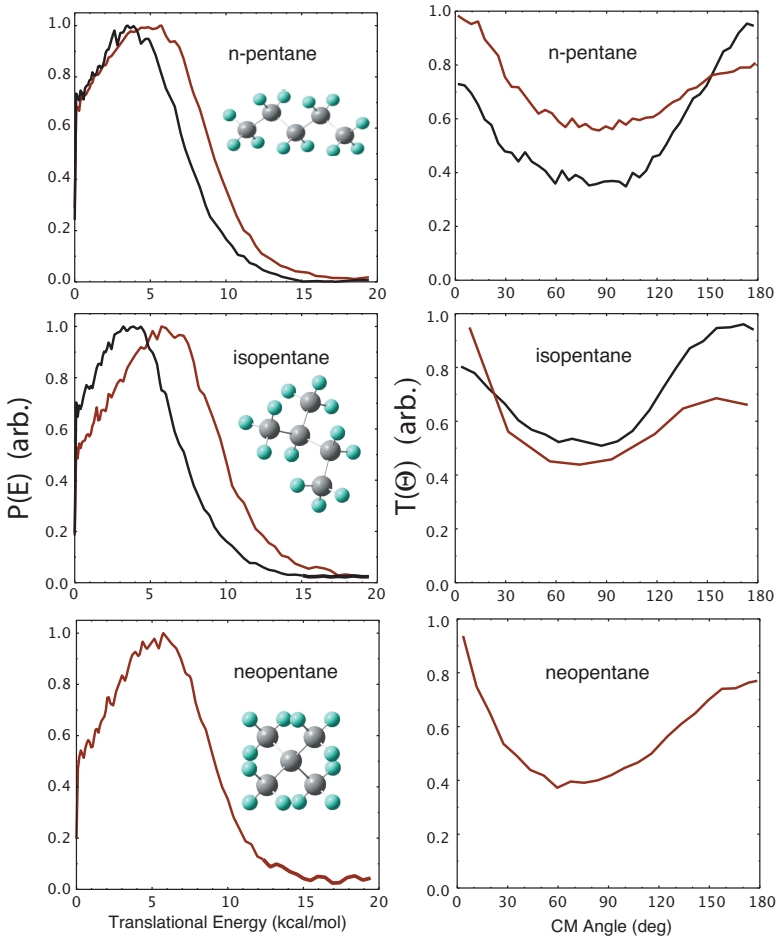

Figure 3.4: Total center-of-mass translational energy distributions (left) and angular distributions (right) for indicated pentane isomer reactions from data in Figure 3.3. Black curves are the low collision energy results from Figs. 3.3a, 3.3b, ∼5 kcal/mol, red curves are high collision energy results, ∼9 kcal/mol from Figs. 3.3c, 3.3d, 3.3e.

the collision energy shows a shift to a more forward peaking trend and much sharper forward scattering for neopentane and isopentane (rising at 30°), less so for n-pentane (∼60°). These trends can be seen clearly in the angular distributions shown in Fig. 3.5, in which all systems at a given collision energy are grouped together.

An important advantage of the slice imaging technique applied to crossed-beam scattering is that the full coupling of the translational energy and angular distributions are directly manifested in the data. In analysis of traditional crossed-beam scattering data, strategic choices in fitting the data are typically made in an effort to explore the detailed nature of the scattering distributions and to reveal the underlying dynamics. Often these choices are

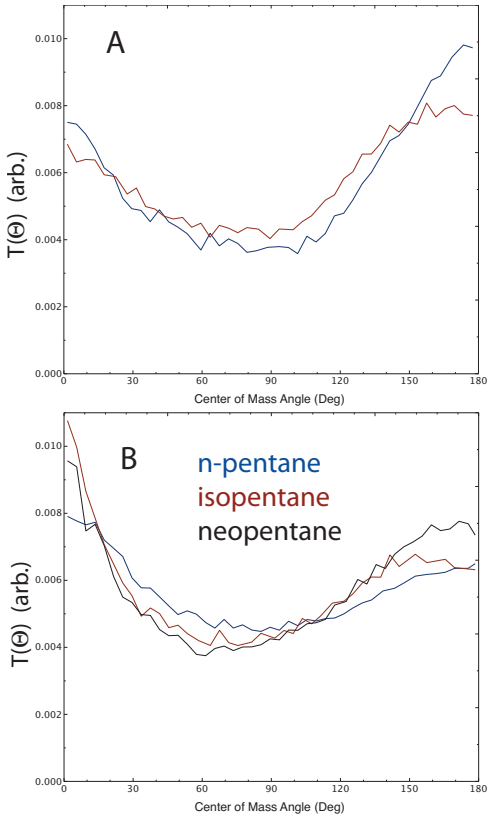

Figure 3.5: Total center-of-mass angular distributions from Figure 3.3 grouped by collision energy. (A) low collision energy; (b) high collision energy.

not based on features in the data, and some ambiguity in interpretation arises as a result. *Photoloc* methods have allowed some investigation of the velocity dependence of the angular distributions, but owing to the inherent averaging these are underdetermined, and only the gross features may be obtained from the fitting. Slice imaging methods do not face this difficulty. The present data show strong coupling of energy release and scattering angle, as can be seen even in the raw images. In all of the images in Figure 3.3, for example, the backscattered distribution is broader than that in the forward direction; moreover, for the high collision energy images, in particular, it is clear that the sideways scattering extends to lower energy than the forward or backscattered distributions. To gain insight into the detailed nature of this coupling, these data are integrated in several different ways. Figure 3.6 shows the translational energy distributions for forward (0°-60°), sideways (60°-120°), and backscattered (120°-180°) regions of the distributions, separately normalized. The forward

scattered translational energy distributions peak sharply and this is quite striking for the higher collision energy result, especially for isopentane and neopentane. For n-pentane, all of the distributions are similar to those for the other isomers but broader, particularly on the low energy side.

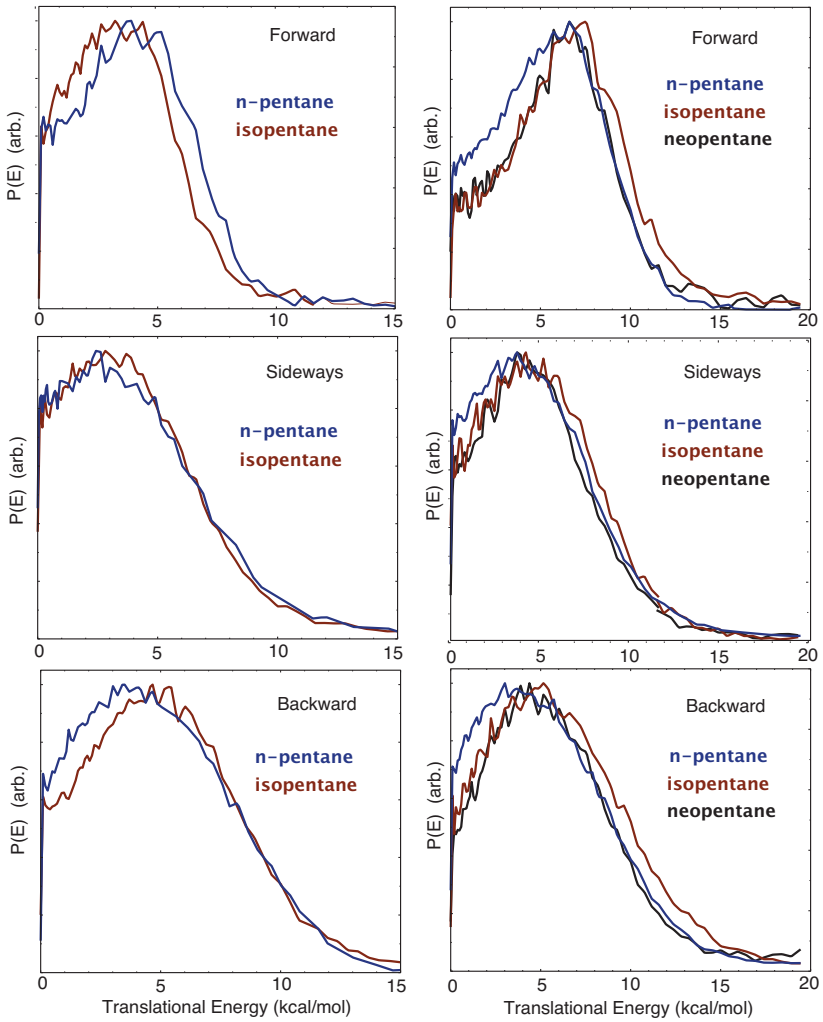

Figure 3.6: Center-of-mass translational energy distributions for indicated pentane isomer and center-of-mass scattering region: Forward (0°-60°); sideways (60°-120°); backward (120°-180°). Left side, low collision energy results; right side, high collision energy results.

Another approach to illustrate the nature of these coupled distributions is to show the angular distributions for selected translational energy ranges. This is shown in Figure 3.7 for the single case of isopentane at high collision energy; the trends in the others are similar. The low recoil energy component of the distributions is nearly isotropic, with slight

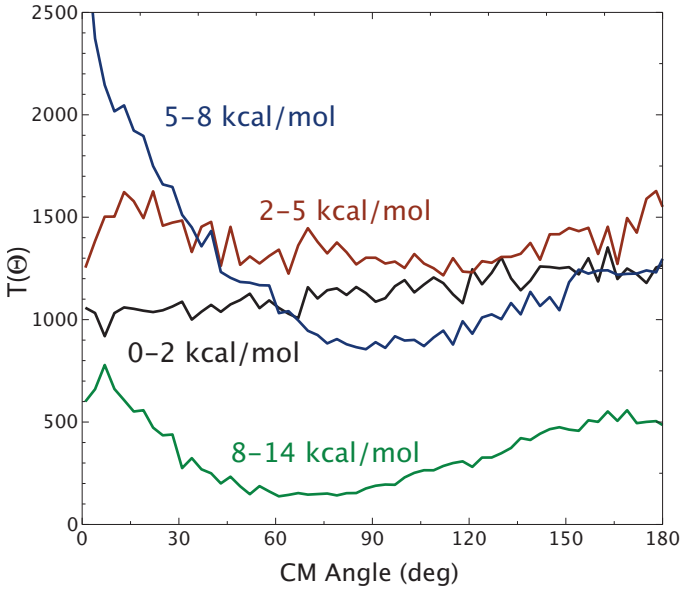

Figure 3.7: Center-of-mass angular distributions for Cl + isopentane at 9.5 kcal/mol and indicated range of total translational energy.

backscattering. The recoil energy regions in the vicinity of the maximum show sharp forward scattering superimposed on a broad distribution that shows some slight backward peaking as well. The highest recoil energy component shows relatively less sideways scattering, as expected based on the appearance of the images.

3.4 Discussion

The translational energy distributions plotted in Figures 3.4 and 3.6 clearly show that the distributions for all pentane isomers are quite similar. This is one of the most remarkable aspects of the present results. As has been seen in the past, the distributions tend to preserve the collision energy into product recoil. This behavior is expected for collinear heavy-light-heavy systems as will be discussed further below, and it suggests plotting all of the translational energy distributions on a reduced scale, as shown in Figure 3.8, with average values compiled in Table 3.2. The plots are extraordinary in the similarity of the trends shown regardless of target isomer. For the high collision energy result averaged over recoil direction, more than 70% of the products possess a translational energy equal to or

less than the collision energy. At low collision energy, this fraction is smaller, i. e., a greater fraction of the energy appears in translation. This trend is not surprising, as the exoergicity is a larger fraction of the collision energy, and some of it finds its way into product recoil. The most probable translational energy release is similar in all cases, about 80% of E_C, independent of target isomer and collision energy.

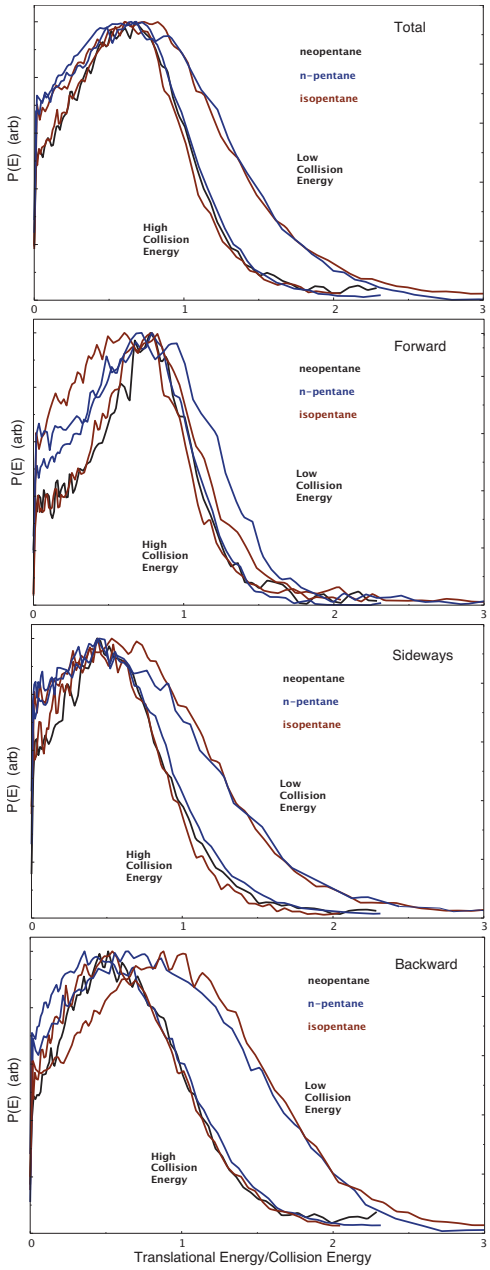

Figure 3.8: Reduced translational energy distributions $P(E_T/E_C)$.

Further insight can be obtained by examining these same trends for different scattering regions, also shown in Figure 3.8 and highlighted in Table 3.1. The forward scattered (0°-60°) distributions show sharp peaking at $0.8E_C$. It is sharpest for neopentane and isopentane, somewhat broader for n-pentane. The forward scattered distributions all show much less variation with collision energy compared to the sideways (60°-120°) or backscattered (120°-180°) contributions. The backscattered distributions show a strong dependence on collision energy, for n-pentane and isopentane there is a change from about $1.02E_C$ at low collision energy to $0.68E_C$ at high collision energy. This observation shows rather clearly that low impact parameter collisions are required to couple the exoergicity into recoil. It is interesting that neopentane, with only primary H sites, shows the highest average recoil at the high collision energy. As can be seen in Figure 3.8, this is owing to the fact that it has the sharpest peak and less very low energy recoil; the high recoil energy portion of the distribution is identical for all three isomers.

Table 3.1: Most probable collision energy, E_C (kcal/mol), average translational energy release, $\langle E_T \rangle$(kcal/mol) in the different regions of the image for the subject reactions.

	E_C	$\langle E_T \rangle$total	$\langle E_T \rangle$forward	$\langle E_T \rangle$sideways	$\langle E_T \rangle$backward
n-pentane	5.4	4.6	4.2	3.7	5.3
	8.4	5.3	5.5	4.8	5.6
Isopentane	5.3	4.6	3.9	4.1	5.5
	9.5	6.3	6.5	5.4	6.6
Neopentane	8.0	5.7	5.9	4.8	6.1

The fraction of available energy appearing in translation is not compiled, in part because

Table 3.2: Most probable collision energy, E_C (kcal/mol), average reduced translational energy, $\langle E_T \rangle^* = \langle E_T \rangle / E_C$, and fraction forward scattered for the subject reactions.

	E_C	$\langle E_T \rangle$*total	$\langle E_T \rangle$*forward	$\langle E_T \rangle$*sideways	$\langle E_T \rangle$*backward	f_{forw}
n-pentane	5.4	0.85	0.78	0.69	0.98	0.45
	8.4	0.63	0.66	0.57	0.67	0.50
Isopentane	5.3	0.87	0.74	0.77	1.04	0.45
	9.5	0.66	0.68	0.57	0.69	0.46
Neopentane	8.0	0.71	0.74	0.60	0.76	0.47

scaling with collision energy is more meaningful than available energy; moreover, it is difficult to assay the available energy, as this will depend on the likelihood of abstraction of primary, secondary, or tertiary H atoms. Nevertheless, for comparison, consider the case of n-pentane at the high collision energy. Assuming all sites equally likely and the average reaction exoergicity for primary or secondary H abstraction, an available energy of 11 kcal/mol is obtained. The fraction of available energy appearing in translation will then be 0.48 overall, with forward, sideways, and backscattered contributions of 0.50, 0.44, and 0.51, respectively. This is significantly lower than the 0.68 reported by Bass *et al.* [86] for n-butane. These scaled angle-dependent translational energy distributions are also helpful for exploring the distinct dynamics of primary, secondary, or tertiary H atom abstraction. A number of studies have probed this issue directly using partially deuterated alkanes with detection of the DCl or HCl product. Koplitz and co-workers [87] examined relative reactivity for partially deuterated propane, butane, and isobutane, and Varley and Dagdigian [88, 89] extended these measurements to examine the site specificity of the dynamics of these reactions using the *photoloc* technique. The experiments clearly showed enhanced reactivity at the secondary or tertiary site, roughly a threefold enhancement on a *per* H atom basis. It is important to bear in mind, however, that this enhancement is likely to decrease significantly with collision energy, as the difference in reactivity is largely a consequence of the difference in energetics. The likelihood of abstraction of primary H atoms should approach that for secondary and tertiary sites in the limit of high collision energy. It is suspected that this reduced reactivity for primary H atom sites is in part responsible for the inability to achieve adequate signal-to-noise ratio for the low collision energy neopentane case. Varley and Dagdigian also reported gross angular distributions obtained assuming a single recoil energy with no internal energy in the hydrocarbon radical. They found, for the reaction with $CD_3CH_2CD_3$, enhanced scattering in the backward hemisphere for both HCl and DCl, but for DCl sideways-backward scattering was dominant. Hemmi and Suits [71], in studies of n-pentane at relatively high collision energy (16.8 kcal/mol) using universal synchrotron vacuum ultraviolet probe, reported overall for-

ward scattering, closely resembling that seen here, but with slightly higher energy release in the forward direction. They decomposed the distribution into two channels and argued for association of the forward scattering with preferential abstraction of secondary H atoms based on the observed translational energy release, following earlier suggestions by Blank *et al.* [70] for reaction with propane. This interpretation was echoed by Bass *et al.* [86] in a study of Cl + n-butane using the *photoloc* imaging method. Although the present results do not directly address this issue by any means, the similarities in the translational energy and angular distributions for the three target pentane isomers clearly show that there is no strong correlation between scattering angle or translational energy with abstraction site. At the high collision energy, n-pentane, with equal numbers of primary and secondary H atoms, shows a nearly identical scaled translational energy release compared to neopentane, with only primary H atoms, and isopentane, that also includes a tertiary H atom. The greatest effect is seen in the broadening of the distributions for n-pentane compared to the others, particularly in the shading of the translational energy release to lower energy. This is consistent with the association of secondary abstraction with greater HCl rotational excitation, as seen by Koplitz and Dagdigian and others.

For the forward scattered peak, a little momentum transfer can be expected, and the spectator stripping limit can be examined, i.e., if the product HCl has the same momentum as the incoming Cl atom. In this case, the predicted translational energy will be $(35/36)^2 E_C$, or about $0.95 E_C$. The values in Table 3.1 and 3.2 are significantly lower than this, suggesting likely rotational excitation of the pentyl radicals even for these collisions. As seen in the raw images and reproduced in the average values in Table 3.1, the sideways scattering consistently shows the lowest average fraction of energy in translation. It is likely that for these intermediate impact parameter collisions, there is efficient rotational excitation of the alkyl radical, but no compensating coupling of the exoergicity into recoil.

The angular distributions shown in Figs. 3.4, 3.5 also show remarkable parallels for all systems. At lower collision energy there is a modest preference for backward scattering, and

this shifts to sharp forward peaking for all cases at the higher collision energy. However, even at the higher collision energy, the integrated distributions still show an overall preference for backward scattering, as seen in Table 3.1. These angular distributions are consistent with those reported by Hemmi and Suits [71] for n-pentane, but show greater backward scattering than the n-butane results of Bass *et al.* [86] at 7.4 kcal/mol obtained using *photoloc* in an imaging configuration. The *photoloc* results are very similar to these in the forward direction, showing a sharp forward peak rising from $\cos\theta = 0.5$ (30°), but no sign of the backscattered peak seen here and in the synchrotron experiment. However, Bass *et al.* noted that their study was blind to backscattered products with less than half of the available energy appearing in translation owing to interference from HCl in the beam. It is somewhat surprising that they did not consider this as one possible source for the discrepancy between the angular distribution measurements. The consequences of this omission can be examined by integrating the images for different recoil energy regions separately, as shown in Fig. 3.7. At the lowest energy contribution, 0-2 kcal/mol, shows some enhanced backscattering, while the next region, 2-5 kcal/mol, is nearly isotropic. The dominant region from 5 to 8 kcal/mol shows strong forward scattering, and the smaller contribution from 8 to 14 kcal/mol also shows enhanced forward scattering. If the contributions below 5 kcal/mol is ignored, a qualitative agreement with the *photoloc* angular distributions for n-butane is obtained.

Many approaches have been developed over the years to model reaction dynamics in polyatomic systems. Zare and co-workers successfully treated the Cl + methane reaction with a combined line-of-centers/hard sphere model. In this treatment, the energy along the normal to the potential at the barrier determines the likelihood of overcoming the barrier, with the angular distribution determined as for hard spheres, sometimes with an adjustable opacity function to model enhanced contributions from peripheral reactions. There are several key differences for pentanes versus methane, however. The first is in potential energy surface: For methane, the barrier is substantial and the reaction endoergic. For pentanes, even for primary H abstraction, there appears to be no barrier and the reaction is significantly

exoergic. Nevertheless, even for pentanes, there is likely a submerged barrier as characterized by Greaves *et al.* [90] for Cl + ethane. This implies that the line-of-centers picture is still relevant, and reaction away from collinear Cl-H-C not necessarily likely. This is the necessary ingredient to generate peaking in the backward direction; without this, a flat scattering distribution would be expected with a cutoff in the forward direction (for pure hard sphere with impulse) or a forward peaking distribution (for a peripheral reaction). The second key difference for methane versus pentanes is that for methane, a purely collinear collision is necessarily a low impact parameter collision. For the pentane isomers, any purely collinear Cl-H-C collision necessarily possesses a nonzero impact parameter. Other models have been developed that take account of these issues to some extent.

3.5 Conclusion

Several conclusions can be drawn from these results: The broad backscattered peaking indicates that even though the barrier may be submerged, it still has an important influence on the dynamics. The shift to forward scattering shows the role of peripheral abstraction and the fact that these are largely nonzero impact parameter collisions. The similarities among all isomers show that the primary and secondary (and perhaps tertiary) H atoms do not show strongly divergent angular or translational energy distributions. The translational energy distributions in the forward direction are very consistent, showing generally sharp peaking at about 80% of the collision energy with the balance perhaps mostly in rotation of the alkyl radical. The backscattered distributions peak at lower energy but also show some of the reaction exoergicity, particularly clearly for the low collision energy cases, in general, manifesting the features of a close collision.

Chapter 4

Dynamics of H and D abstraction in the reaction of Cl atom with butane-1,1,1,4,4,4-d_6

4.1 Introduction

The insights obtained from the many dynamical studies on the interaction of free radicals with hydrocarbons (RH) [11, 54, 60, 61, 75, 91–94] has helped build a foundation for understanding the processes involved in combustion, atmospheric, and marine environments. However, in fundamental studies involving polyatomic reactants and polyatomic products, both experimentalists and theoreticians are faced with challenging dynamical issues. Polyatomic reactants may have multiple reaction sites that can exhibit distinct reactive behavior. For example, H-atom abstraction from RH with three or more carbon atoms are complicated by the nature of H-atom type being abstracted, i. e. competing primary, secondary, or tertiary H-atoms may be present with different energetics and distinct products. Despite long interest in these questions, little direct probing of these dynamics has been achieved, and the quantity of speculation in the literature perhaps exceeds that of concrete evidence. Crossed-beam imaging methods have now developed to the point that these issues can be addressed more directly, and this paper represents the first of the efforts on this problem.

The dynamics associated with the abstraction at the different H atom sites in alkanes was studied in a widely cited set of papers of Andresen and Luntz [91] on the reaction of

$O(^3P)$ with neopentane, cyclohexane, and isobutane. These were chosen as prototype systems for study of abstraction of primary, secondary, and tertiary hydrogens, respectively. This crossed-beam study relied on laser-induced fluorescence to probe the OH product state distributions, but without translational energy or differential cross section determinations. Interestingly, in all systems the OH rotational distributions were found to be cold and they this ascribed to a collinear O-H-C transition state with low impact parameter collisions. The OH vibrational distributions, however, showed a dependence on the type of H-atom abstracted, with increasing vibrational excitation for primary, secondary and tertiary hydrogen atoms. This trend was attributed to the increasing exoergicity in this sequence, and the movement of the reaction barrier toward the reactant geometries. These findings were confirmed in the quasiclassical trajectory calculations by Luntz and Andresen [92].

There have been several studies on site-selective hydrogen atom abstraction by Cl atoms from RH with three or more carbon atoms, obtained using various kinetic techniques [95–97]. Tyndall *et al.* [97] used relative rate technique to quantify the contributions of primary and secondary H-atoms in the reaction of Cl atoms with propane and butane. They found room temperature reaction of Cl atoms with C_3H_8 yields 43±3% 1-propyl and 57±3% 2-propyl radicals, while the reaction of Cl + n-C_4H_{10} produces 29±2% and 71±2% for abstraction of primary and secondary hydrogen atoms, respectively. Sarzynski and Sztuba [96] in their study of Cl + butane using the relative rate method reported a slightly positive temperature dependence for abstraction of primary hydrogen atom and slightly negative for secondary hydrogen abstraction, suggesting small barriers for the former reactions.

In addition to many kinetics studies, the reaction dynamics of chlorine atoms with hydrocarbons have also been studied in great detail in the past two decades. In contrast to $O(^3P)$ + RH reactions, these reactions have little or no barriers to reaction and are exoergic, with the exception of Cl + methane with $\Delta H = +1.82$ kcal mol^{-1}. Zare and coworkers [60, 61, 93, 94, 98]and Varley and Dagdigian [56] investigated the dynamics of chlorine atom reactions with small hydrocarbons and their deuterated analogues using *photoloc* with core

extraction techniques combined with resonance-enhanced multiphoton ionization (REMPI) to probe the nascent HCl (DCl) product. Results showed cold HCl and DCl rotational distributions [54]. An earlier report on the secondary abstraction reaction of Cl + c-C_6D_{12} using diode laser absorption technique also showed cold DCl rotation distributions. These cold HCl(DCl) rotational distributions have been exhibited by Cl atom reaction in a wide range of target alkane reactants [11, 99]. The most direct investigation involving the site-specific dynamics of Cl + RH reaction was by Koplitz and co-workers [87] using selectively deuterated propane. They found that the yield of DCl is nearly equal for either primary and secondary labeled propane while the HCl yield was 1.5 times greater for $CH_3CD_2CH_3$ than $CD_3CH_2CD_3$. Varley and Dagdigian [88, 89] extended this study to a *photoloc* investigation of partially deuterated propane and isobutane deuterated on the tertiary carbon. For the Cl + $CD_3CH_2CD_3$ reaction, results suggested sideways scattered DCl product while the HCl peaked in the backward direction. For Cl + $(CH_3)_3CD$, the nascent DCl product was mainly backscattered, suggesting that abstraction of a tertiary hydrogen atom proceeds through a near collinear transition state. Abstraction of the primary hydrogen to yield the HCl product was sideways peaked in qualitative agreement to the primary abstraction in the Cl + partially deuterated propane system.

Numerous studies have demonstrated the efficiency of crossed molecular beam ion imaging techniques in providing detailed information on the dynamics of many bimolecular reactions. This technique has also been exploited in studying the dynamical consequence of isotope effects on several systems. Using crossed molecular beam ion velocity imaging techniques, Liu and coworkers [100] studied reaction of Cl with CHD_3 to examine vibrational mode selectivity in that system. They found that CH stretch excitation was no more effective than translation in promoting reaction. Despite the number of studies on deuterated methane and ethane and on the dynamics of Cl atom reaction with fully hydrogenated systems, there have been no studies yet bringing the power of imaging methods to explore the dynamics of H *vs*. D abstraction in selectively deuterated alkanes.

In this section, the reaction of chlorine atoms with butane-1,1,1,4,4,4-d_6 using crossed molecular beams and dc slice imaging techniques is reported. In this reaction, the Cl beam crosses the partially deuterated butane beam and H- or D-atom abstraction occurs forming HCl (4.1a) or DCl (4.1b) and a butyl radical:

$$\mathrm{Cl} + \mathrm{CD_3CH_2CH_2CD_3} \longrightarrow \quad \mathrm{HCl} + \mathrm{CD_3CH_2CHCD_3} \quad \Delta_r H(0\ \mathrm{K}) = -6.0\mathrm{kcal/mol} \tag{4.1a}$$

$$\mathrm{Cl} + \mathrm{CD_3CH_2CH_2CD_3} \longrightarrow \quad \mathrm{DCl} + \mathrm{CD_3CH_2CH_2CD_2} \quad \Delta_r H(0\ \mathrm{K}) = -1.7\mathrm{kcal/mol} \tag{4.1b}$$

The reaction enthalpies used here are from *ab initio* calculations performed by Visger-Kiefer [101] using the GAUSSIAN 09 [102] suite of software at the CBS-QB3 [103, 104] level corrected for zero point energy. The butyl radical products resulting from the H-atom and D-atom abstraction were probed via single photon ionization using a 157 nm excimer laser. Previous results from Suits group group have shown improved detection and sensitivity of single photon ionization in probing the dynamics of a variety of reactions [105, 106]. The key issue addressed here is to compare the dynamics of abstraction at the primary to that of the secondary carbon sites.

4.2 Experiment

The experiments were performed in a crossed beam imaging apparatus described elsewhere [66, 78]. The apparatus is partitioned into a main scattering chamber and two source chambers differentially evacuated to 10^{-7} Torr base pressure and 10^{-5} Torr operational pressure by turbomolecular pumps. The Cl atom beam was then generated by photodissociation of tetrachloroethylene, TCE, 5% seeded in helium, using the 193 nm output of an ArF excimer laser (60 mJ, 10 Hz) at the nozzle of a piezoelectric pulsed valve. The Cl atom product was entrained in the beam, which was skimmed before traveling into the interaction region. Butane-1,1,1,4,4,4-d_6 (98% D, Isotec Inc.) seeded 5% in Ar, He, or H_2, was expanded from a total pressure of 4 bar through another pulsed valve, collimated by a single skimmer, and

crossed the Cl beam at 90° in the interaction region. Recent measurements in Suits laboratory show that photodissociation of TCE gives 30% spin-orbit excited Cl atoms at 202 nm, and a similar yield at 193 nm is expected, as it is the same absorption band [107]. However, efficient quenching to the ground state during the expansion is anticipated as seen in similar experiments with oxalyl chloride as the Cl atom precursor.

The scattered butyl radical products resulting from H- or D-atom abstraction with m/z = 63 or m/z = 62, respectively, were detected by single photon ionization. Ionization of the products was achieved by a 157 nm F_2 excimer laser (OPTEX, 0.5 mJ, 10 Hz) focused loosely using a MgF_2 lens (f = 135 cm) into the interaction region of the two crossed beams. Although the primary butyl radical products nominally possess an ionization energy slightly higher than the secondary radical, and slightly above the 7.9 eV probe photon energy, previous studies found essentially identical detection efficiencies for these two products at 157 nm, and no evidence of a dependence on internal energy [85]. The ions were accelerated perpendicular to the plane formed by the molecular beams via a four-electrode dc slice ion optics assembly [14] to impact on a 75 mm diameter dual microchannel plate (MCP) detector coupled to a fast phosphor screen held at 5 kV (Photonis/Burle, Sturbridge, MA). The front of the MCP assembly was held at ground potential and the back plate was pulsed to gate the central slice of the reaction products at a specific mass by application of a high voltage pulse (+2.2 kV/+1 kV bias, 100 ns width) using a commercial pulser (DEI PVX-4140, Fort Collins, CO). The timing of the pulsed molecular beam nozzles, firing of the photolysis and probe lasers, and detector gate pulse were controlled using a delay generator (BNC 555, San Rafael, CA). The resulting image was recorded using a charged coupled device (CCD) camera (Mintron 2821e, 512×480 pixels, Taipei, Taiwan) and transferred to a computer for analysis. The dc slice imaging detection scheme, centroiding and megapixel acquisition program IMACQ were used to accumulate the raw images [84]. Image accumulation to reach a satisfactory signal to noise ratio took 13 h at a given collision energy.

4.3 Results

Crossed-beam scattering with single photon ionization has shown to be a sensitive approach to investigating many complex bimolecular processes [72, 73, 75–79, 105, 106, 108]. With the use of 157 nm excimer laser as product probe, partially deuterated butyl radicals formed from the H- and D-atom abstraction from Cl + butane-d_6 reaction can be examined selectively. Here, the H-abstraction reaction at nominal collision energies 10.4 kcal mol^{-1} and 12.9 kcal mol^{-1} and D-atom abstraction at three different collision energies ranging from 5.2 kcal mol^{-1} to 12.8 kcal mol^{-1} is studied. The spread in the collision energy is roughly 25% full-width half maximum. Image obtained in the H-abstraction at the lowest collision energy is not reported owing to interfering background in the backward hemisphere of the image.

Figure 4.1 shows the DC sliced images of the butyl radical products from both H and D abstraction of butane deuterated at the terminal carbons, with the nominal Newton diagrams superimposed on the images. These are after background subtraction and density-to-flux correction as described fully in previous reports [105, 106]. The latter correction is modest, but one significant challenge often associated with the use of 157 nm probe in crossed-beam imaging is a large photochemical background in the forward scattered portion of the image arising from photodissociation of the parent hydrocarbon. This issue has been mitigated in the present configuration with an intense source of Cl radical, and are able to obtain accurate reactive signals for the full range of scattering except within 5-10° of the hydrocarbon beam.

The total translational energy distributions, integrated over all angles, are given in Fig. 4.2. The translational energy distributions of the butyl radical products due to H-atom abstraction (m/z = 63) peak at higher translational energy than that of D-abstraction (m/z = 62) at comparable collision energy of ∼10 kcal mol^{-1}. At ∼13 kcal mol^{-1} this difference is even more pronounced. Figure 4.3 shows the center-of-mass angular distributions, integrated over all recoil directions, derived from the images. The butane beam defines the forward

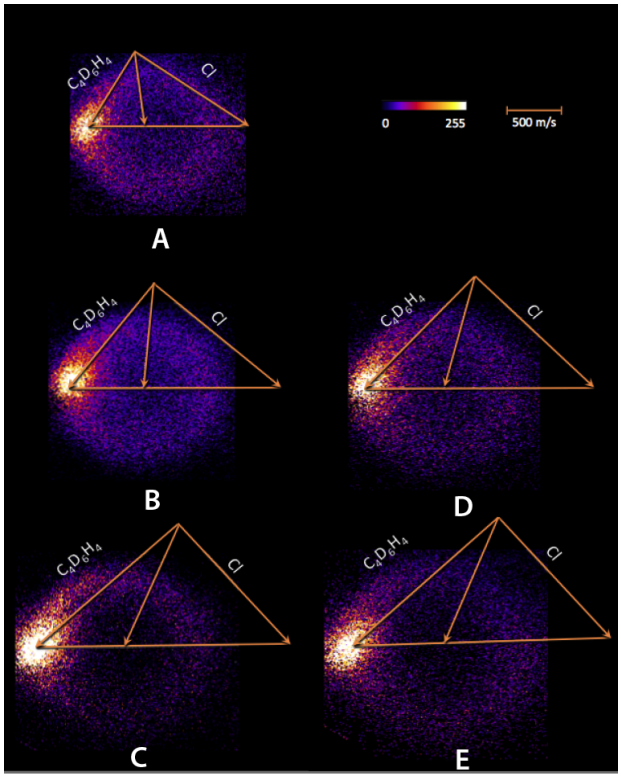

Figure 4.1: DC sliced images for butyl radical products resulting from the H- and D-atom abstraction from Cl atom reaction with butane-1,1,1,4,4,4-d_6 and superimposed Newton diagrams. Left panel are results from D-atom abstraction; (a) collision energy 5.2 kcal mol^{-1}; (b) collision energy 9.1 kcal mol^{-1}; (c) collision energy 12.8 kcal mol^{-1}. Right Panel are results from H-atom abstraction; (d) collision energy 10.4 kcal mol^{-1}; (e) collision energy 12.9 kcal mol^{-1}.

direction (0°). The angular distributions at low collision energy show flux in all directions, with modestly enhanced scattering in the forward direction. As the collision energy increases, the scattering for both the H- and D-atom abstraction shifts to the forward direction for all cases while the backward scattering is reduced. The angular distributions for both channels are remarkably similar.

The average energy release data for the two abstraction channels at each collision energy is compiled in Table 4.1. For D-abstraction, the fraction of energy appearing in translation is 65% but is consistently lower for H-abstraction. To gain further insight into the dynamics of the two abstraction channels, the product translational energy distribution is examined in two ways. First, the H and D abstraction channels are compared at comparable collision

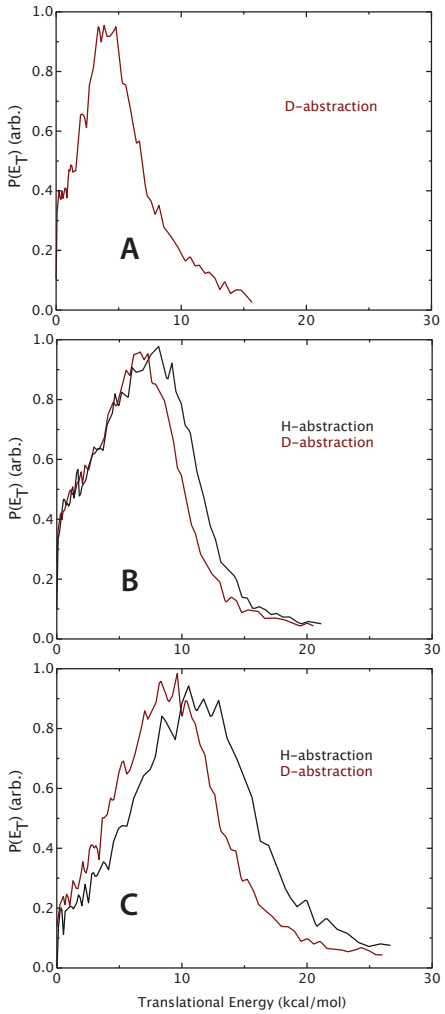

Figure 4.2: Total translational energy distributions from data in Figure 4.1. (A) D-abstraction at 5.2 kcal mol^{-1} collision energy; (b) H-abstraction (black curve) and D-abstraction (red curve) at ∼10.0 kcal mol^{-1}; (c) H-abstraction (black curve) and D-abstraction (red curve) at ∼13.0 kcal mol^{-1}.

energies for the forward (10°-60°), sideways (60°-120°), and backward (120°-180°) scattered products, by integrating the signals separately in each portion of the image. These are plotted in Figure 4.4. For these heavy-light-heavy systems, it is well known that the kinematics favor conservation of translational energy in the reaction [109, 110]. It is therefore revealing as found in earlier studies to plot the translational energy distributions scaled by the collision energy. This allows dynamical deviations from the dominant kinematic trend to be seen more clearly. The scaled translational energy distributions for each of the two channels separately

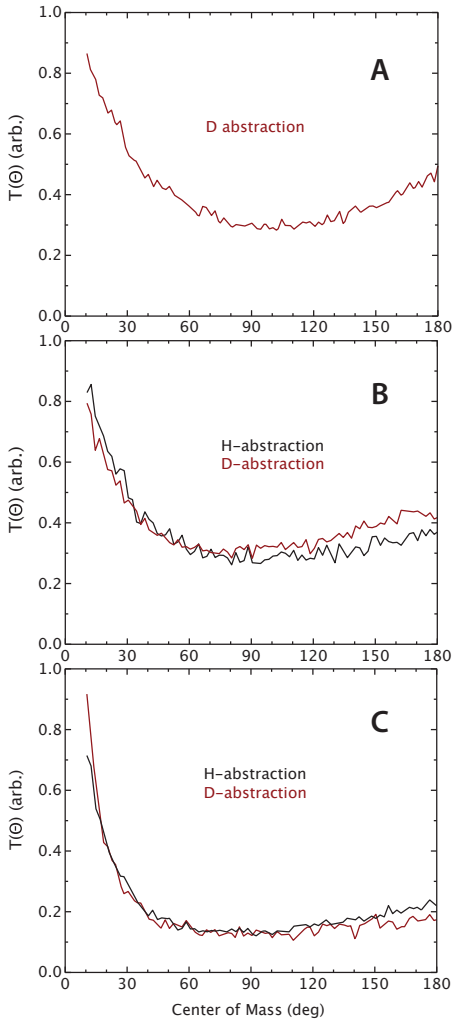

Figure 4.3: Total angular distributions from data in Fig. 4.1. (A) D-abstraction at 5.2 kcal mol^{-1} collision energy; (b) H-abstraction (black curve) and D-abstraction (red curve) at ∼10.0 kcal mol^{-1}; (c) H-abstraction (black curve) and D-abstraction (red curve) at ∼13.0 kcal mol^{-1}.

are shown in Figure 4.5 and the average values compiled in Table 4.2 and Table 4.3.

4.4 Discussion

The most direct study comparable to the results here is that of Varley and Dagdigian [88, 89] on the reaction of chlorine atoms with propane deuterated at the secondary site, and isobutane deuterated at the tertiary site. Both systems showed cold DCl and HCl rotational distribution, similar to the distributions of Cl reactions with several small hydrocarbon

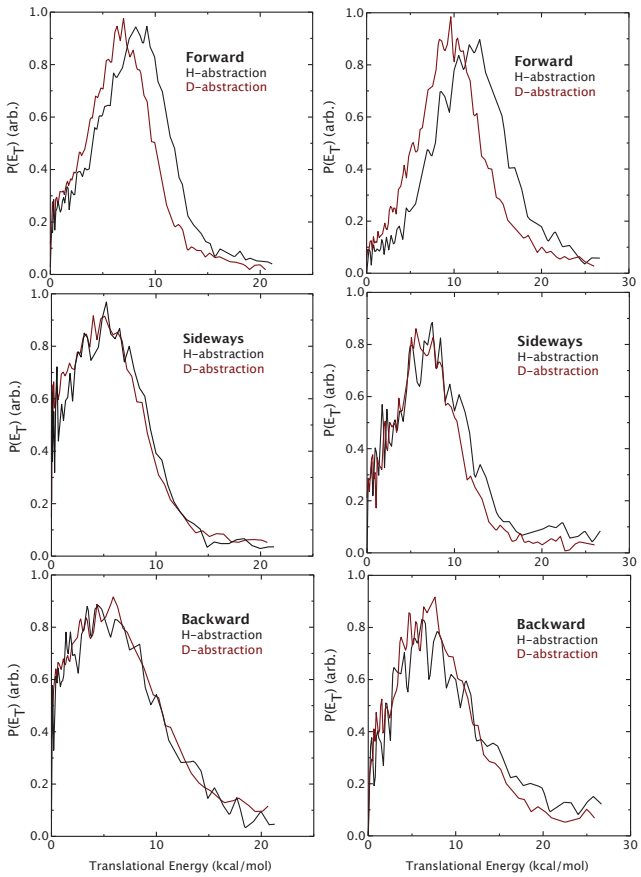

Figure 4.4: Center-of-mass translational energy distributions for $Cl(^2P_{3/2})$+butane-1,1,1,4,4,4-d_6 reaction and center of mass scattering region: Forward (10°-60°); sideways (60°-120°); backward (120°-180°). Left panel: ∼10 kcal mol^{-1} collision energy results; right panel: ∼13 kcal mol^{-1} collision energy results.

molecules [11]. They reported the angular distributions to be mainly backward for DCl and sideways for HCl; however they faced a number of challenges in their studies, including a broad collision energy spread, a spread in initial reagent velocities, and the assumption of a single product recoil velocity was necessary to fit the data.

It is important to note that in this study the D-atoms are attached to primary C atom sites and the H-atom is on the secondary C-atoms. As shown in Fig. 4.3, at ∼10.0 kcal mol^{-1} collision energy, the backscattering for the D abstraction is slightly greater than that of the H-abstraction. The difference however is not very significant. At a collision energy of 7.4 kcal mol^{-1}, Bass and coworkers [86] studied the nascent HCl($v = 0$, J) from the reaction of Cl atom with n-butane using *photoloc*, and reported forward scattering for the abstraction

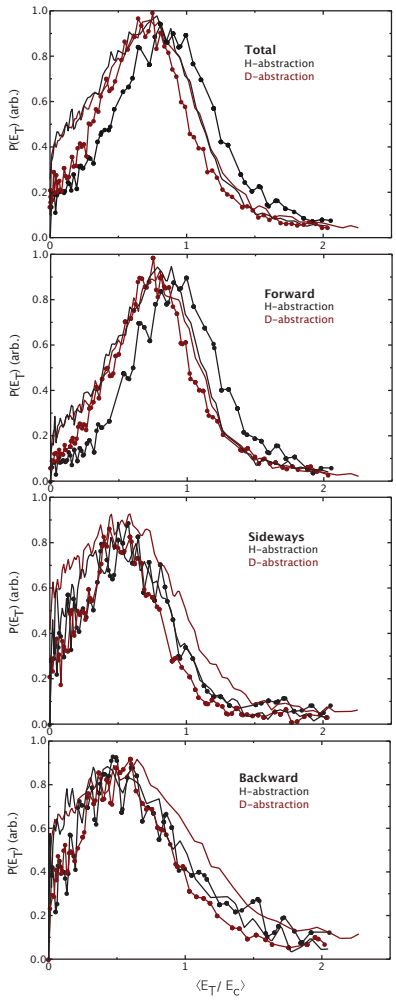

Figure 4.5: Reduced translational energy distributions $P(E_T/E_C)$. Red curves are for D-abstraction; solid line: $\sim$10 kcal mol^{-1} collision energy, dotted line: $\sim$13 kcal mol^{-1} collision energy. Black curves are for H-abstraction; solid line: $\sim$10 kcal mol^{-1} collision energy, dotted line: $\sim$13 kcal mol^{-1} collision energy.

of H at the primary carbon site while abstraction of H atom at the secondary site was seen to be more isotropic and less forward peaking. This was based on inferences about the energetics for the two channels, and was not a direct probe of the two channels. However, this experiment was not able to report the full range of the backward distribution owing to the interference of HCl in the beam. Forward-peaking secondary abstraction was argued based on the energy release in crossed-beam studies of Blank *et al.* [70] and in particular Hemmi and Suits [71] in the reaction of Cl with propane and pentane, respectively. However,

Table 4.1: Collision energy, available energy, average total translational energy release, and fraction of available energy appearing in translation.

	E_C	E_{avail} (kcal mol^{-1})	$\langle E_T \rangle$total (kcal mol^{-1})	f_t
H-abstraction	10.4	16.4	7.7	0.46
	12.9	18.9	11.2	0.58
D-abstraction	5.2	6.9	4.5	0.65
	9.1	10.8	6.9	0.64
	12.8	14.5	9.0	0.62

Table 4.2: Most probable collision energy, E_C (kcal/mol), average translational energy release, $\langle E_T \rangle$(kcal/mol) in the different regions of the image for the subject reactions.

	E_C	$\langle E_T \rangle$total	$\langle E_T \rangle$forward	$\langle E_T \rangle$sideways	$\langle E_T \rangle$backward
H-abstraction	10.4	7.7	8.3	6.6	7.3
	12.9	11.2	12.1	8.7	9.3
D-abstraction	9.1	6.9	7.3	6.6	8.2
	12.8	9.0	10.1	7.6	8.6

the results shown in the present work clearly indicate that the overall scattering angular distributions are surprisingly insensitive to the nature of the H atom site that is the target.

At the highest collision energies studied here, the key feature is the sharp forward peaking, which is essentially identical for both H and D abstraction. Recent investigation of the Cl + pentane [105] isomers showed a similar tendency toward forward scattering with increasing collision energy, but did not examine collision energies as high as in the present studies. In relative kinetics studies, Sarzynski and Sztuba [96] showed that abstraction of primary H-atoms suggested a positive activation energy indicating a small barrier towards abstraction, while secondary hydrogen abstraction was barrierless in the reaction of Cl atom with n-

Table 4.3: Most probable collision energy, E_C (kcal/mol), average reduced translational energy, $\langle E_T \rangle^* = \langle E_T \rangle / E_C$.

	E_C	$\langle E_T \rangle$*total	$\langle E_T \rangle$*forward	$\langle E_T \rangle$*sideways	$\langle E_T \rangle$*backward
H-abstraction	10.4	0.74	0.79	0.63	0.70
	12.9	0.86	0.93	0.67	0.72
D-abstraction	9.1	0.76	0.80	0.73	0.90
	12.8	0.70	0.79	0.60	0.67

butane. The sharp forward peaking seen at high energy suggests that large impact parameter collisions show no evidence of this barrier.

Conformational isomerism is an important issue in large molecules in general, and in alkanes in particular. Butane is the simplest hydrocarbon molecule that possesses different conformational minima. The most stable is the *anti* conformation, while a *gauche* conformer lies 0.62 kcal mol^{-1} higher than the *anti*, and there is a barrier of 3.5 kcal mol^{-1} separating them [111]. Under the conditions of the experiment, the *gauche* conformer should be present at a level of $\sim$25% prior to the expansion, and given the high barrier, quenching to the minimum is not likely to occur to any significant extent. Roughly one fourth of the alkane target molecules possess a *gauche* geometry. The dynamical consequence of this is not entirely clear, but can expect the secondary sites to be less stereochemically constrained. This is expected to blur the distinction between the primary and secondary dynamics to some extent.

The distinct dynamics for primary *vs.* secondary abstraction are only clearly manifested in the total translational energy distributions, as shown in Fig. 4.2 and in the scaled distributions shown in Fig. 4.5. At collision energy of 10 kcal mol^{-1}, the translational energy distribution for D-abstraction peaks at slightly lower energy compared to the H-abstraction distribution. The difference is even more pronounced at the highest collision energy of 13 kcal mol^{-1}. This is likely a consequence of the much greater exoergicity for the secondary abstraction reaction, and also the broader range of approach geometries accessible for the barrierless H abstraction. This is also seen in the marked difference of the scaled translational energy of H-abstraction and D-abstraction as a function of scattering region. As seen in Fig. 4.5 and Table 4.3, the scaled translational energy release of the D-atom abstraction (red curves) showed strong dependence on collision energy in the backward (120°-180°) scattered distributions, i.e. $\langle E_T \rangle^* = \langle E_T \rangle / E_C = 0.90$ at low collision energy and 0.67 at high collision energy. This suggests that low impact parameter collisions are required to couple the reaction exoergicity into product recoil for the primary abstraction. For the secondary

abstraction, distinct behavior is observed: in the backward direction there is little change in the scaled translational energy with collision energy, while in the forward direction, there is a larger fraction of the energy in translation as the collision energy increases: $\langle E_T \rangle^*$ rises from 0.79 to 0.93.

The observed average translational energy in the backward directions is about 2/3 of the collision energy except for the D-abstraction at the lowest collision energy where it is 0.90. To help explain this, the simple kinematic model of Evans *et al.* [110] can cited. This model predicts the average translational energy release to be given by:

$$\langle E_C \rangle = E_C \cos^2 \beta + E_R \sin^2 \beta \tag{4.2a}$$

where β is the skew angle for the reaction, E_C is the collision energy, and E_R is the energy release in the reaction. For heavy-light-heavy reactions, the skew angle is acute [109, 112] such that the second term is negligible. For the deuterium abstraction considered here, $\cos^2\beta$ is 0.92, while it is 0.96 for hydrogen abstraction. In all cases the observed translational energy release is substantially lower than the values predicted by the kinematic model by Evans *et al.* [110]. This model is intended for collinear collisions (hence the application to the backscattered product) and in general it works well for three-atom systems. The discrepancy between the predicted average translational energy and the observed energy release is not surprising because the reaction system has a large number of degrees of freedom that are not accounted in this model. Vibration or rotations of the alkyl radical products are two of the factors that are not taken into consideration in this kinematic model. A Franck-Condon picture was invoked by Liu and Suits [75] in the study of $O(^3P)$ with butane. They calculated the relaxation energy of the alkyl from the transition state geometry to be 4-5 kcal mol^{-1} and argued that this value is not available for recoil of the detected alkyl products. In cases herein, there is also likely considerable rotational excitation of the butyl radical products. For the forward scattered products, similar reduced translational energy release in the forward direction (and below the model prediction) is seen, except for primary (D) abstraction at the lower collision energy. It can be speculated that these large impact parameter collisions (for

forward scattering from primary abstraction) result in little momentum transfer, giving rise to lower rotational excitation in general and a lower likelihood of A-axis rotational excitation in particular.

Perhaps the most surprising feature of these results is the absence of any strong signature of the distinct dynamics for these two reaction channels in the angular distribtions. It may be that these systems, with little or no barrier and large reaction cross sections, are less sensitive to these issues than analogous reactions with significant barriers, such as for oxygen atoms.

4.5 Conclusion

The abstraction reaction of Cl atom towards butane-1,1,1,4,4,4-d_6 has been studied using single-photon ionization using crossed molecular beam dc slice imaging methods. This allows comparison in detail the dynamics associated with these two abstraction channels. The angular distributions showed a dramatic increase in the forward scattered product with collision energy for both reaction channels but were very similar for H or D abstraction at all collision energies studied. The translational energy distribution showed some differences for the two channels, with a larger fraction of the collision energy appearing in translation for the H abstraction channel in the forward direction, but an opposite trend for the D abstraction channel.

Chapter 5

Imaging the dynamics of chlorine atom reactions with alkenes

5.1 Introduction

The dynamics of chlorine atom reactions with alkanes have been extensively studied and are now understood at a considerable level of detail. These reactions are particularly attractive because the process proceeds via direct hydrogen abstraction by the chlorine atom generating an alkyl radical and HCl as products. Both products have been investigated by several detection schemes such as photoloc and crossed-beam methods. Theoretical and experimental investigations showed that the nascent HCl(v,J) product distributions are rotationally cold and the reaction is characterized by a collinear Cl-H-C transition state. Detailed reviews on this subject have been published elsewhere [9, 11, 13, 112, 113].

The chemistry of Cl + alkene reactions is very rich, albeit more complicated than the saturated hydrocarbons owing to the presence of the double bonds and the dramatic variations in CH bond energies across the various reaction sites. The interactions of chlorine atoms with unsaturated hydrocarbons (URH) are of considerable importance in understanding the processes involved in combustion, atmospheric, marine, and environmental chemistry. To date, numerous kinetic studies of chlorine with simple alkenes have been reported [114–123] but no detailed dynamical investigations. The rate constants reported in these thermal studies represent three dynamically distinct processes: (5.1a) addition to the double bond with

stabilization of the adduct by a third body, (5.1b) addition-elimination giving HCl and an alkenyl radical, and (5.1c) direct hydrogen abstraction the molecule giving the same products as (5.1b):

$$\mathrm{Cl} + \mathrm{C}_n\mathrm{H}_{2n} \longrightarrow \quad \mathrm{C}_n\mathrm{H}_{2n}\mathrm{Cl}\cdot + \mathrm{M} \tag{5.1a}$$

$$\mathrm{Cl} + \mathrm{C}_n\mathrm{H}_{2n} \longrightarrow \quad (\mathrm{C}_n\mathrm{H}_{2n}\mathrm{Cl})^* \longrightarrow \quad \mathrm{C}_n\mathrm{H}_{2n-1}\cdot + \mathrm{HCl} \tag{5.1b}$$

$$\mathrm{Cl} + \mathrm{C}_n\mathrm{H}_{2n} \longrightarrow \quad \mathrm{C}_n\mathrm{H}_{2n-1}\cdot + \mathrm{HCl} \tag{5.1c}$$

The C-H bond strengths and associated reactivity vary quite dramatically, as will be investigated in detail in what follows. Abstraction of an allylic H atom is strongly exoergic owing to the formation of the resonantly stabilized radical product, so this is the energetically preferred path. The addition channel (5.1a) produces a chloroalkyl radical and is barrierless and exoergic (-20 kcal mol^{-1}). The products of addition-elimination (5.1b) and direct abstraction (5.1c) mechanisms are identical on the basis of chemical formula, but formation of distinct product isomers for these two pathways is clearly possible. Moreover, their relative importance is not clear and the branching may change significantly with temperature and pressure. Since all of these channels are simultaneously operative in the Cl+URH reactions, several techniques have been used to disentangle the individual contributions to the whole. The total reaction rate coefficient dependence on pressure was used to separate addition from metathesis (i.e., abstraction or addition-elimination). The kinetic isotope effect method has been used to deconvolute addition and abstraction mechanisms. Extracting the contribution of direct abstraction from the addition-elimination channel can be modeled by probing the vibrational energy disposal of the diatomic product HCl [119]. The vibrational energy disposals for the direct abstraction and addition-elimination channels are significantly different [124, 125]. The reaction of Cl with propene, for example, involves addition, direct abstraction of allylic hydrogen, and addition-elimination channels that also involve reaction at the allylic site. This system has been the subject of numerous rate studies using different methodologies. Kaiser and Wallington [118] measured the total rate coefficient using end

product analysis by Fourier transform infrared and gas chromatography to separate addition and metathesis contributions. They reported a net rate constant to be $(3.7\pm0.3)\times10^{-11}$ cm^3 molecule^{-1} s^{-1} and about 60% (2.3×10^{-11}) of this is attributed to direct abstraction and the remainder to the addition-elimination path. Pilgrim and Taatjes [119] measured the fraction of the vibrationally excited HCl produced in the same reaction. Results showed that a sizable fraction, (48±6)%, of the HCl were vibrationally excited at 293 K. They ascribed this result to the predominance of direct abstraction in the reaction. A comprehensive review on this subject has been reported by Taatjes [126].

Over the years, ion imaging [18, 20] has become a premier technique in studying photochemical reactions and recently it has provided deep insight in crossed-beam investigations of complicated atom + polyatom reactions [11, 58, 127–129]. One advantage of crossed-beam experiments is the capability of the experimentalist to control the initial state (e.g., energize the reagents mode independently) and the direction of the reactants. Crossed-beam methods also present the advantage of confining the radical and the target molecules in separate supersonic beams, ensuring reactions at specified collision energy [8, 130]. In addition, the reaction differential cross section and the product translational energy distributions can be deduced directly from the image of the product to elucidate the details of molecular dynamics of the reaction.

In contrast to Cl + RH reactions, the dynamics of Cl + URH reactions is a rich area that has received much less attention. In this chapter, results for the reaction of Cl atoms with a series of target monounsaturated alkene molecules (1-pentene, 1-hexene, 2-hexene, and cyclohexene) is presented. The advances in sensitivity in probing the alkyl radical in Cl + RH reactions prompted to extend the efforts to Cl + URH reactions using crossed-beam dc slice ion imaging. The detection strategy involves the use of a single photon ionization of the alkenyl radical product utilizing a 157 nm excimer laser [72, 73, 75–78, 108]. In the experiments, the hydrocarbon radical product are probed, so the experiments are only sensitive to reactions of larger (C5 and higher) systems whose radical products have low enough

ionization energies for 157 nm ionization. This work aims to provide the global picture of the dynamics of the Cl atom reactions with monounsaturated hydrocarbon reactions. One of the fundamental questions addressed in this study is the relative importance of direct abstraction versus addition-elimination mechanism as a function of collision energy. In addition, the experiments sought to gain insight into the energetics for larger monounsaturated hydrocarbons and radicals, and probe relative importance for abstraction at the various H-atom sites in the molecule.

5.2 Methods

5.2.1 Experimental Methods

The reactive scattering experiments reported here were performed in a crossed-beam imaging apparatus described elsewhere [66, 78]. The experimental details of the present study have been described in greater length in previous report [105]. Briefly, the apparatus consists of a main chamber and two source chambers ($\sim 10^{-7}$ Torr base, $\sim 10^{-5}$ Torr operational pressure), fixed at 90° to each other. In the radical source chamber, a molecular beam of oxalyl chloride $(ClCO)_2$ was produced by passing helium through a bubbler containing $(ClCO)_2$ held at 0°C. The Cl atom beam was subsequently generated by photolyzing $(ClCO)_2$ using the 193 nm output of an ArF excimer laser (60 mJ, 10 Hz) at the nozzle of a piezoelectric pulsed valve. The Cl beam was skimmed before entering into the collision region. Photodissociation of $(ClCO)_2$ at 230 nm by Ahmed *et al.* [81] reported Cl, $Cl^*(^2P_{1/2})$, and CO as products of the dissociation process and Hemmi and Suits extended this study to 193 nm [82]. Both studies reported the production of two Cl atoms per photon absorbed. The excited spin-orbit $Cl^*(^2P_{1/2})$ produced at 230 nm is anticipated at 193 nm. However, after entrainment in the supersonic expansion, most of the $Cl^*(^2P_{1/2})$ atoms are likely to be quenched to the ground state [23, 83, 131].

The alkene (1-pentene, 1-hexene, 2-hexene, and cyclohexene), seeded 5% in Ar or He, was expanded from a total pressure of 4 bar through another pulsed valve, collimated by

a single skimmer, and crossed the Cl beam at 90° in the interaction region. The alkenyl radical products of interest were detected by single photon ionization at 157 nm using an F_2 excimer laser (GAM EX-10, ∼0.5 mJ, 10 Hz) focused loosely using a MgF_2 lens (f = 135 cm) into the collision region of the two crossed molecular beams. The ions were accelerated via a four-electrode dc slice ion optics assembly to impact on a 75 mm diameter dual microchannel plate (MCP) detector coupled to a fast phosphor screen held at 5 kV (Photonics/Burle, Sturbridge, MA). The front of the MCP assembly [14] was held at ground potential and the back plate was pulsed to "gate" the central slice of the reaction products at a specific mass by application of a high voltage pulse (+2.2 kV/+1 kV bias, 70 ns width) using a commercial pulse generator (DEI PVX-4140, Fort Collins, CO). The timing of the pulsed molecular beam nozzles, firing of the photolysis and probe lasers, and detector gate pulse were controlled using a delay generator (BNC 555, San Rafael, CA). The resulting image was recorded using a charged coupled device camera (Mintron 2821e, 512×480 pixels, Taipei, Taiwan). The dc slice imaging detection scheme and megapixel acquisition program IMACQ were used to accumulate the raw images containing centroided data [84]. Image accumulation to reach a satisfactory signal to noise ratio took 13 h per system at a given collision energy. The conditions of a typical experiment are illustrated in an accompanying video shown in previous publication [105].

5.2.2 Theoretical Methods

Ab initio calculations were carried out using the GAUSSIAN 09 [102] suite of software. The geometries of each alkene studied, as well as the radicals formed following removal of a hydrogen atom from each distinct carbon atom, were optimized in the initial step of the compound method CBS-QB3 [103, 104]. The bond dissociation energies and reaction enthalpies were then obtained from the CBS-QB3 (0 K) energies including zero point energy. Adiabatic ionization energies were also obtained using the CBS-QB3 method to optimize the corresponding ion structures. The vertical ionization energies were calculated using the

CBS-QB3 methodology without the initial geometry optimization for the ion. Instead, the geometries used were those of the optimized radical associated with each ion. Further details (energies, optimized structures, vibrational frequencies, and rotational constants) may be found in the online supplementary material [http://dx.doi.org/10.1063/1.3473049].

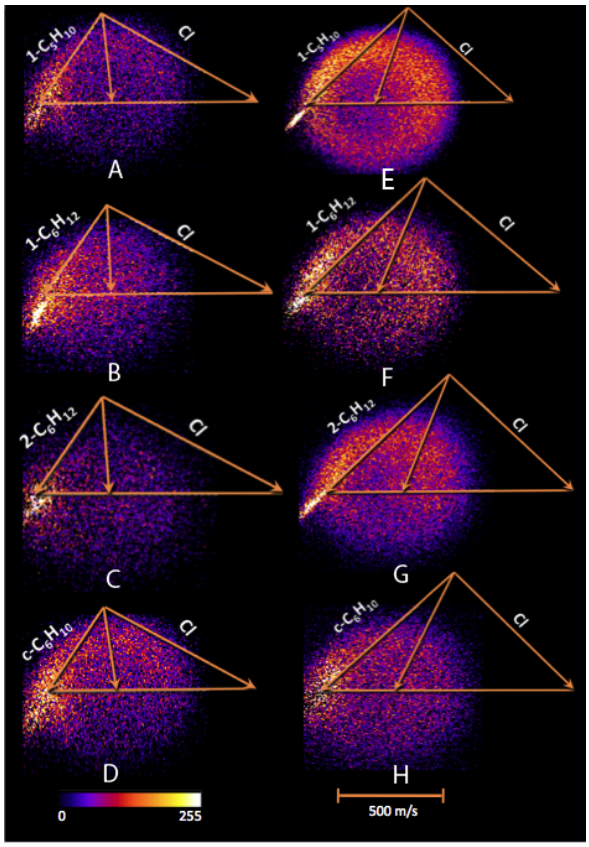

Figure 5.1: DC sliced images of alkenyl radical product from reactions of Cl($^2P_{3/2}$) with indicated alkene reagents and superimposed Newton diagrams. (A) 1-pentene, collision energy 4.3 kcal/mol; (b) 1-hexene, collision energy 4.2 kcal/mol; (c) 2-hexene, collision energy 4.1 kcal/mol; (d) cyclohexene, 4.3 kcal/mol; (e) 1-pentene, collision energy 7.2 kcal/mol; (f) 1-hexene, collision energy 7.1 kcal/mol; (g) 2-hexene, collision energy 7.0 kcal/mol; and (h) cyclohexene, collision energy 7.3 kcal/mol.

5.3 Results

Figure 5.1 shows the reactive scattering images of the alkenyl radical from the reaction of Cl atoms with 1-pentene, 1-hexene, 2-hexene, and cyclohexene at collision energies (E_C)

of 4.0 and 7.3 kcal/mol. The spread in the collision energy is roughly 25% full-width at half maximum. The most probable Newton diagram for each detected radical is overlaid on the image. These images are background subtracted and density-to-flux corrected from the raw images obtained in the experiment as described in detail previously [105]. Background subtraction is performed by recording an image with the 193 nm photolysis laser off and the 157 nm probe on to isolate the reactive scattering signals from the radicals produced by photodissociation of the parent alkene. The 157 nm probe, albeit highly sensitive in detecting the alkenyl product, can also generate signal from photodissociation of the parent hydrocarbon [75–79]. The integrated intensity of the background photochemistry signal is on the order of 20% of the total and it is comparable in magnitude to the reactive signal in the region of the image in which it appears. It is straightforward to subtract this reliably. One point that is not apparent in the images in Fig. 5.1 is that the subtracted images are signed values so that, for example, a region containing only background will integrate to zero after correction even if the background counts arrive in different pixels in the laser-on and laser-off images.

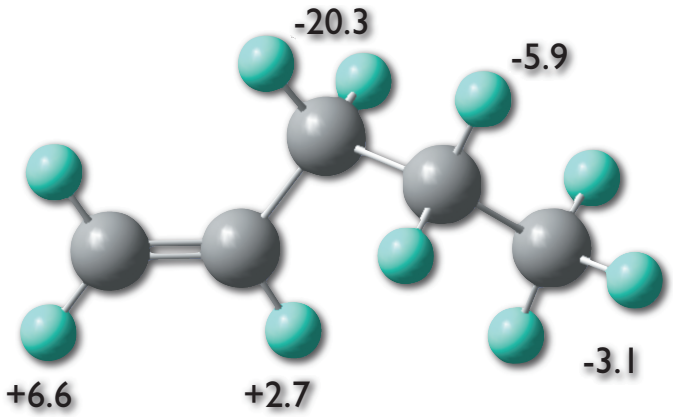

Figure 5.2: Possible H-atom abstraction sites for 1-pentene and the associated reaction enthalpies (CBS-QB3). Values are in kcal/mol.

Abstraction of a hydrogen atom from the C5 and C6 unsaturated hydrocarbons is a much more complicated process than that of the corresponding saturated systems. Figure 5.2 shows the different positions of H-atom abstraction for 1-pentene, for example, along with

the energetics involved in the process. Aside from the varying sites of possible abstraction, it is also important to note that the chemical environments (i.e., C atom hybridization) to which these hydrogen atoms are attached are markedly different. Abstraction of the allylic (β-C) hydrogen and the vinylic (α-C) hydrogen can occur at widely different rates. For higher alkenes (n $\geq$ 4), as in the case here, alkyl hydrogens can also be the site of abstraction. The reaction enthalpies (0 K) are shown in the figure 5.2, based on bond dissociation energies calculated at the CBS-QB3 level by Visger [106]. Reaction energetics and ionization energies for the target molecules and various radical products are compiled in Table 5.1. On the basis of thermochemistry alone, one might predict that abstraction of the allylic hydrogen atom might be dominant owing to its lower dissociation energy. However, in the case of 1-pentene, for example, reactions involving any of the allylic and alkylic hydrogen abstractions are exoergic, with the latter values similar to those for analogous alkanes studied recently [105]. While the calculated vertical ionization energy values are somewhat higher than the probe energy (7.9 eV) in some cases, the recent study of the relative ionization efficiency for products of heptane isomer photodissociation at 157 nm showed little variation in detection of various radical products even for those with vertical ionization energies slightly above the probe energy. The exception here is for the radicals produced by abstraction of the vinylic H atoms: these are both significantly endoergic channels and the radicals possess higher ionization energies. Abstraction at these sites is highly unlikely and neglect these reactions. For abstraction at the allylic or alkylic H-atom sites, based on the calculations in Table 5.1, strong variation in ionization efficiency is not expected. In what follows, variations in detection efficiency for different radical products is not explicitly considered [85].

Figure 5.3 shows the total translational energy distributions, integrated over all angles, and the center-of-mass angular distributions, integrated over all recoil speeds, derived from the images after background subtraction and density-to-flux correction. The translational energy at low collision energy peaks at around 2-3 kcal/mol and extends beyond 10 kcal/mol. The peak is shifted to slightly higher energies at high collision energy. The angular distribu-

Table 5.1: CBS-QB3 bond dissociation energies and reaction enthalpies (0 K) for reaction at indicated carbon atom for each reactant molecule. Also given are vertical and adiabatic ionization energies for each product radical. Allylic radicals are indicated by asterisks.
[a]Bond dissociation energy, [b]Cl + URH → HCl + UR·,[c]Ionization energy

	BDE (kcal/mol)[a]	ΔH_{rxn}(kcal/mol)[b]	Vertical IE[c] (eV)	Adiabatic IE (eV)
1-pentene				
C1	110.0	6.6	8.8	7.9
C2	106.1	2.7	8.4	7.3
C3*	83.1	-20.3	7.6	7.5
C4	97.5	-5.9	7.8	6.8
C5	100.3	-3.1	8.4	7.5
1-hexene				
C1	110.0	6.6	8.9	7.8
C2	106.2	2.8	8.4	7.3
C3*	83.0	-20.4	7.6	7.4
C4	97.9	-5.5	7.7	6.8
C5	97.4	-6.0	7.7	7.2
C6	100.3	-3.1	8.4	7.1
2-hexene				
C1*	85.5	-17.9	7.5	7.4
C2	106.6	3.2	8.2	7.2
C3	106.8	3.4	8.2	7.1
C4	82.9	-20.5	7.1	7.0
C5	97.5	-5.9	7.6	6.3
C6	100.3	-3.2	8.3	7.6

tions at low E_C show flux in all directions and are largely isotropic. Increasing the collision energy shows a shift to a more forward peaking trend for all cases, superimposed on the isotropic component. This can be clearly seen in Figure 5.5 where the angular distributions are grouped by collision energies. To gain further insight on the dynamics, the translational energy distributions for the forward (0°-60°), sideways (60°-120°), and backward (120°-180°) directions are examined by integrating the signal in these regions separately, as shown in Figure 5.4. The translational energy distributions in the forward direction show a modest peak at low collision energy that grows dramatically with collision energy. If the sharp forward scattered contribution is assumed as a dynamically distinct feature, it is useful to quantify its contribution relative to the isotropic component and evaluate it for each reactant

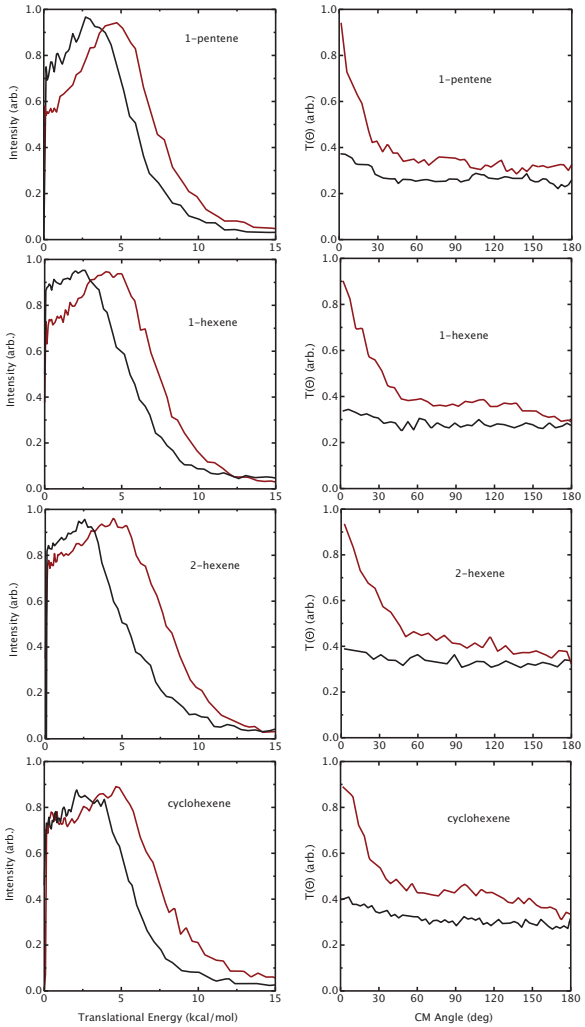

Figure 5.3: Total center-of-mass translational energy distributions (left) and angular distributions (right) for the indicated alkene reactions from data in Fig. 5.1. Black curves are the low collision energy results from Figs. 5.1a, 5.1b, 5.1c, 5.1d; red curves are high collision energy results from Fig. 5.1e, 5.1f, 5.1g, 5.1h.

molecule and collision energy. This will be justified further below. The result of this analysis is shown in Table 5.3 as the excess forward scattering, i.e., the deviation from an isotropic distribution. The most probable collision energy and average translational energy release are compiled in Table 5.2.

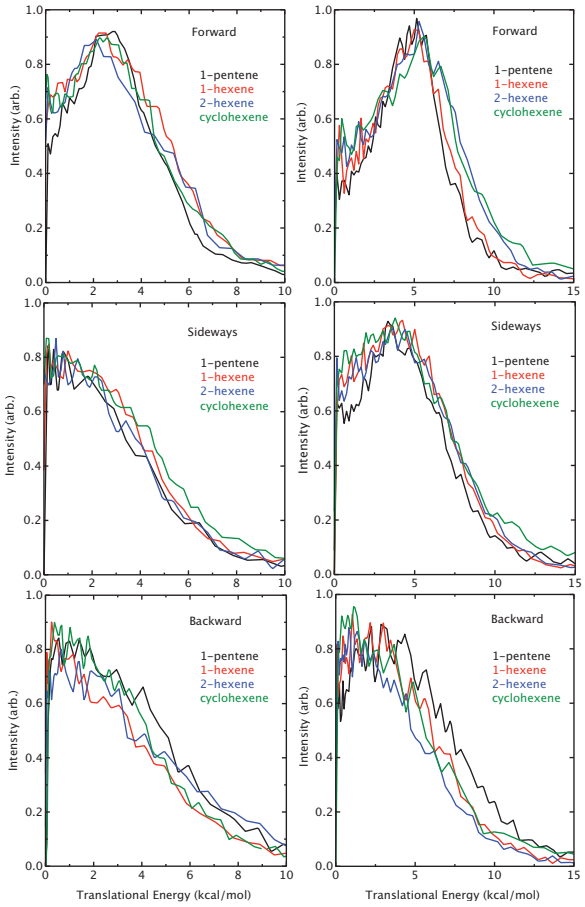

Figure 5.4: Center-of-mass translational energy distributions for the indicated Cl($^2P_{3/2}$) + alkene reactions and center-of-mass scattering region: Forward (0°-60°), sideways (60°-120°), and backward (120°-180°). Left side: low collision energy results; right side: high collision energy results.

5.4 Discussion

This study presents the first crossed-beam study of the reaction of Cl atoms with monounsaturated hydrocarbons. This section begins by addressing the issue of the competition of direct abstraction versus the addition-elimination mechanism by looking at the center-of-mass product angular distributions grouped by E_C as shown in Fig. 5.5. At the low collision energy, around 4 kcal/mol, the distribution is seen to be largely isotropic with a small forward scattered contribution; the latter growing markedly as the collision energy is increased to 7 kcal/mol. The isotropic component is a strong suggestion of the formation of a collision complex [132] that has a lifetime longer than its rotational period. Schmoltner

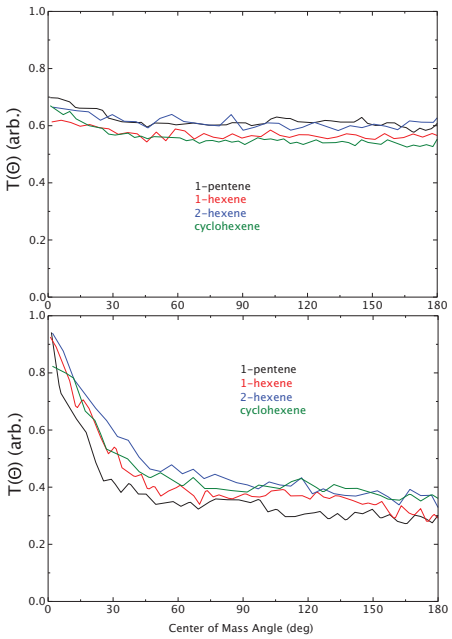

Figure 5.5: Total center-of-mass angular distributions from Fig. 5.1 grouped by collision energy. (A) Low collision energy; (b) high collision energy.

and co-workers [133–135] observed this trend in their studies of O(^{3}P) reaction with different unsaturated hydrocarbons. Similar behavior was also observed in the reaction of pseudohalogen CN($X^2\Sigma^+$) with different unsaturated hydrocarbons by Kaiser and co-workers [136–139]. Crossed-beam reactions of CN($X^2\Sigma^+$)+unsaturated hydrocarbons with mass spectrometric detection combined with *ab initio* calculations showed that the reaction undergoes complex formation initiated by addition of CN to the π electron density of the olefin to give a long-lived intermediate. A significant difference, however, is that the newly formed C-C bond is quite strong in that case, so that H loss is a dominant process rather than simply HCN elimination, which would be analogous to the HCl elimination that is the sole reaction channel here. In addition to the ∼20 kcal/mol deep minimum for the URH-Cl addition complex, the adducts in the systems studied here have at least 16 atoms and thus a much higher density of states and correspondingly longer lifetime at the same collision energy.

As seen in Figs. 5.3 and 5.5, with increased collision energy, the distributions show a significant gain in intensity in the forward scattered peak in addition to the isotropic distribution. This suggests the presence of another pathway to products that becomes important

Table 5.2: Most probable collision energy, E_C (kcal/mol), average reduced translational energy, $\langle E_T \rangle^* = \langle E_T \rangle / E_C$.

	E_C	$\langle E_T \rangle$total	$\langle E_T \rangle$forward	$\langle E_T \rangle$sideways	$\langle E_T \rangle$backward
Pentene	4.3	4.7	4.7	4.6	3.7
	7.2	5.9	6.1	5.5	5.1
1-hexene	4.2	6.2	5.0	5.8	4.3
	7.1	6.1	4.7	6.1	5.5
2-hexene	4.1	6.1	4.8	5.8	3.5
	7.0	4.1	5.4	5.3	4.4
Cyclohexene	4.3	5.2	4.9	4.7	3.9
	7.3	6.5	6.2	6.5	6.0

with increasing collision energy. There are two possible explanations for this behavior. One is the "osculating complex" model of Herschbach [140], in which the scattering distributions lose forward-backward symmetry as the lifetime of the collision complex approaches its rotational period. An alternative explanation is that a distinct, direct component grows in with collision energy and is superimposed on the long-lived complex component. The translational energy distributions in the forward direction (see Fig. 5.4) clearly support the latter picture. For a pure collision complex, it is expected that the forward and backward translational energy distributions to be the same. At the low collision energy, the sideways and backscattered distributions all peak near zero recoil energy, while for the forward direction one can easily see a sharp forward peak superimposed on the same distribution as in the backward direction. As the collision energy is increased, the sharp forward peak grows dramatically and begins to extend into the sideways direction, while the backscattered component is little changed.

It is thus suggested that the significant increase in the forward component at higher collision energy marks the onset of direct abstraction of hydrogen to compete with the addition/elimination mechanism. As stated in Sec. 4.1, for Cl + alkanes, abstraction reactions favor a collinear Cl-H-C transition state geometry which is associated with the cold nascent HCl(v, J) rotational product distribution [11]. This may be the case in the abstraction process in Cl + alkene reactions. Literature search indicates that there is no experimental

measurement reported on the nascent HCl(v, J) rotational distribution of these class of reactions. We can, however, draw a theoretical estimate on the extent of linearity of Cl-H-C transition state structure from the report of Braña and Sordo [141]. Their theoretical studies in the abstraction channel of Cl + propene reaction showed almost linear transition state structures for H abstraction in the five chemically different environments. *Ab initio* calculation at the MP2/aug-cc-pVDZ level of theory give values of <Cl-H-C ∼176.4°-179.9° for the abstraction of the three vinylic H atoms and <Cl-H-C ∼176.6°-177.9° for the allylic H atoms. Qualitatively, the rapid approach of Cl atom to the C5 and larger alkene molecule can result in abstraction of an alkylic hydrogen atom producing the corresponding hydrocarbon radical and HCl. This is reasonable since the H-atom site is at least two carbons away from the unsaturation site; thus the reactivity is not strongly influenced by the π bond. The present results clearly suggest the contribution of direct H-atom abstraction in the forward peaking distributions, reminiscent of the energy dependence of the Cl + pentane results [105].

One significant difference in the direct scattering component seen here is the absence of a direct component in the backward direction that was seen in Cl + pentane results [105]. This strongly suggests that the low impact parameter collisions that lead to backscattering for alkanes are depleted here and lead instead to complex formation and the addition/elimination reaction.

The integrated translational energy distributions are similar in all target alkene molecules and peak at 65% E_C for the low collision energy and shift to higher values at high collision energy as highlighted in Figure 5.3. It is sharpest in the 1-pentene systems and broader for cyclohexene. What is distinct in the present result is the similarity of the sideways (60°-120°) and backward (120°-180°) translational energy distributions for the reaction at low collision energy. While the Cl + pentane results show strong coupling of the translational energy and angular distributions, the present results reveal otherwise, especially in the low collision energy. The forward peaking component reveals another interesting fact that even at low E_C, direct H abstraction (∼3%) seems operative as shown in Figure 5.6 and Table 5.3. It

is clearly more pronounced in the high collision energy experiments as summarized in Table 5.3.

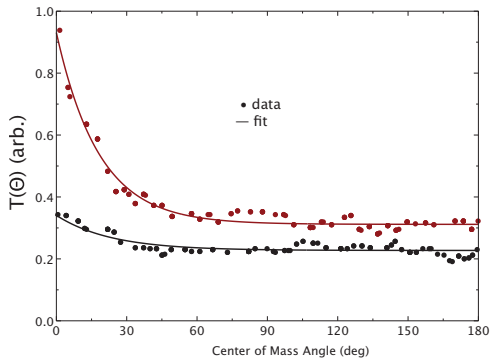

Figure 5.6: Total center-of-mass angular distributions for 1-pentene from Fig. 5.1 fitted as distinct isotropic and forward scattered components. Black curves are low collision energy results and red curves are high collision energy results.

One challenging aspect in the Cl + alkene experiment is to assay the available energy of the reaction because of the varying energetics for different reaction sites. The calculations shown in Table 5.1 are consistent with the limited values available in literature, but provide a consistent overall picture. Reaction at the vinylic carbon sites can largely be neglected under the conditions owing to significant endoergicity. Reaction at the allylic site is strongly exoergic, approaching that of F atom reaction with alkanes. Reaction at the more remote sites shows energetics quite similar to the alkanes, as discussed above. At low energy, addition/elimination is expected to dominate forming mostly the allylic radical. This suggests the observed average recoil energies of 4-5 kcal/mole represent on the order of 20% of the available energy in recoil. This is vastly different from the alkane case and, again, entirely consistent with addition/elimination. This further leads to the question of energy disposal.

Table 5.3: Percent excess forward scattering from Figure 5.6

	Low collision energy	High collision energy
1-pentene	3.5 ± 0.01	11.0 ± 0.008
1-hexene	3.2	12.0
2-hexene	3.7	13.5
Cyclohexene	3.4	11.0

Pilgrim and Taatjes measured the HCl vibrational energy disposal in the Cl + propene reaction and found that significant amount of reaction exothermicity (28±3%) was found to be channeled into HCl vibration with 0.48±0.006 formed in vibrationally excited levels. This could account for a significant fraction of the missing energy. The addition/elimination reaction will also give rise to much hotter hydrocarbon radical products, again consistent with the lower fraction of energy in recoil.

5.5 Conclusion

This work represents the first crossed-beam study of Cl atom reactions with monounsaturated alkene molecules. The results of the experiment show two distinct mechanisms for the reaction of chlorine atoms with a series of molecules studied. At low collision energy, the angular distributions are highly isotropic with small (∼3%) forward component. This suggests the formation of a long-lived intermediate that indicates addition-elimination mechanism with minimal direct H-atom abstraction contribution. At higher collision energy, the contribution of direct H-atom abstraction increases to ∼13.5% of the product flux. The dynamics associated with the interaction of chlorine atoms with unsaturated hydrocarbons present a rich ground that merits further dynamical research. In particular, state-resolved scattering studies probing the distinct dynamics for formation of HCl $v = 0$ and $v = 1$ should be very revealing.

Chapter 6

Reaction dynamics of Cl + butanol isomers by crossed-beam sliced ion imaging

6.1 Introduction

Over the years, a wide array of theory, experiments, and computations has been performed in establishing the dynamics associated with the reaction of Cl atoms with hydrocarbons (RH) [11, 112, 113]. However, related studies on the dynamics of Cl atom reactions with oxygenated hydrocarbons like alcohols are relatively limited. These oxygenated hydrocarbon (ROH) systems offer special dynamical interest to both theory and experiments. In addition to its multiple reactive sites and the degree of polarity of the molecule, the complexity of the potential energy surfaces present some serious setbacks on the part of the researchers in interpreting the results.

Only a few of the experiments on the dynamics of Cl + ROH reactions involve probing the hydroxyalkyl radical or the nascent HCl (v, J) products using various detection methods. Ahmed *et. al* [77, 78] first combined crossed molecular beam with velocity map imaging techniques for the reaction of Cl($^2P_{3/2}$) atoms with smaller alcohol such as methanol, ethanol, and 2-propanol using single photon ionization as a product probe of the scattered hydroxylalkyl products. Results showed that 30-40% of the available energy of the reaction was deposited into product translation with the detected product angular distributions to

be predominantly sideways/backward scattered with respect to the alcohol beam suggesting direct rebound dynamics. Rudic and coworkers [142] measured the rotational distribution of the HCl($v = 0$) products formed from the reaction of Cl atoms with methanol, ethanol, and dimethyl ether to be relatively hotter compared to that of Cl + RH reactions. These results, coupled with *ab initio* calculations [143], were ascribed to the dipole-dipole interaction of the HCl and the radical co-product in the exit channel of the potential energy surface (PES). In a state-to-state experiments of the Cl + $CH_3OH \rightarrow HCl(v, J) + CH_2OH$ reaction, Bechtel and coworkers [144] employed *photoloc* technique combined with REMPI methods to investigate the nascent HCl (v, J). The probed HCl ($v = 0, 1$) products reveal direct reaction with both stripping and rebound mechanism for $v = 0$ and stripping reactions for $v = 1$ with the CH_2OH co-products act as spectator in direct contrast to $v = 0$. In the imaging study of the differential cross sections (DCS) of Cl+CH_3OH, Murray and coworkers [145] found that the nascent HCl ($v = 0$) products are forward scattered for $J = 2$ and backwards for $J = 5$.

Recently, there has been a growing interest in the chemistry of butanol isomers primarily because of the possibility to use these alcohols as an alternative transportation fuel to address the problem of diminished natural oil and gas resources [146]. A significant number of detailed kinetic investigations [147–153] and theoretical calculations [154–156] have been performed to establish an accurate kinetic model in the combustion of butanol. These alcohols are produced from fermentation and non-fermentative biosynthesis and possess energy densities closer to gasoline and do not readily absorbed moisture from the atmosphere [157–160]. In addition, branched alcohols have octane numbers higher than the straight chain counterparts. Substantial kinetic database have been established for the reaction of Cl with smaller alcohols such as methanol, ethanol, and propanol [161–166]. Few kinetic studies involving Cl + butanol involve determining the rate constant and mechanism of the reaction [167–171]. However, the associated dynamics of the reaction has not been touched upon. The kinetics of these reactions has been investigated in a variety of independent studies. Kinetic measurements have shown that the rate constant for Cl + n-butanol is (1.96 ± 0.19)

$\times 10^{-10}$ cm^3 molec^{-1} s^{-1} [168], Cl + sec-butanol is $(1.32 \pm 0.14) \times 10^{-10}$ cm^3 molec^{-1} s^{-1} [167], Cl + iso-butanol is $(1.82 \pm 0.14) \times 10^{-10}$ cm^3 molec^{-1} s^{-1} [169] and Cl + tert-butanol is $(3.26 \pm 0.19) \times 10^{-11}$ cm^3 molec^{-1} s^{-1} [169].

In this section, a non-state selective study of the H-abstraction reaction of Cl(^{2}P$_{3/2}$) with butanol isomers (n-butanol, sec-butanol, iso-butanol, and tert-butanol) by crossed-beam dc slice imaging is presented. The product hydroxyalkyl radical were probed via single photon ionization at 157 nm. As has seen in the past, this product probe is a sensitive and systematic approach to studying the underlying dynamics of complicated polyatomic chemical reactions [72–79, 101, 105, 106, 108].

6.2 Experiment

The scattering experiments were performed using a crossed-beam dc slice ion-imaging set-up described elsewhere [66, 78]. Briefly, both beams were confined in separate supersonic expansion in two source chambers ($\sim 10^{-7}$ base Pressure and $\sim 10^{-5}$ operational Pressure) fixed at 90° to each other and collimated by a skimmer before it enters the differentially pumped interaction region. The Cl atom beam was generated from the photolysis of oxalyl chloride, $(COCl)_2$ using the 193 nm output of an ArF excimer laser (60 mJ, 10 Hz) at the nozzle of a piezoelectric pulsed valve. The dissociation dynamics of $(COCl)_2$ was known to produce Cl, Cl*(^{2}P$_{1/2}$), and CO as reported by Ahmed and coworkers [81] at 230 nm and further investigated by Hemmi and Suits [82] at 193 nm. The excited spin-orbit Cl(^{2}P$_{1/2}$) produced at 230 nm is anticipated at 193 nm. However, after entrainment in the supersonic expansion, most of the Cl(^{2}P$_{1/2}$) are likely to be quenched to the ground state [23] .

The alcohols (n-butanol, sec-butanol, iso-butanol, and tert-butanol), seeded 5% in He or H_2, was expanded from another pulsed valve in another source chamber with a total pressure of 4 bar, and crossed the Cl beam at 90° in the interaction region. An excimer F2 laser (GAM EX-10, ∼0.5 mJ, 10 Hz) was used to effect ionization of the hydroxyalkyl radical products (m/z = 73) of the reactions. The probe laser was loosely focused using a

MgF_2 lens (f=135 cm) into the collision region of the two crossed molecular beams. The ions were accelerated via a four-electrode dc slice ion optics assembly [14] to impact on a 75 mm diameter dual microchannel plate (MCP) detector coupled to a fast phosphor screen held at 5kV (Burle Electro-Optics). The front of the MCP assembly was held at ground potential and the back plate was pulsed to "gate" the central slice of the reaction products at a specific mass by application of a high voltage pulse (+2.2 kV/+1 kV bias, 70 ns width) using a commercial pulse generator (DEI PVX-4140). The timing of the pulsed molecular beam nozzles, firing of the photolysis and probe lasers, and detector gate pulse were controlled using a delay generator (BNC 555). The resulting image was recorded using a charged coupled device camera (Mintron 2821e, 512×480 pixels). The dc slice imaging detection scheme and megapixel acquisition program IMACQ were used to accumulate the raw images containing centroided data [84]. Image accumulation to reach a satisfactory signal to noise ratio took 1-3 hours.

6.3 Results

The reactively scattered hydroxyalkyl radical from the Cl atom reactions with butanol isomers are shown in Figure 6.1 with the nominal Newton diagram overlaid in the images. The improved instrumental resolution and the ability to produce intense source of Cl radicals enabled us to obtain considerably more detailed images of the hydroxyalkyl radical than was previously possible. The spread in the collision energy is roughly 25% full-width half maximum.

The butanol isomers have two fundamentally different abstraction sites: One in the hydroxyl end of the molecule and the C-H groups. Thermochemical data indicates the bond strength to be 104 and 94 kcal/mol for H abstraction in the O-H and C-H sites, respectively. From this data alone, the C-H bond abstraction site is seen to be favorable. Moreover, kinetics investigation on the specificity of H atom abstraction showed preference of H-atom abstraction on the alkyl backbone with ∼3% contribution from the hydroxyl end [163, 164].

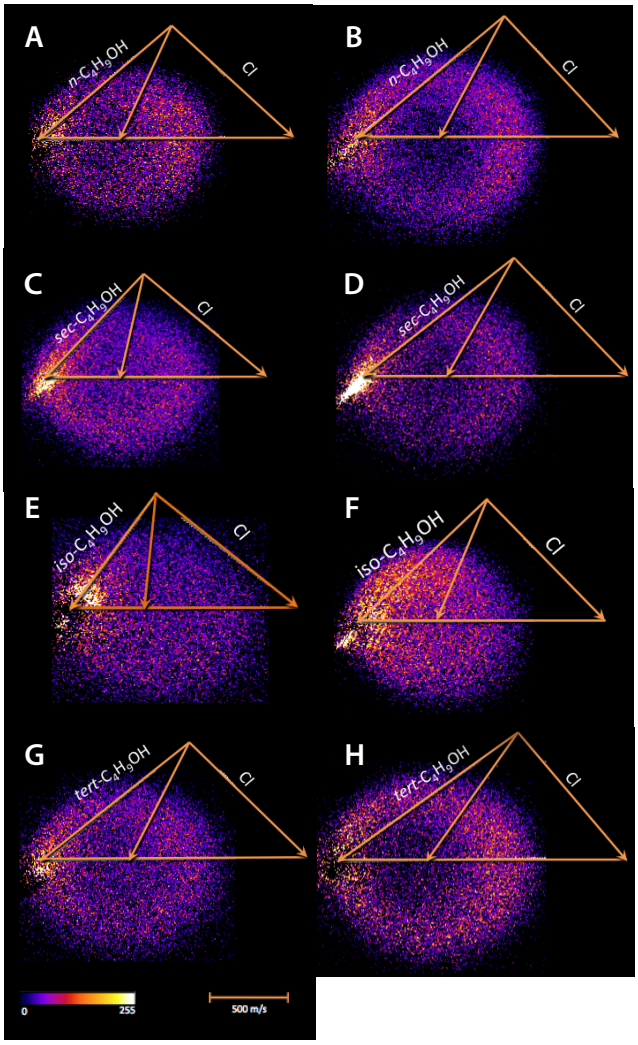

Figure 6.1: Sliced scattering data for reaction of Cl with butanol isomers. A, B: n-butanol at 6.8 and 8.0 kcal/mol; C, D: 2-butanol at 5.7 and 8.0 kcal/mol; E, F: iso-butanol at 5.3 and 7.0 kcal/mol, and G, H: tert-butanol at 7.0 and 9.2 kcal/mol, respectively.

A dynamical study on the reaction of Cl atom with deuterated methanol: CH_3OD and CD_3OH showed no DCl products for the former and measured only the nascent DCl for the latter [144].

Figure 6.2A shows the total translational energy distributions, integrated over all angles. The distributions peak at lower energy and grow with collision energy. Figure 6.2B are the corresponding angular distributions, integrated over all recoil directions derived from the hydroxyalkyl images after background subtraction and density-to-flux correction, described

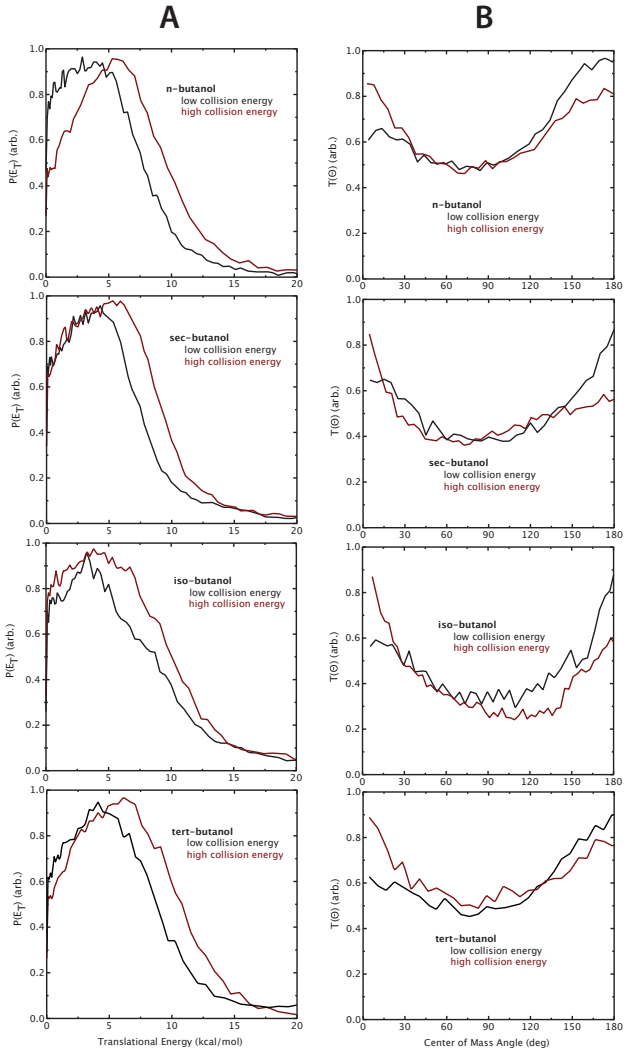

Figure 6.2: Global translational energy and angular distributions extracted from Figure 6.1.

in detail in previous reports [105, 106] . The angular distributions at low collision energy (E_C) show flux in all direction with preference in the backward direction with respect to the alcohol beam. Increasing the E_C shows a shift to a more forward peaking trend.

To gain further insight on the dynamics, the translational energy distributions for the forward (0°-60°), sideways (60°-120°), and backward (120°-180°) regions of the distributions is shown in Fig. 6.3 and tabulated in Table 6.1.

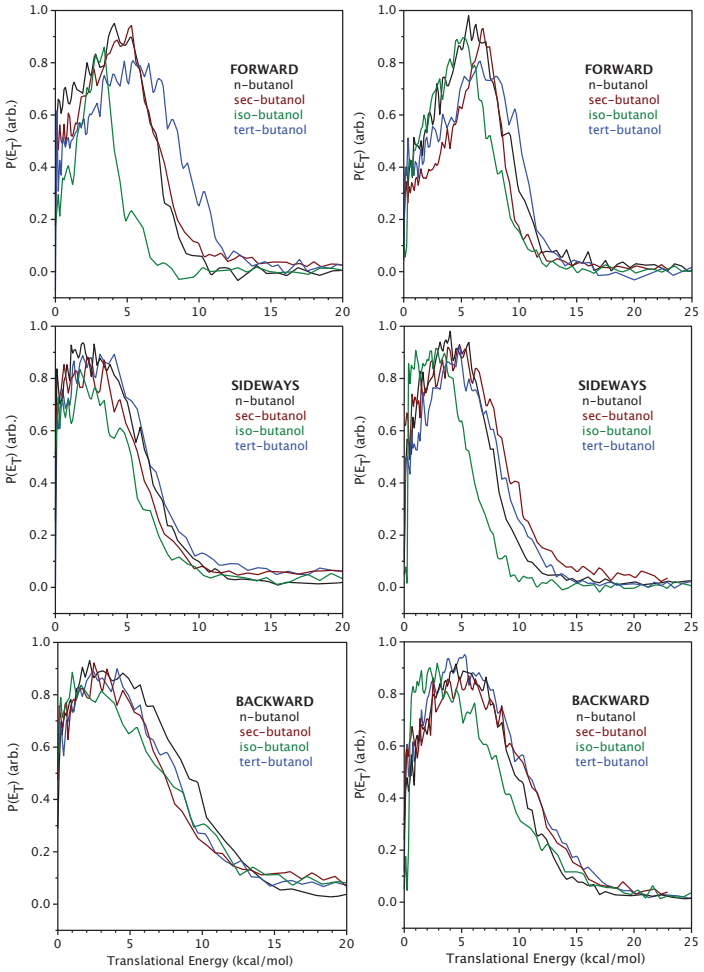

Figure 6.3: Angle-dependent translational energy distributions from more detailed analysis of images in Fig. 6.1. Left panel: low collision results, right panel: high collision energy results.

6.4 Discussion

A surprising result here is the similarity of the dynamics of the title reaction with that of Cl + pentane reaction as will be discussed here. One of the significant differences of Cl atom reactions with alcohols compared to alkanes is the degree of rotational excitation of the nascent HCl (v, J) products. It is rotationally cold in alkane while it is modestly rotationally excited in alcohol [11, 142] . This warmer HCl rotational distribution is ascribed to a dipolar interaction between HCl and the hydroxyalkyl moieties in the exit channel of the potential energy surface [142]. The difference in rotational distributions may suggest a marked con-

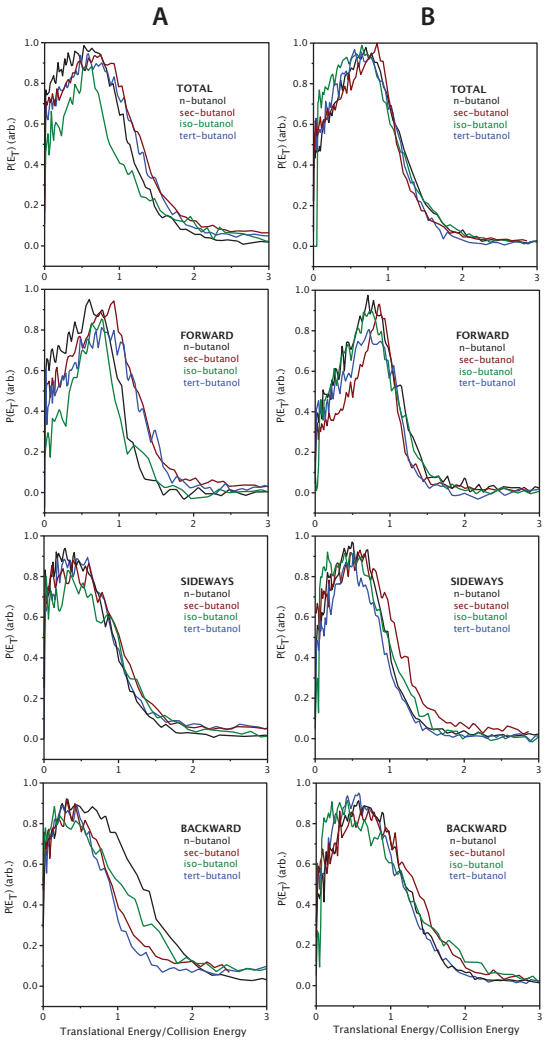

Figure 6.4: "Reduced" translational energy distributions highlighting tendency for translation to follow collision energy. Left panel: low collision energy results, right panel: high collision energy results.

trast in overall dynamics between saturated and oxygenated hydrocarbons towards reactions with chlorine atoms but may also prove otherwise. We first turn to the angular distributions shown in Figure 6.2B. At lower collision energy, the product flux are scattered on the backward direction with respect to the direction of the alcohol beam (0°). The product angular distribution shifted to forward distribution as the collision energy is increased. The absence of symmetric angular distributions supported the hypothesis of a direct or rebound dynamics at low collision energy as a result of low impact parameter collisions and stripping for high collision energy coupled to high impact parameter collisions. However, in the *ab*

Table 6.1: Most probable collision energy, E_C (kcal/mol), average translational energy release, $\langle E_T \rangle$(kcal/mol) in the different regions of the image for the subject reactions.

	E_C	$\langle E_T \rangle$total	$\langle E_T \rangle$forward	$\langle E_T \rangle$sideways	$\langle E_T \rangle$backward
n-butanol	6.8	5.8	4.0	4.1	5.5
	8.0	5.4	6.3	5.4	6.6
sec-butanol	5.7	4.7	4.9	4.7	5.2
	8.0	5.2	6.6	6.1	6.8
iso-butanol	5.3	4.2	4.0	3.1	4.8
	7.0	4.3	5.3	4.0	6.0
tert-butanol	7.0	5.8	6.2	6.0	6.3
	9.2	6.4	6.7	4.9	7.4

Table 6.2: Most probable collision energy, E_C (kcal/mol) and average reduced translational energy release, $\langle E_T \rangle^* = \langle E_T \rangle / E_C$ in the different regions of the image for the subject reactions.

	E_C	$\langle E_T \rangle$*total	$\langle E_T \rangle$*forward	$\langle E_T \rangle$*sideways	$\langle E_T \rangle$*backward
n-butanol	6.8	0.86	0.59	0.60	0.81
	8.0	0.68	0.79	0.68	0.83
sec-butanol	5.7	0.82	0.86	0.82	0.91
	8.0	0.65	0.83	0.76	0.85
iso-butanol	5.3	0.79	0.75	0.58	0.91
	7.0	0.61	0.76	0.57	0.86
tert-butanol	7.0	0.83	0.86	0.86	0.90
	9.2	0.70	0.73	0.53	0.80

initio MP2/6-311G** calculation of Garzon and coworkers [168], it was found out that the reaction of Cl + butanol proceed *via* molecular complexes appearing along the reaction pathway, with values 5.25 kcal/mol and 3.60 kcal/mol below the reactants for the pre-transition state and post-transition state complex, respectively. Conventional wisdom reasoned that for complex mediated reaction, the angular distribution is expected to be highly symmetric in the forward-backward regions or a highly isotropic distribution [132]. Although the current results show otherwise, a critical parameter influencing the dynamics is, of course, the collision energy. Global statements such as the reaction is complex-mediated (or direct) must be associated with a particular collision energy to be meaningful. Unfortunately these reactions at thermal energies or below have not yet examined .

This subtle difference in behavior of Cl + butanol is reminiscent to the previously observed distribution in Cl + smaller alcohols. *Ab initio* calculations for Cl + $CH_3OH \rightarrow$ HCl + CH_2OH characterize molecular complexes appearing in the potential energy surface suggesting pre-reactive complexes, however, these van der Walls and weak H-bonds wells are too shallow to allow reaction complexes to exist at the collision energies employed [142, 143]. In separate experimental investigations, Ahmed and co-workers [77, 78] found the reaction to be backward-sideways scattered suggesting direct rebound dynamics using single photon ionization as a product probe for the hydroxyalkyl radical at 8.7 kcal/mol collision energy. Bechtel and coworkers [144] revisited the reaction using co-expansion technique probing the nascent HCl (v, J) by 2 + 1 REMPI. Their findings suggest stripping mechanism for HCl (v = 1) and both stripping and rebound mechanism for HCl ($v = 0$) products. At 5.6 kcal/mol mean collision energy of Cl + CH_3OH, a state-to-state probing of HCl products showed propensity for forward scattering for $J = 2$, and more pronounced backward scattering for $J = 5$. These results provide additional support to the experimental findings for butanol isomers.

The question now is how to reconcile this experiment-theory discrepancy? One of the factors to consider is the issue of the stability of the complex formed in the reaction. The osculating complex model by Herschbach [140] postulated that the collision complex lifetime τ, has to survive of at least 5 times its rotational period τ_r, to qualify a reaction to be a long-lived complex-mediated mechanism. For a short-lived complex, the initial approach of the reactants is not scrambled causing the angular distribution, $I(\theta)$ to be asymmetric. One of the major problems in dealing with large polyatomic systems such as the case herein is the presence of stereoisomers that potentially blur the angular distributions. Although great success has been achieved in separating different conformers in unimolecular dissociation [172–175], studying its effects in full collision reactions remain a challenge [101]. For butanol alone, the presence of 14 stereoisomers with small differences in energetics [176, 177], in addition to the anisotropic shape of the molecule, foil the distribution as Cl atom approach

the butanol at all possible angles. It is however, noteworthy to mention that all rotational and vibrational levels of the hydroxyalkyl radical are ionized, *i. e.* universal detection. The angular distribution may show a forward-backward symmetry in a state-to-state probing of the nascent HCl (v, J) products at collision energy values near or at the collision energy in combustion engine just like the way the HCl rotational distribution is different in the two set of hydrocarbons. One of the problems in the current report is the inability to go to low collision energy especially for the n-butanol case.

A closer inspection of the translational energy distribution provides additional information in the reaction dynamics. Figure 6.2A shows the total translational energy distributions integrated over all angles. The distributions show to preserve the collision energy into product recoil as expected for a heavy-light-heavy reaction, where a heavy atom abstracts a light atom attached to another heavy atom [16, 178]. The translational energy distributions are scaled by dividing the distribution values by the collision energy and the plots are shown in Figure 6.4 and summarized in Table 6.1. At high collision energy, ∼70% of the product have $P(E_T)$ equal to or less than the collision energy. This fraction is smaller in the low collision energy. The translational energy for the forward scattered product can be predicted using the spectator-stripping model [179] where the departing HCl product has the same momentum as the approaching Cl atom: $(35/36)^2 \times E_C$. The values reported in Table 6.1 are significantly lower than the predicted value, *i. e.* 4.0 kcal/mol (experiment) against 6.5 kcal/mol (model) for the 6.8 kcal/mol collision energy for the Cl + n-butanol reaction, suggesting likely rotational excitation of the hydroxyalkyl radical. The forward distributions peak at ∼80% of the collision energy in sharp similarity with Cl + pentanes reaction [105]. The backward scattered peak, which results from the low-impact parameter collisions and collinear collisions, can be modeled by:

$$\langle E_C \rangle = E_C \cos^2 \beta + E_R \sin^2 \beta \tag{6.1a}$$

where β is the skew angle for the reaction, E_C is the collision energy, and E_R is the energy release in the reaction. Since the reaction considered here is a heavy-light-heavy reaction,

the second term of the equation above vanishes because the skew angle is highly acute, $\beta \sim 11.5°$. In all cases, the observed translational energy release for the backward scattered products are lower than the predicted value from the model of Evans *et. al* [110]. The disagreement can be due to the fact that this model works well for triatom systems and not for polyatomic molecules. Polyatomic systems possess several repositories for the excess energies: vibrations or rotation of the alkyl radical product are two of the possibilities. A Franck-Condon argument by Liu and Suits [75] for the reaction of $O(^3P)$ + butane, showed 4-5 kcal/mol for the relaxation energy of the alkyl radical from the transition state geometry is not available for product recoil. The sideways-scattered product resulting from intermediate impact parameter collisions, showed with consistency, the lowest average fraction of energy in translation (see Table 6.1). It is likely that in this case, there is efficient rotational excitation of the hydroxyalkyl radicals but with no compensating coupling of the exoergicity into recoil. The fraction of available energy appearing in translation is not reported because of the lack of scientific reports on the enthalpy of reactions for the different butanol isomers with chlorine atom.

As mentioned at the outset of this section, one puzzling aspect of the dynamics of the title reaction is its similarity to the pentane reaction with chlorine atom. The energies for the C-H bonds in pentane and butanol are very similar and the structures resemble each other with mass difference of only 2 amu. One key difference between the two is in the potential energy surface: Cl + pentanes appears to be a barrierless reaction and is significantly exoergic. For Cl + butanol reactions, a classical barrier of 1.34 kcal/mol has calculated for the most energetically favored pathway, *i. e.* H abstraction in the β-C position. Even with the presence of potential well in the Cl + butanol reaction, it is not "deep enough to cause long-lived complex to survive," [142, 144, 180] thus the direct mechanism observed in the crossed-beam experiments.

6.5 Conclusion

Understanding the chemistry of butanol and its isomers has attracted attention from the fields of theory and computation and experimental chemical kinetics following its importance in combustion. The first dynamics approach to this important molecular system is studied by crossed beam imaging of the hydroxyalkyl products generated from the reaction of chlorine atoms with butanol isomers. While the HCl product distributions for oxygenated hydrocarbons are markedly different from the HCl product distribution of saturated hydrocarbons, the results presented here for Cl + butanol isomers reaction showed similarity with that of Cl + pentanes. The product angular distribution showed backward scattering at low collision energy with enhanced forward scattering with respect to the alcohol beam with increased collision energy. The product translational energy distributions further support the similarity of these reactions. At high collision energy, a sharp peak of $\sim$80% of the collision energy is seen in the forward scattered products. The sideways-scattered product showed the lowest fraction of energy appearing in translation.

Chapter 7

Dynamics of CN + alkane reactions by crossed-beam dc slice imaging

7.1 Introduction

The CN radical is one of the simplest organic radicals and is a key intermediate in nitrogen bearing fuel combustion [181], in dense interstellar clouds [182–184], in comets, and in the atmosphere of the outer planets and their moons, notably Titan [185]. Due to the strong C-N bond (7.76 eV) and the large electron affinity [186], it is often considered a pseudohalogen, with similar high reactivity. It reacts with both saturated hydrocarbons except methane [187, 188] and unsaturated hydrocarbons without barriers. CN radical reactions are believed to be one way to produce long chain hydrocarbons and complex organic molecules in astrochemical environments and in combustion of nitrogen-rich fuels.

There are numerous kinetic studies of the reactions of CN radical with hydrogen [189–193] and hydrocarbons [187, 188, 194–200] with measurements spanning a temperature range from 25 to 1200 K. All literature data show the large rate coefficients and negative temperature dependencies for reactions of CN with unsaturated hydrocarbons. Investigations of CN radical reaction dynamics with unsaturated hydrocarbons have been reported by Kaiser and co-workers using crossed-molecular beams scattering. They examined the reactions of CN ($X^2\Sigma^+$) with C_2H_2 [139, 201], C_2H_4 [138], CH_3CCH [202], C_6H_6 [136], CH_3CCCH_3 [137], and other unsaturated hydrocarbons. All these experimental studies, combined with ab initio

calculations, showed that these reactions have no entrance barriers, complex forming reaction dynamics, and are initiated by addition of CN ($X^2\Sigma^+$) to the π electron density to give a long-lived intermediate. CN addition and H atom elimination is the main channel observed for these reactions.

The rate coefficients for CN + alkane reactions are smaller than for the reactions of CN ($X^2\Sigma^+$) with unsaturated hydrocarbons. Furthermore, they show an unusual temperature dependence, with the rate decreasing from nearly gas kinetic at 25 K, to a minimum at 200 K, and then increasing again with temperature. This has recently been ascribed by Georgievskii and Klippenstein [203] to the existence of a "submerged" transition state (TS) at close range which dominates the rate at high temperature, and an outer variational TS that governs the rate at low temperature. The former will show conventional Arrhenius behavior while the latter shows a decreasing rate with temperature. Although there are many studies on the reactions of CN ($X^2\Sigma^+$) with unsaturated hydrocarbons and kinetic studies of CN reactions with saturated hydrocarbons, to our knowledge, there have been no investigations at the microscopic level on CN ($X^2\Sigma^+$)+alkane reaction to date, despite their role in combustion processes. However, Che and Liu [204, 205] have reported crossed-beam studies of the related CN radical reaction with D_2. Their results, obtained using (1 + 1) resonance enhanced multiphoton ionization-time of flight mass spectrometry (REMPI-TOFMS) to detect the D atom products, yielded both the integral and differential cross sections for the reaction. They showed that the D atom products were backward scattered, which indicates that rebound dynamics is dominant in that reaction. The ratio of forward to sideways scattering decreased with increasing collision energy, implying that the stereodynamics might play a role in the reaction. Although, by analogy with Cl, for example, we suspect that hydrogen abstraction will be the dominant mechanism for the reactions of CN ($X^2\Sigma^+$) with hydrogen and saturated hydrocarbons, the reaction dynamics is as yet unknown.

Here, crossed-beam slice imaging studies of the reactions of CN ($X^2\Sigma^+$) with saturated hydrocarbons (n-butane, n-pentane, n-hexane, and cyclohexane) is reported . The product

alkyl radical images were obtained via single photon ionization at 157 nm.

7.2 Experiment

The experiments were carried out in a crossed-beam imaging apparatus described elsewhere [66, 78]. Briefly, The CN beam was generated by photodissociation of BrCN seeded in He (3%), using the 193 nm output of a ArF excimer laser (80 mJ, 10 Hz) at the nozzle of a piezoelectric pulsed valve. At this wavelength, essentially only the ground state of CN ($X^2\Sigma^+$) is produced. Previous photodissociation studies and other previous studies confirmed that only less than 6% CN ($X^2\Sigma^+$) radicals were vibrationally excited [206]. Although the nascent CN rotational distribution is highly excited, after entrainment in the supersonic expansion, most of the CN ($X^2\Sigma^+$) radicals are likely to be rotationally cooled. It should be noted, however, that no measurement of the rotational distributions was performed and there could be some residual rotationally excited CN present.

Target alkane molecules were seeded in hydrogen or helium in order to vary the collision energy. These two molecular beams are generated by expanding from a piezoelectric pulsed valve having a 1 mm orifice into differently pumped source chambers. After passing through collimating skimmers, 2 and 1 mm skimmers for the CN ($X^2\Sigma^+$) beam and alkane beams, respectively, the two beams cross at an angle of 90° in the main chamber. The backing pressures were typically 1.0 bar for both the BrCN beam and alkane beam. For the gas sample butane, the backing pressure was increased up to 5.0 bars. The collision energy was 7.5±0.5 kcal/mol for all the reactions except butane. For this case, the experiments are extended to high collision energy, 10.8 kcal/mol. The typical spread in the collision energy was 8% full width at half maximum or better. The operating pressures were maintained at $\sim 10^{-5}$ torr in the source chambers and at $\leq 2\times 10^{-7}$ torr in the main chamber.

The alkyl products were detected with 157 nm vacuum ultraviolet soft ionization [38, 73, 77, 207]. In the experiments, the power of the 157 nm laser is ∼0.6 mJ/pulse with loose focusing in the chamber, which avoids multiphoton ionization process. The dc slice imaging

detection scheme and megapixel acquisition program IMACQ were used to accumulate the raw images. The detector is a 75 mm diameter dual microchannel plate (MCP) coupled to a fast phosphor screen held at 5 kV (Burle Electro-Optics). The front of the MCP assembly was held at ground potential and the back plate was pulsed to gate the central slice of the reaction products at a specific mass by application of a high voltage pulse (+2.2 kV/+1 kV bias, 60 ns width) using a commercial pulser (DEI PVX-4140). The timing of pulsed molecular beam nozzles, firing of photolysis and probe lasers, and detector gate pulse was controlled using a delay generator (BNC 555). The resulting image was then recorded using a charge coupled device camera (Mintron 2821e, 512×480 pixels). Accumulation of the image took about 1-4 h to reach a satisfactory signal to noise ratio.

7.3 Results

Images for reaction of CN with n-butane are shown in Fig. 7.1. Although 157 nm provides a sensitive universal probe for C3 and higher alkyl radical reaction products, one shortcoming is that photochemistry of the parent hydrocarbon at 157 nm also gives the radical, which can then be detected as well. This gives rise to a photochemical background signal centered at the hydrocarbon beam. If the reactive signal is strong enough relative to the background, as seen in Fig. 7.1A for reaction with n-butane at 10.8 kcal/mol, then the photochemistry signal can be subtracted to get information on scattering in the forward direction, albeit with lower signal-to-noise ratio and larger inherent uncertainty. In many cases shown here, however, the photochemical background is too large to allow for reliable subtraction. In that case, the forward scattered portion of the image is suppressed and results for the region of interference are not reported.

Figure 7.1 shows the typical raw images of butyl radical reaction products with the background subtracted. These are images obtained from the CN ($X^2\Sigma^+$) + C_4H_{10} reaction at the collision energies of 10.8 and 7.5 kcal/mol, respectively. In crossed molecular beams experiments, the fast products in the laboratory frame can fly away and low speed products

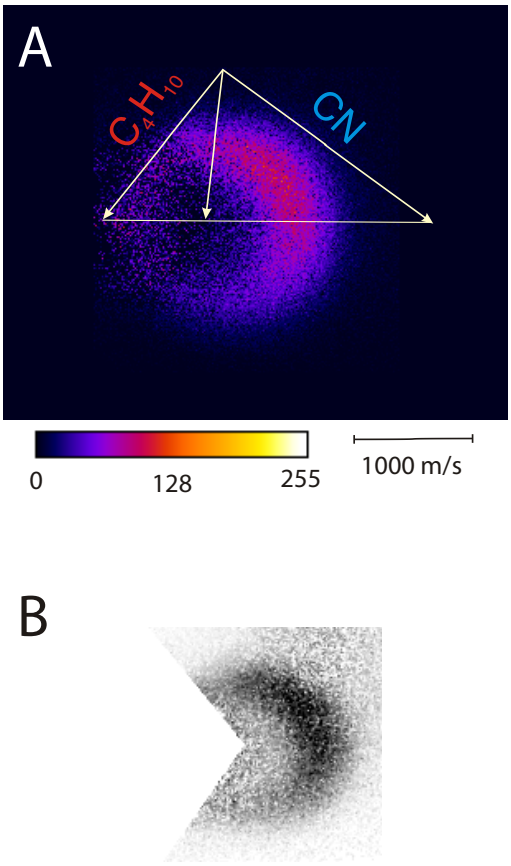

Figure 7.1: Raw images of butyl product from reactions of CN ($X^2\Sigma^+$) with butane at a collision energy of (a) 10.8 kcal/mol and (b) 7.5 kcal/mol. The Newton diagram is imposed on the image at 10.8 kcal/mol collision energy.

will remain in the detection region and can accumulate. The slower products thus have higher detection efficiency. The raw images show some asymmetry across the relative velocity vector arising from this effect, although it is clear that this number density to flux correction is not large in this case. The effect is accounted for in the analysis, as described elsewhere [105, 106]. After doing background subtraction and the density-to-flux correction, the translational energy and angular distributions are derived from the alkyl images directly. Figure 7.2 shows the angular distributions of the CN ($X^2\Sigma^+$) + C_4H_{10} reaction obtained from the images shown in Figure 7.1. At the higher collision energy, the angular distributions show flux in all direction, but with a clear preference for backward scattering with respect to the alkane beam, and a nearly monotonic decrease to the forward direction. The results

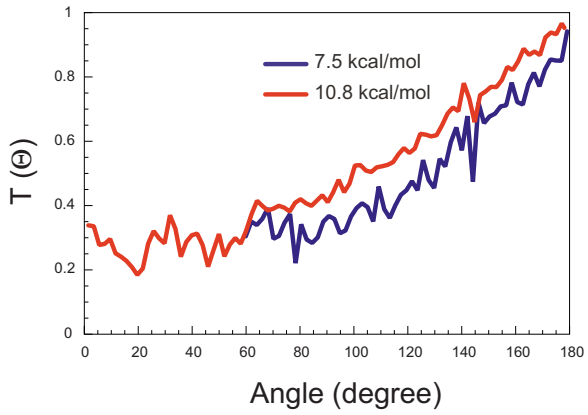

Figure 7.2: Total angular distributions for reactions of CN ($X^2\Sigma^+$) with butane.

at the lower collision energy for the region from 60° to 180° show no significant changes from the higher collision energy case. The translational energy distributions are shown in Fig. 7.3. Both of them peak at ∼20% of the available energy. For the high collision energy butane results, the translational energy distributions for the forward and backward scattered portion of the distribution are plotted separately. It can be seen that the forward scattered component has a peak at slightly higher translational energy release. The detailed energy release data is compiled in Table 7.1.

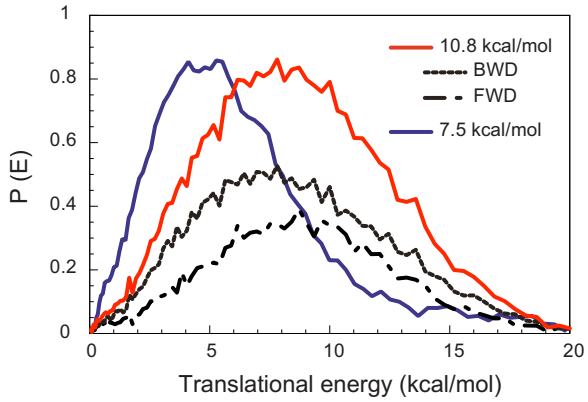

Figure 7.3: Translational energy distributions for reactions of CN ($X^2\Sigma^+$) with butane at 10.8 and 7.5 kcal/mol. For 10.8 kcal/mol collision energy: red solid line, total translational energy distribution; black dotted line, backward scattered; black dot-dashed line, forward scattered. The blue solid line shows the total translational energy distribution at a collision energy of 7.5 kcal/mol.

In order to gain insight into the dynamics of primary hydrogen atom abstraction and

other issues, reactions of CN ($X^2\Sigma^+$) with a series of other alkane molecules are also studied at the same 7.5 kcal/mol collision energy. The raw images are shown in Fig. 7.4, while Fig. 7.5 shows the angular distributions derived from the images. Results were obtained for reaction with butane, pentane, hexane, and cyclohexane. All the angular distributions are similar. Indeed, they all show preferential backward scattering. Although these results are blind to the region forward of 60°, the angular distributions all show a decrease from 90° to 60° and a marked forward-backward asymmetry. Guided by the high collision energy butane results, and for additional reasons discussed below, the forward scattered contribution is at most quite modest. For the reaction with cyclohexane, an even broader angular distribution is obvious than the other reactants. Figure 7.6 shows the translational energy distributions for these reactions.

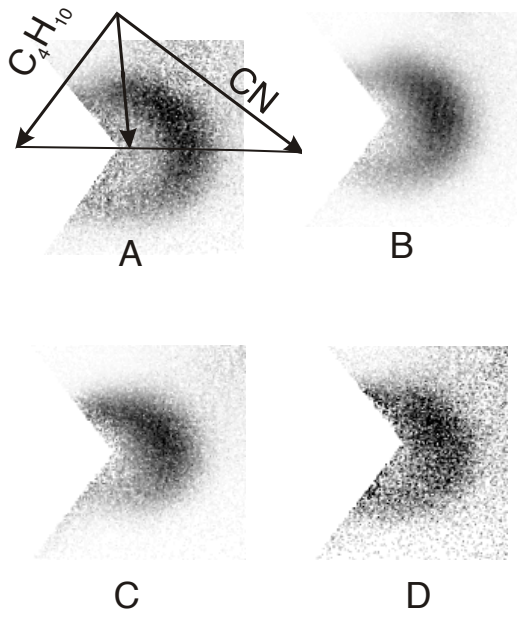

Figure 7.4: Raw images of alkyl radical product from reactions of CN ($X^2\Sigma^+$) with alkane reagents at a collision energy of 7.5 kcal/mol: (a) butane, (b) pentane, (c) hexane, and (d) cyclohexane. The Newton diagram is imposed on the butane image.

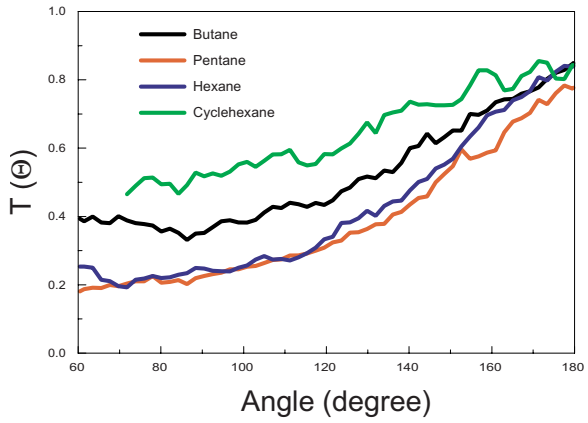

Figure 7.5: Total angular distributions of reactions of CN ($X^2\Sigma^+$) with indicated alkane reagents.

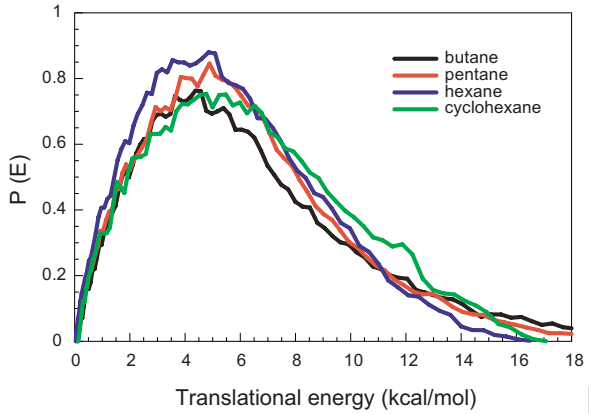

[h]

Figure 7.6: Total translational energy distributions of reactions of CN ($X^2\Sigma^+$) with indicated alkane reagents.

7.4 Discussion

These results are the first to study the detailed reaction dynamics of CN ($X^2\Sigma^+$) with alkane molecules, but they may be compared to related halogen atom [11, 62, 63, 75, 208–210] and oxygen atom [75, 91, 92, 211–214] reactions for which a growing body of detailed work now exists. Consider the similarities and differences among these reactions. For X + C_2H_6 → HX + C_2H_5, the exoergicity decreases in the order X = F>CN>Cl>O, with 0 K ΔH_R values of -39.1, -28.1, -5.95, and -5.49 kcal/mol, respectively. For F, Cl, and CN reactions, the barrier is close to zero; for F and Cl, it may be slightly positive, while high level calculations for the CN reaction find it slightly below zero, consistent with the

Table 7.1: Collision energy and translational energy release for indicated reactions (kcal/mol). E_C is the collision energy, E_{avail} is the total available energy, $\langle E \rangle$ is the average translational energy release, and f_t is the fraction of the total available energy appearing in translational.

Alkane	E_C(kcal/mol)	E_{avail}	$\langle E \rangle$	f_t
Butane	10.8	36.0	8.8	0.24
	7.5	32.7	5.0	0.15
Pentane	7.7	33.6	4.6	0.14
Hexane	7.9		5.2	
Cyclohexane	7.1	35.4	6.3	0.18

Table 7.2: Energy partitioning of CN ($X^2\Sigma^+$) + C_4H_{10} reaction at 10.8 kcal/mol.

E_C(kcal/mol)	E_{avail}	$\langle E \rangle_{fwd}$	$\langle E \rangle_{bwd}$	f_{fwd}	f_{bwd}
10.8	63.0	9.0	8.6	0.25	0.24

fast reaction seen at 25 K [203]. For O(^{3}P) reaction, there is a sizable barrier of about 8 kcal/mol, which has a profound effect on primary versus secondary H atom abstraction rates, as the final product energies and barrier heights are lower by ∼2 kcal/mol for secondary H atom abstraction.

For both F and CN, the barrier, such as it is, is an early one, so that the HX product is likely to be formed with substantial vibrational excitation. In unique crossed-beam studies of the F atom reaction with ethane using a high resolution IR absorption probe, Whitney *et al*. [208] found product HF vibrational populations of 0.28:0.43:0.12:0.17 for v = 3:2:1:0. For the CN reaction, the TS structure calculated by Georgievskii and Klippenstein [203] shows the C-H bond stretched to 1.8 Å(about 75% beyond the equilibrium distance), significantly longer than the 1.4 Å(53% beyond r_e) reported for the F-C_2H_6 TS by Bottoni and Poggi [209]. It can thus be anticipated perhaps even greater vibrational excitation in HCN than in HF. Clearly, the bulk of the exoergicity of the reaction is deposited into the new H-CN bond. For Cl and O abstraction of primary H atoms, the barrier is not early, and vibrational excitation in the HX product is minimal. One key finding of the classic O + alkane studies of Andresen and Luntz [91, 92] is that the barrier moves toward reagents for secondary

and tertiary H abstraction, so that vibrational excitation in the new bond increases in this progression. The same is likely true for the Cl case, but this is less likely to be important for CN, with a very early barrier even for primary H abstraction.

With these issues in mind, the translational energy distribution is examined. These are consistently broad but do not extend to the limit of the available energy. This is consistent with the minimal HCN $v = 0$ products expected. Approximately 15%-20% of the available energy in translation of the products, implying more than 1 eV internal energy distributed between HCN and the alkyl radical. The distributions show an average translational energy release typically about 2/3 the value of the collision energy, except for the cyclohexane case in which it is nearly 90%. This can be compared to the O or Cl reactions, which can be understood using a simple kinematic picture such as that suggested by Evans *et al* [110]. In this model, the average translational energy release is given by

$$\langle E_C \rangle = E_C \cos^2 \beta + E_R \sin^2 \beta \tag{7.1a}$$

where β is the skew angle for the reaction, E_C is the collision energy, and E_R is the energy release in the reaction. This is essentially a linear triatomic model, and the remaining energy is then allotted to vibrational excitation of the new bond. This picture provides a rough limiting view of the behavior of some aspects of the Cl and O+alkane reactions, particularly if modified to account for relaxation of the alkyl radical from the transition state geometry. Typically, for all of these heavy-light-heavy hydrogen transfer reactions, the skew angle is acute and the first term dominates, so that the translational energy of the reaction is well conserved; for the CN reactions considered here, $\cos^2 \beta$ is $\sim$0.95. This further implies that 95% of the substantial exoergicity is to be found in the new HCN bond. However, this model also implies that the average translational energy release should be larger than the collision energy, on the order of 8.5 kcal/mol for the nominal 7.5 kcal/mol collision energies, and 11.6 kcal/mol for the high collision energy butane case. Instead, the results are significantly less: The values cluster around 60% of the model prediction except for the case of cyclohexane, for which it is 80%. There are two likely possible repositories of this excess energy that are

not included in the kinematic model: vibration or rotation of the alkyl radical product. A Franck-Condon argument has been proposed to account for some of this: The relaxation energy of the hydrocarbon radical from the transition state geometry, typically on the order of 4-5 kcal/mol, will not be available for recoil [75]. The results are largely consistent with this picture. On the other hand, there is likely to be considerable rotational excitation of the alkyl radical product. This has been accounted for in a hybrid Franck-Condon/impulsive treatment in analysis of the F + ethane work from Whitney *et al.* [208]. It would be difficult to implement the same approach here because there is a mixture of abstraction sites with varying impact parameters and lever arms. Further detailed study will be necessary to disentangle the precise partitioning of energy between alkyl radical vibration and rotation.

A complication in these experiments arises owing to the nature of the 157 nm probe. There are both primary and secondary CH bonds involved in these reactions, except for the case of cyclohexane, in which all H atoms are secondary. The secondary H atoms are generally more reactive as the saddle points are lower in energy, but for the CN reactions, all H atoms will be reactive targets. However, the 7.9 eV probe is nominally below the reported values for the ionization energy of the 1-butyl radical: 8.02 eV (adiabatic) and 8.5 eV (vertical). It is thus not immediately clear in the butane case if we are selecting a subset of the reaction products, i.e., the 2-butyl radicals. To gain some insight into the relative sensitivity to 1-butyl and 2-butyl radicals, a preliminary investigation of the photodissociation of 2-methylhexane and 2,3-dimethylpentane at 157 nm have been performed [85]. These both will give isopropyl radical and butyl radicals as primary products, with 1-butyl in the former case and 2-butyl in the latter. Using the isopropyl signals to scale them, the relative sensitivity is found to be 1:0.64 for 2-butyl versus 1-butyl ionization at 157 nm. This implies that both radical products are detected, though probably not with equal sensitivity. Moreover, this is consistent with the observation that the butane signals are not at all weaker than for the pentane or hexane reactions, and for these we should certainly be above the ionization energy for any radical product. It may be that the density of Rydberg states at this energy allows for efficient 1 +

1 ionization, and this may also preclude any strong tendency for a vibrational dependence of the detection probability.

The angular distributions for these reactions, as discussed in the preceding section, show broad backward scattering clearly implying direct dynamics. Although in most cases here the most forward scattered part of the distribution is truncated, in the one instance where it is clear, no evidence of forward peaking is seen. This is perhaps a bit surprising. It is similar to the O(^{3}P) + alkane results [75, 211, 212] but very different from the widely studied Cl + alkane reactions. Even for Cl + ethane, with only primary H atoms, broad angular distributions are seen with both forward and backward peaking components [66]. Bass *et al.* [110] and Retail *et al.* have reported that Cl reaction with butane shows a similar broad angular distribution, while Cl + tetramethylsilane shows primarily backscattering [215]. The calculated TS for CN + ethane indicated possibly a submerged saddle point, and this is even more likely for the secondary H abstraction cases. Nevertheless, this may constrain reaction to a near collinear C-H-CN geometry. However, it remains somewhat puzzling that the CN angular distributions resemble those of O(^{3}P), with the highest barrier, while the Cl reactions often show very broad angular distributions.

It is clear that the kinetic energy and the angular distribution are somewhat coupled. The reaction products have broader translational energy distributions in the backward direction than in the forward direction. Due to interference from the photochemistry background in the forward direction, we only give the average translational energy $\langle E \rangle$ at the lower collision energy, as shown in Table 7.1. However, the coupling is clear at the higher collision energy (10.8 kcal/mol) for the reaction of CN ($X^2\Sigma^+$) with butane. The translational energy spectra of forward (0°-90°) and backward (90°-180°) scattering were obtained by integrating the signal in these regions, as shown in Fig. 7.3. All results show a significant fraction of available energy in the internal excitation of either the alkyl radical or HCN or both regardless which alkane reagent is used. As discussed above, the bulk of the internal energy is almost certainly to be found in the new HCN bond, with only modest excitation of the

alkyl radical product likely. Secondary decomposition of the radical products is thus not likely, and no lower mass products were detected from these reactions. For the reaction of CN ($X^2\Sigma^+$) with butane at collision energy of 10.8 kcal/mol, the results show a broad distribution and peaking at lower translational energy for the backward scattering. The average translational energy and energy partitioning were calculated and listed in Table 7.2.

One additional point merits some comment. It is noted in the introduction of this chapter that these reactions are believed to be barrierless, with a rate that has a minimum at ~200 K but rises both to higher and lower temperature, while the results here clearly show direct dynamics. However, the results, at collision energies of 7-10 kcal/mol, clearly address the dynamics at the high energy domain of the kinetics studies, and the conclusions should not be directly extrapolated to very low energies.

7.5 Conclusion

Crossed molecular beam technique combined with dc sliced ion imaging have been used to investigate the reaction of CN ($X^2\Sigma^+$) with several target alkane molecules at collision energies of 7.5 and 10.8 kcal/mol. Center-of-mass translational energy and angular distributions were directly obtained from the experiments. The results are consistent with very high vibrational excitation of HCN as the early barrier results in reaction at extremely stretched NC-H distances. Simple models are used to suggest that structure in the alkyl radicals plays an important role in the energy disposal, although the precise partitioning of rotational and vibrational energy in the alkyl product is not yet clear.

Chapter 8

Crossed-beam imaging of the H abstraction channel in the reaction of CN with 1-Pentene

8.1 Introduction

The cyano radical ($CN(X^2\Sigma^+)$) is an extremely reactive species that can abstract hydrogen from saturated hydrocarbons without a barrier and add to bonds of unsaturated hydrocarbons to form strongly bound intermediates also without a barrier. These may then be stabilized by collision or decay through a variety of pathways, predominantly via atomic hydrogen or alkyl radical elimination, forming nitriles. Owing to its ability to react without barriers and its relative abundance in the atmosphere of Titan, the cyano radical plays a key role in the low-temperature chemistry on Titan, including hydrocarbon growth processes and nitrogen incorporation into the haze particles that are a dominant feature of its atmosphere [216–218].

Cyano radical reactions with unsaturated hydrocarbons have been examined in a variety of kinetics studies, including some using supersonic flows at temperatures down to 20 K [187, 219, 220]. The reaction rates are found to be extremely fast and show a negative temperature dependence, with rates of $2.5 \pm 0.2 \times 10^{-10}$ cm^3 molecule^{-1} s^{-1} reported for the reaction of cyano with ethylene at 298 K [221]. Two recent kinetics studies are particularly noteworthy in that products were detected for reaction with propene. The Seakins group

[222] at Leeds detected H atom elimination following CN addition and determined absolute yields for this channel; then, they compared these to a master equation calculation using a model potential surface. Trevitt *et al.* [223] also studied the CN + propene reaction in a flow reactor using tunable synchrotron radiation to obtain isomer-specific detection of products. They detected H and CH_3 elimination and identified distinct product isomers but saw no evidence for formation of the allyl radical when the ionization energy was tuned above the threshold for detection of allyl but below that for ionization of other products. In addition to these kinetic studies, a number of crossed-beam studies for cyano radical plus unsaturated hydrocarbons have been reported, notably from the Kaiser laboratory [138, 224]. Also, Huang *et al.* [225] used *ab initio* theory at the CBS-CCSD(T) level to examine the possible product channels for crossed beam results at a detailed level for this reaction. They found slight barriers to H abstraction but acknowledged that these may disappear at higher levels of theory. Gannon *et al.* [222] used an IRC search at the UMP2/6-311+G(d,p) level and concluded there was no barrier. In any case, the traditional crossed-beam approach has little sensitivity to the abstraction reaction, owing to unfavorable kinematics and background at the product masses; therefore, this pathway has often been omitted in the analysis.

8.2 Experiment

In the crossed-beam DC slice imaging approach [14, 66, 105], a beam of photolytically prepared radicals are crossed with a beam of the target reactant in a vacuum chamber and detect the radical products by single-photon ionization using a compact 157 nm excimer laser. Owing to the limited photon energy of the probe (7.9 eV), the detection is largely confined to C4 and larger radical products. The relevant slice of the detected product is imaged directly, which is then readily converted into the velocity-flux contour map that embodies the reaction dynamics. Cyano radicals are prepared by 193 nm photolysis of cyanogen (Apogee Technology, 98.5%), [77, 115] after which it is entrained in the helium carrier gas. The target reactant, 1-pentene (Sigma-Aldrich, 98%) is seeded in various carrier

gases (He, H_2) chosen to give the collision energy of interest. As seen in some cases in the past, 157 nm photolysis of the 1-pentene also gives the product radical, which is then also detected. This gives an interfering signal centered at the pentene beam velocity that, for these reactions, precludes determination of the reactive scattering within 60° of the beam direction.

8.3 Results

Crossed-beam slice imaging [14, 18, 20] with single-photon ionization at 157 nm is a sensitive and direct probe of bimolecular reactive scattering for a variety of reactions [75, 77, 78]. Earlier studies on cyano radical reaction with n-alkanes have been reported [79] and recently the Suits group embarked on systematic studies of chlorine atoms with alkanes [105] and alkenes [106].

In the present study, the reaction between the cyano radical and 1-pentene at four collision energies from 5 to 9 kcal/mol is investigated. The sliced images of the C_5H_9 radical, corrected for the density-to-flux effects [105, 106], are shown in Figure 8.1 with the most probable Newton diagrams superimposed. As discussed in the Section 8.2, the photochemistry background interferes in the vicinity of the pentene beam, so that portion of the image is suppressed. From these images, the center-of-mass translational energy and angular distributions is shown in Figure 8.2. The translational energy distributions are given separately for the sideways (60°-120°) and backwards (120°-180°) portions of the scattering distributions. Neglecting the undetected forward-scattered part of the distribution, the angular distributions are isotropic at all collision energies studied. The translational energy distributions peak near zero, despite very large exoergicity for some of the HCN-forming channels, as shown in Figure 8.3. This figure gives 0 K reaction enthalpies for H abstraction by CN based on CBS-QB3 [103, 104] calculations of the bond dissociation energies given in Ref 105. The average translational energy release is given in Figure 8.2, but the fraction of available energy is not shown because, as shown in Figure 8.3, this depends very strongly on the particular H

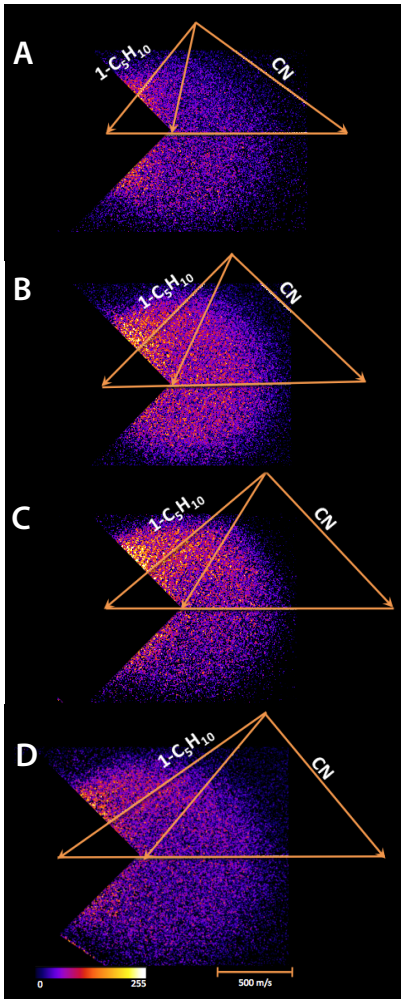

Figure 8.1: DC sliced images of pentenyl radical product from reactions of CN($X^2\Sigma^+$) with 1-pentene at different collision energies and superimposed Newton diagrams. (A) 5.1, (B) 6.0, (C) 7.3, and (D) 9.2 kcal/mol.

atom that is abstracted. It is, in any case, likely that the products are highly vibrationally excited, in particular, the HCN product, as has been seen in CN + alkane reactions [194].

8.4 Discussion

The present results unambiguously show the occurrence of hydrogen abstraction in the CN + 1-pentene reaction. The isotropic angular distributions and relatively low kinetic energy release are consistent with complex formation, as is the similarity between the sideways- and backwards-scattered translational energy distributions. This is the generally assumed

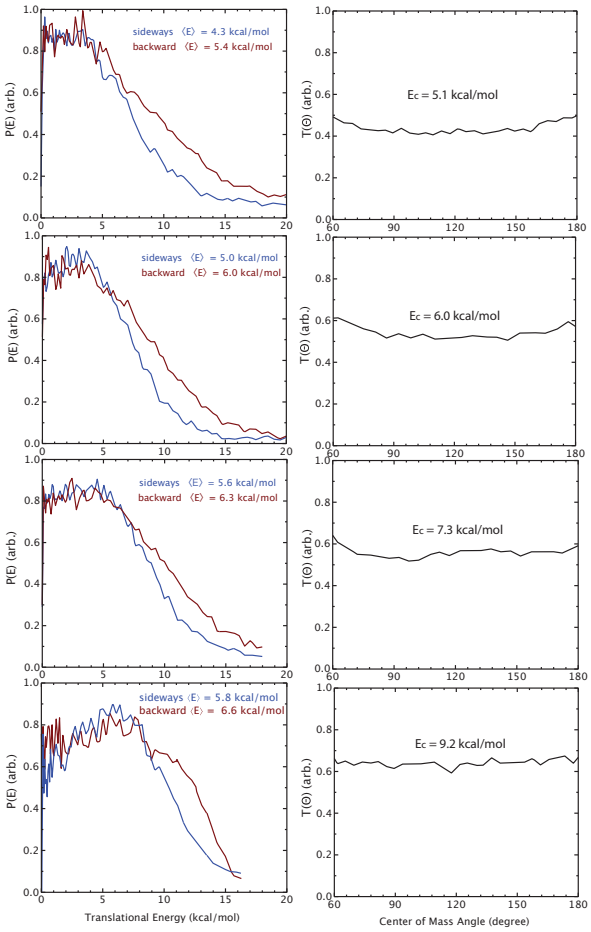

Figure 8.2: Left side: Center-of-mass translational energy distributions at the sideways (60°-120°) and backwards (120°-180°) regions and the average translational energy release at each region. Right side: Center-of-mass angular distributions at indicated collision energies.

entrance path for these reactions given the very high reaction rates, negative temperature dependence, and relatively stable addition complex. It is roughly estimated the yield of the product radical in this reaction relative to that of the C_5H_{11} radical in reaction of CN with n-pentane. On the basis of total integrated image intensities for a comparable acquisition time, the yields are roughly the same, within experimental uncertainties of at least ±25%, owing to possible differences in beam intensities, ionization cross sections, and so forth. The room-temperature rate for the reaction of CN with n-pentane is 1.6×10^{-10} cm^3 molecule^{-1} s^{-1} [197]. This reaction only gives rise to H abstraction. At the time of writing this dissertation, no literature report on the rate determination for CN + 1-pentene has been reported,

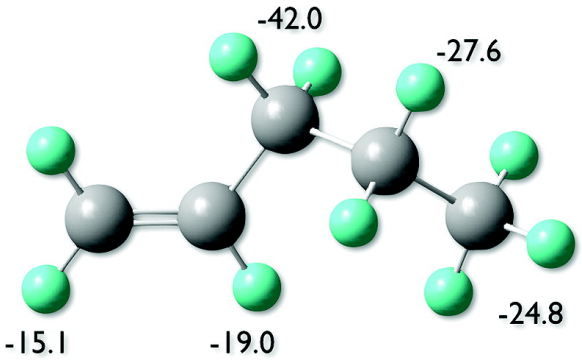

Figure 8.3: Structure of 1-pentene with 0 K reaction enthalpies (kcal/mol) for H abstraction by CN at indicated carbon atoms.

but Gannon *et al.* [222] give the rate for 2-butene at room temperature as 2.93 $\times$ 10^{-10} cm^3 $molecule^{-1}$ s^{-1}, and we suspect that for 1-pentene will be similar. At 5 kcal/mol, much above room temperature, the pentane rate will likely increase, and the pentene rate will likely decrease. By using the room-temperature rates to estimate the branching for HCN production, a lower bound can thus be calculated. On this basis, it is estimated that the branching to H abstraction in reaction of CN with 1-pentene to be 1.6/2.93, or about 50%. Although there are many approximations and uncertainties in this determination, the HCN production is probably not a minor channel.

A key question is whether this may occur in smaller systems such as propene or propyne that possess similar strongly exoergic channels giving rise to the resonantly stabilized allyl and propargyl radicals, respectively. Gannon et al. [222] examined this question indirectly in the kinetic study of CN + propene mentioned previously. They calculated barriers for isomerization of the addition complex and its dissociation giving H or CH_3. The surface included a barrierless abstraction channel forming HCN and the allyl radical, the most exoergic reaction pathway, but this was not included in the master equation modeling, owing to the difficulty of treating the barrierless process. They found that methyl loss branching slightly exceeds H loss under all conditions. They obtained satisfactory agreement with the experimental results for H atom yield and concluded that the calculations "support but cannot confirm the absence of a direct channel." Trevitt and co-workers [223] also

studied the CN + propene reaction with direct vacuum ultraviolet probe of the products using a time-resolved multiplexed mass spectrometer coupled to a flow reactor at 5 Torr. Most relevant to the results presented here was their failure to detect the allyl radical, despite attempts to probe this species directly at a photoionization energy of 9.68 eV. This energy was chosen, just below the ionization onset for propene, to eliminate interference from propene itself. They concluded that the branching must be less than 2%. The obvious explanation for the absence of the H abstraction channel in the propene study despite what is seen in pentene is that these are two different systems with different dynamics and reaction pathways. Given the similar energetics for these two systems, the present results suggest that it may be worthwhile to attempt more theoretical and experimental investigations to unravel the origin of this distinct behavior.

This similarities between the cyano radical plus alkene reactions and those for chlorine atoms with alkenes, which were studied in some detail recently, [106] warrant some discussion. The angular distribution that is observed here is consistent, over the detected angular range, with the results for the analogous chlorine plus alkene reactions [106]. In the latter reactions, however, it manifested a sharp forward-scattered peak that rose with collision energy, accounting for 3% of the scattered flux at 4 kcal/mol and 11% at 7 kcal/mol. Furthermore, for the Cl reaction, this collision-energy-dependent forward-scattered flux has a distinct translational energy distribution. As it strongly resembles the translational energy distribution for the forward scattering in Cl + alkane reactions, it is associated with abstraction of the alkyl H atoms in pentene and hexene, rather than the allylic H atoms. Unfortunately, the current results are blind to this portion of the angular distribution in the CN + pentene experiments; therefore, it cannot be determined whether a similar direct component is present. On the other hand, this feature in the Cl reactions only became significant at high collision energy; therefore, it is unlikely to be relevant to Titan.

Chapter 9

Conclusions and Prospectus

The single-photon ionization technique provides a sensitive approach in studying the global dynamics of chlorine atom and cyano radical reactions with hydrocarbons. The alkyl radicals probed in these reactions reveal an identifying mark unique for each system. In the case of Cl + pentane isomers, the nature of the abstraction site has little influence on the dynamics as seen in the similarity of the scattering results. For the selectively deuterated butane, the angular distributions for primary and secondary abstraction are surprisingly similar. The only difference can be seen in the translational energy distributions. This is likely owing to the relatively high collision energy employed; future studies will examine a lower temperature regime where greater sensitivity to the distinct reactive sites can be studied in great detail. Chlorine reactions with alkenes showed interesting dynamics as the collision energy increased, revealing both a complex addition-elimination component and a direct abstraction reaction. A detailed state-resolved detection of the nascent HCl ($v = 0, 1$; J) products is foreseen to completely disentangle the individual contributions of the various reaction pathways.

A variety of CN($X^2\Sigma^+$) radical reaction with polyatomic hydrocarbons is a rich field to tackle owing to the many competing pathways of the reaction. Given the right precursor for CN($X^2\Sigma^+$) radicals, an improved signal to noise ratio can be achieved that will therefore allow full extraction of the translational energy and angular distributions in full angular range. Nitrogen chemistry on Titan is an area of active investigation with a number of

puzzling aspects. In the reaction of CN($X^2\Sigma^+$) with unsaturated hydrocarbons, the HCN vertical distribution is not well-reproduced by photochemical models, and an extra sink term has been incorporated in several of them to account for this [226]. A significant additional source of HCN would increase this discrepancy. There is also uncertainty about the contribution of nitrogen-containing radicals in the lower stratosphere produced by cosmic rays [227]. The branching in the subject reactions between nitrogen incorporation and chain lengthening versus HCN production along with resonantly stabilized radicals can have a significant impact on models, and further investigation is clearly warranted. A new model to help experimentalist to account for polyatomic molecular systems is also needed.

The field of molecular reaction dynamics, however not new, has been an integral field in understanding numerous reactions relevant to several environments as well as to fundamental theoretical understanding. The efforts put forth by the pioneers of this field have brought our understanding of how chemical reactions occur to an unprecedented level of detail especially in the atom + diatom systems. One key goal for chemical dynamics studies now is to extend the insights learned in the A + BC type reactions to a large variety of polyatomic systems and properties. As illustrated by several research groups, including the Suits group, the products of chemical reactions can now be imaged directly as soon as they exit the interaction region rather than imagining the process. While considerable progress has been achieved on the use of time-of-flight mass spectrometric detection in studying a variety of crossed-beam reactions, ion-imaging methods are still not widely exploited in this area. There are still uncharted territories where the capability of ion imaging can be brought to the fore. For one, reactions of chlorine atoms with long chain alcohols are important in combustion industry in the continued effort to provide a cleaner and efficient fuel. Another area where crossed-beam imaging technique can be used is in the challenging radical-radical reactions. These are fundamental reactions that are ubiquitous in the atmospheric and interstellar environments.

BIBLIOGRAPHY

[1] Dudley R. Herschbach. Molecular dynamics of elementary chemical reactions (Nobel Lecture). *Angewandte Chemie International Edition in English*, 26(12):1221–1243, 1987.

[2] Yuan Tseh Lee. Molecular beam studies of elementary chemical processes. *Science*, 236:793–798, 1987.

[3] John C. Polanyi. Some concepts in reaction dynamics. *Science*, 236:680–690, 1987.

[4] R. I. Kaiser and N. Balucani. The formation of nitriles in hydrocarbon-rich atmospheres of planets and their satellites: Laboratory investigations by the crossed molecular beam technique. *Accounts of Chemical Research*, 34(9):699–706, 2001.

[5] X. Gu and R. I. Kaiser. Reaction dynamics of phenyl radicals in extreme environments: A crossed molecular beam study. *Accounts of Chemical Research*, 42(2):290–302, 2009.

[6] J. J. Lin. Dynamics of reactions between two closed-shell molecules. *Physical Chemistry Chemical Physics*, 13:19206–19213, 2011.

[7] N. Balucani. Elementary reactions and their role in gas-phase prebiotic chemistry. *International Journal of Molecular Sciences*, 10(5):2304–2335, 2009.

[8] P. Casavecchia, F. Leonori, N. Balucani, R. Petrucci, G. Capozza, and E. Segoloni. Probing the dynamics of polyatomic multichannel elementary reactions by crossed molecular beam experiments with soft electron-ionization mass spectrometric detection. *Physical Chemistry Chemical Physics*, 11:46–65, 2009.

[9] X. Yang. State-to-state dynamics of elementary bimolecular reactions. *Annual Review of Physical Chemistry*, 58(1):433–459, 2007.

[10] Xueming Yang. Probing state-to-state reaction dynamics using H-atom Rydberg tagging time-of-flight spectroscopy. *Physical Chemistry Chemical Physics*, 13:8112–8121, 2011.

[11] C. Murray and A. J. Orr-Ewing. The dynamics of chlorine-atom reactions with polyatomic organic molecules. *International Reviews in Physical Chemistry*, 23(3):435–482, 2004.

[12] Jong-Ho Choi. Radical–radical reaction dynamics: A combined crossed-beam and theoretical study. *International Reviews in Physical Chemistry*, 25(4):613–653, 2006.

[13] S. J. Greaves, R. A. Rose, and A. J. Orr-Ewing. Velocity map imaging of the dynamics of bimolecular chemical reactions. *Physical Chemistry Chemical Physics*, 12:9129–9143, 2010.

[14] D. Townsend, M. P. Minitti, and A. G. Suits. Direct current slice imaging. *Review of Scientific Instruments*, 74(4):2530–2539, 2003.

[15] J. J. Lin, J. Zhou, W. Shiu, and K. Liu. Application of time-sliced ion velocity imaging to crossed molecular beam experiments. *Review of Scientific Instruments*, 74(4):2495–2500, 2003.

[16] M. Brouard and C. Vallance. *Tutorials in Molecular Reaction Dynamics*. Royal Society of Chemistry, Cambridge, 2010.

[17] J. M. Bowman, B. J. Braams, S. Carter, C. Chen, G. Czakó, B. Fu, X. Huang, E. Kamarchik, A. R. Sharma, B. C. Shepler, Y. Wang, and Z. Xie. Ab-initio-based potential energy surfaces for complex molecules and molecular complexes. *Journal of Physical Chemistry Letters*, 1(12):1866–1874, 2010.

[18] D. W. Chandler and P. L. Houston. Two-dimensional imaging of state-selected photodissociation products detected by multiphoton ionization. *Journal of Chemical Physics*, 87(2):1445–1447, 1987.

[19] W. C. Wiley and I. H. McLaren. Time-of-flight mass spectrometer with improved resolution. *Review of Scientific Instruments*, 26(12):1150–1157, 1955.

[20] A. T. J. B. Eppink and D. H. Parker. Velocity map imaging of ions and electrons using electrostatic lenses: Application in photoelectron and photofragment ion imaging of molecular oxygen. *Review of Scientific Instruments*, 68(9):3477–3484, 1997.

[21] Roger Campargue, editor. *Atomic and Molecular Beams*. Springer, 2001.

[22] Paul L. Houston. *Chemical Kinetics and Reaction Dynamics*. McGraw-Hill Companies, Inc., New York, 2001.

[23] S. Y. T. van de Meerakker, H. L. Bethlem, and G. Meijer. Taming molecular beams. *Nature Physics*, 4:595–602, 2008.

[24] D. H. Levy. The spectroscopy of very cold molecules. *Science*, 214:263–269, 1981.

[25] Giacinto Scoles, editor. *Atomic and Molecular Beam Methods*. Oxford University Press, 1988.

[26] R. E. Continetti, B. A. Balko, and Y. T. Lee. Crossed molecular beams study of the reaction D + H_2 → DH + H at collision energies of 0.53 and 1.01 eV. *Journal of Chemical Physics*, 93(8):5719–5740, 1990.

[27] L. Schnieder, K. Seekamp-Rahn, E. Wrede, and K. H. Welge. Experimental determination of quantum state resolved differential cross sections for the hydrogen exchange reaction H + D_2 → HD + D. *Journal of Chemical Physics*, 107(16):6175–6195, 1997.

[28] L. Schnieder, K. Seekamp-Rahn, J. Borkowski, E. Wrede, K. H. Welge, F. J. Aoiz, L. Bañares, M. J. D'Mello, V. J. Herrero, V. Sáez Rábanos, and R. E. Wyatt. Experimental studies and theoretical predictions for the H + D_2 → HD + D reaction. *Science*, 269:207–210, 1995.

[29] T. N. Kitsopoulos, M. A. Buntine, D. P. Baldwin, R. N. Zare, and D W. Chandler. Reaction product imaging: The H + D_2 reaction. *Science*, 260:1605–1610, 1993.

[30] F. J. Aoiz, L. Bañares, V. J. Herrero, V. Sáez Rábanos, K. Stark, and H. J. Werner. Classical dynamics for the F + H_2 → HF + H on a new ab initio potential energy surface. A direct comparison with experiment. *Chemical Physics Letters*, 223(3):215–226, 1994.

[31] D. M. Neumark, A. M. Wodtke, G. N. Robinson, C. C. Hayden, and Y. T. Lee. Experimental investigation of resonances in reactive scattering: The F + H_2 reaction. *Physical Review Letters*, 53:226–229, 1984.

[32] D. M. Neumark, A. M. Wodtke, G. N. Robinson, C. C. Hayden, and Y. T. Lee. Molecular beam studies of the F + H_2 reaction. *Journal of Chemical Physics*, 82(7):3045–3066, 1985.

[33] L. Che, Z. Ren, X. Wang, W. Dong, D. Dai, X. Wang, D. H. Zhang, X. Yang, L. Sheng, G. Li, H.-J. Werner, F. Lique, and M. H. Alexander. Breakdown of the Born-Oppenheimer approximation in the F + o-D_2 → DF + D reaction. *Science*, 317:1061–1064, 2007.

[34] S.-H. Lee and K. Liu. Exploring the spin-orbit reactivity in the simplest chlorine atom reaction. *Journal of Chemical Physics*, 111(14):6253–6259, 1999.

[35] F. Dong, S.-H. Lee, and K. Liu. Direct determination of the spin-orbit reactivity in Cl($^2P_{3/2}$,$^2P_{1/2}$) + H_2/D_2/HD reactions. *Journal of Chemical Physics*, 115(3):1197–1204, 2001.

[36] M. Alagia, N. Balucani, L. Cartechini, P. Casavecchia, E. H. van Kleef, G. G. Volpi, F. J. Aoiz, L. Bañares, D. W. Schwenke, T. C. Allison, S. L. Mielke, and D. G. Truhlar. Dynamics of the simplest chlorine atom reaction: An experimental and theoretical study. *Science*, 273:1519–1522, 1996.

[37] X. Wang, W. Dong, C. Xiao, L. Che, Z. Ren, D. Dai, X. Wang, P. Casavecchia, X. Yang, B. Jiang, D. Xie, Z. Sun, S.-Y. Lee, D. H. Zhang, H.-J. Werner, and M. H. Alexander. The extent of non–Born-Oppenheimer coupling in the reaction of Cl(^2P) with para-H_2. *Science*, 322:573–576, 2008.

[38] M. Ahmed, D. S. Peterka, and A. G. Suits. Crossed-beam reaction of O(^1D) + D_2 → OD + D by velocity map imaging. *Chemical Physics Letters*, 301:372–378, 1999.

[39] D.-C. Che and K. Liu. Reactive scattering of O(^1D) + HD: Product speed and angle distributions. *Journal of Chemical Physics*, 103(12):5164–5167, 1995.

[40] Y.-T. Hsu, K. Liu, L. A. Pederson, and G. C. Schatz. Reaction dynamics of O(^{1}D) + HD. I. The insertion pathway. *Journal of Chemical Physics*, 111(17):7921–7930, 1999.

[41] F. J. Aoiz, L. Banares, J. F. Castillo, B. Martinez-Haya, and Marcelo P. de Miranda. The stereodynamics of the O(^{1}D) + HD reaction on the ground 1^1A' and excited 1^1A" potential energy surfaces. *Journal of Chemical Physics*, 114(19):8328–8338, 2001.

[42] P. A. Whitlock, J. T. Muckerman, and E. R. Fisher. Quasiclassical trajectory investigation of the reaction O(^{1}D) + H_2. *Journal of Chemical Physics*, 76(9):4468–4489, 1982.

[43] S. D. Chao, S. A. Harich, D. X. Dai, C. C. Wang, X. Yang, and R. T. Skodje. A fully state- and angle-resolved study of the H + HD $\rightarrow$ D + H_2 reaction: Comparison of a molecular beam experiment to ab initio quantum reaction dynamics. *Journal of Chemical Physics*, 117(18):8341–8361, 2002.

[44] Dongxu Dai, Chia C. Wang, Steven A. Harich, Xiuyan Wang, Xueming Yang, Sheng Der Chao, and Rex T. Skodje. Interference of quantized transition-state pathways in the H + D_2 $\rightarrow$ D + HD chemical reaction. *Science*, 300:1730–1734, 2002.

[45] A. G. Suits, S. D. Chambreau, and S. A. Lahankar. State-correlated dc slice imaging of formaldehyde photodissociation: Roaming atoms and multichannel branching. *International Reviews in Physical Chemistry*, 26(4):585–607, 2007.

[46] J. D. DeSain, S. J. Klippenstein, C. A. Taatjes, M. D. Hurley, and T. J. Wallington. Product formation in the Cl-initiated oxidation of cyclopropane. *Journal of Physical Chemistry A*, 107(12):1992–2002, 2003.

[47] M. D. Hurley, W. F. Schneider, T. J. Wallington, D. J. Mann, J. D. DeSain, and C. A. Taatjes. Kinetics of elementary reactions in the chain chlorination of cyclopropane. *Journal of Physical Chemistry A*, 107(12):2003–2010, 2003.

[48] B. J. Finlayson-Pitts. The tropospheric chemistry of sea salt: A molecular-level view of the chemistry of NaCl and NaBr. *Chemical Reviews*, 103(12):4801–4822, 2003.

[49] M. J. Molina, L. T. Molina, and C. E. Kolb. Gas-phase and heterogeneous chemical

kinetics of the troposphere and stratosphere. *Annual Review of Physical Chemistry*, 47(1):327–367, 1996.

[50] S. F. Rowland. Stratospheric ozone depletion. *Annual Review of Physical Chemistry*, 42(1):731–768, 1991.

[51] R. Atkinson, D. L. Baulch, R. A. Cox, Jr. R. F. Hampson, J. A. Kerr, and J. Troe. Evaluated Kinetic and Photochemical Data for Atmospheric Chemistry: Supplement IV. IUPAC Subcommittee on Gas Kinetic Data Evaluation for Atmospheric Chemistry. *Journal of Physical and Chemical Reference Data*, 21(6):1125–1568, 1992.

[52] R. Atkinson, D. L. Baulch, R. A. Cox, Jr. R. F. Hampson, J. A. Kerr, M. J. Rossi, and J. Troe. Evaluated kinetic, Photochemical and Heterogeneous Data for Atmospheric Chemistry: Supplement V. IUPAC Subcommittee on Gas Kinetic Data Evaluation for Atmospheric Chemistry. *Journal of Physical and Chemical Reference Data*, 26(3):521–1011, 1997.

[53] R. Atkinson, D. L. Baulch, R. A. Cox, Jr. R. F. Hampson, J. A. Kerr, M. J. Rossi, and J. Troe. Evaluated Kinetic and Photochemical Data for Atmospheric Chemistry, Organic Species: Supplement VII. *Journal of Physical and Chemical Reference Data*, 28(2):191–393, 1999.

[54] J. Park, Y. Lee, J. F. Hershberger, J. M. Hossenlopp, and G. W. Flynn. Chemical dynamics of the reaction between chlorine atoms and deuterated cyclohexane. *Journal of the American Chemical Society*, 114(1):58–63, 1992.

[55] W. R. Simpson, T. P. Rakitzis, S. A. Kandel, T. Lev-On, and R. N. Zare. Picturing the transition-state region and understanding vibrational enhancement for the Cl + $CH_4 \rightarrow HCl + CH_3$ reaction. *Journal of Physical Chemistry*, 100(19):7938–7947, 1996.

[56] D. F. Varley and P. J. Dagdigian. Product state distributions and angular differential cross sections from photoinitiated reactions of chlorine atoms with small hydrocarbons. *Journal of Physical Chemistry*, 99(24):9843–9853, 1995.

[57] C. Murray, B. Retail, and A. J. Orr-Ewing. The dynamics of the H-atom abstraction

reactions between chlorine atoms and the methyl halides. *Chemical Physics*, 301:239–249, 2004.

[58] C. Murray, J. K. Pearce, S. Rudić, B. Retail, and A. J. Orr-Ewing. Stereodynamics of chlorine atom reactions with organic molecules. *Journal of Physical Chemistry A*, 109(49):11093–11102, 2005.

[59] N. E. Shafer, A. J. Orr-Ewing, W. R. Simpson, H. Xu, and R. N. Zare. State-to-state differential cross sections from photoinitiated bulb reactions. *Chemical Physics Letters*, 212:155–162, 1993.

[60] W. R. Simpson, A. J. Orr-Ewing, and R. N. Zare. State-to-state differential cross sections for the reaction Cl ($^2P_{3/2}$) + CH_4 ($v_3 = 1$, $J = 1$) → HCl (v' = 1, J') + CH_3. *Chemical Physics Letters*, 212:163–171, 1993.

[61] W. R. Simpson, T. P. Rakitzis, S. A. Kandel, A. J. Orr-Ewing, and R. N. Zare. Reaction of Cl with vibrationally excited CH_4 and CHD_3: State-to-state differential cross sections and steric effects for the HCl product. *Journal of Chemical Physics*, 103(17):7313–7335, 1995.

[62] S. A. Kandel, T. P. Rakitzis, T. Lev-On, and R. N. Zare. Angular distributions for the Cl + C_2H_6 → HCl + C_2H_5 reaction observed via multiphoton ionization of the C_2H_5 radical. *Journal of Physical Chemistry A*, 102(13):2270–2273, 1998.

[63] S. Alex Kandel, T. Peter Rakitzis, Topaz Lev-On, and Richard N. Zare. Dynamical effects of reagent vibrational excitation in the Cl + $C_2H_6(v_5 = 1)$ → HCl + C_2H_5 reaction. *Chemical Physics Letters*, 265:121–128, 1997.

[64] M. J. Bass, M. Brouard, C. Vallance, T. N. Kitsopoulos, P. C. Samartzis, and R. L. Toomes. The dynamics of the Cl + C_2H_6 → HCl(v', j') + C_2H_5 reaction at 0.24 eV: Is ethyl a spectator? *Journal of Chemical Physics*, 119(14):7168–7178, 2003.

[65] W. Li, C. Huang, M. Patel, D. Wilson, and A. Suits. State-resolved reactive scattering by slice imaging: A new view of the Cl + C_2H_6 reaction. *Journal of Chemical Physics*, 124(1):011102, 2006.

[66] C. Huang, W. Li, and A. G. Suits. Rotationally resolved reactive scattering: Imaging detailed Cl + C_2H_6 reaction dynamics. *Journal of Chemical Physics*, 125(13):133107, 2006.

[67] W. Shiu, J. J. Lin, K. Liu, M. Wu, and D. H. Parker. Imaging the pair-correlated excitation function: The F + CH_4 → HF(v') + CH_3(v = 0) reaction. *Journal of Chemical Physics*, 120(1):117–122, 2004.

[68] J. Zhou, W. Shiu, J. J. Lin, and K. Liu. Rotationally selected product pair correlation in F + CD_4 → DF(v') + CD_3(v = 0, N). *Journal of Chemical Physics*, 120(13):5863–5866, 2004.

[69] J. Zhou, W. Shiu, J. J. Lin, and K. Liu. Rotationally selected product pair correlation: F + CD_4 → DF(v') + CD_3(v_2 = 0 and 2, N). *Journal of Chemical Physics*, 124(10):104309, 2006.

[70] D. A. Blank, N. Hemmi, A. G. Suits, and Y. T. Lee. A crossed molecular beam investigation of the reaction Cl + propane → HCl + C_3H_7 using VUV synchrotron radiation as a product probe. *Chemical Physics*, 231:261–278, 1998.

[71] N. Hemmi and A. G. Suits. The dynamics of hydrogen abstraction reactions: Crossed-beam reaction Cl + n-C_5H_{12} → C_5H_{11} + HCl. *Journal of Chemical Physics*, 109(13):5338–5343, 1998.

[72] H. U. Stauffer, R. Z. Hinrichs, P. A. Willis, and H. F. Davis. Competing reaction pathways from Y + C_2H_2 collisions. *Journal of Chemical Physics*, 111(9):4101–4112, 1999.

[73] P. A. Willis, H. U. Stauffer, R. Z. Hinrichs, and H. F. Davis. Crossed beams study of C-H bond activation: Mo($^5S_2$) + CH_4 → $MoCH_2$ + H_2. *Journal of Chemical Physics*, 108(7):2665–2668, 1998.

[74] R. L. Gross, X. Liu, and A. G. Suits. O(^{3}P) versus O(^{1}D) reaction dynamics with n-pentane: a crossed-beam imaging study. *Chemical Physics Letters*, 376:710–716, 2003.

[75] X. Liu, R. L. Gross, G. E. Hall, J. T. Muckerman, and A. G. Suits. Imaging $O(^3P)$ + alkane reactions in crossed molecular beams: Vertical versus adiabatic H abstraction dynamics. *Journal of Chemical Physics*, 117(17):7947–7959, 2002.

[76] X. Liu, R. L. Gross, and A. G. Suits. Differential cross sections for $O(^3P)$ + alkane reactions by direct imaging. *Journal of Chemical Physics*, 116(13):5341–5344, 2002.

[77] M. Ahmed, D. S. Peterka, and A. G Suits. H abstraction dynamics by crossed-beam velocity map imaging: Cl + $CH_3OH \rightarrow CH_2OH$ + HCl. *Chemical Physics Letters*, 317:264–268, 2000.

[78] M. Ahmed, D. S. Peterka, and A. G. Suits. Imaging H abstraction dynamics in crossed molecular beams: Cl + ROH reactions. *Physical Chemistry Chemical Physics*, 2:861–868, 2000.

[79] C. Huang, W. Li, A. D. Estillore, and A. G. Suits. Dynamics of CN + alkane reactions by crossed-beam dc slice imaging. *Journal of Chemical Physics*, 129(7):074301, 2008.

[80] H.-B. Qian, D. Turton, P. W. Seakins, and M. J. Pilling. A laser flash photolysis/IR diode laser absorption study of the reaction of chlorine atoms with selected alkanes. *International Journal of Chemical Kinetics*, 34(2):86–94, 2002.

[81] M. Ahmed, D. Blunt, D. Chen, and A. G. Suits. UV photodissociation of oxalyl chloride yields four fragments from one photon absorption. *Journal of Chemical Physics*, 106(18):7617–7624, 1997.

[82] N. Hemmi and A. G. Suits. Photodissociation of oxalyl chloride at 193 nm probed via synchrotron radiation. *Journal of Physical Chemistry A*, 101(36):6633–6637, 1997.

[83] G. S. Tyndall, J. J. Orlando, and C. S. Kegley-Owen. Rate coefficients for quenching of $Cl(^2P_{1/2})$ by various atmospheric gases. *Journal of the Chemical Society, Faraday Transactions*, 91:3055–3061, 1995.

[84] W. Li, S. D. Chambreau, S. A. Lahankar, and A. G. Suits. Megapixel ion imaging with standard video. *Review of Scientific Instruments*, 76(6):063106, 2005.

[85] R. Silva, W. K. Gichuhi, M. B. Doyle, A. H. Winney, and A. G. Suits. Photodissociation

of heptane isomers and relative ionization efficiencies of butyl and propyl radicals at 157 nm. *Physical Chemistry Chemical Physics*, 11:4777–4781, 2009.

[86] M. J. Bass, M. Brouard, C. Vallance, T. N. Kitsopoulos, P. C. Samartzis, and R. L. Toomes. The dynamics of the Cl + n-C_4H_{10} → HCl (v', j') + C_4H_9 reaction at 0.32 eV. *Journal of Chemical Physics*, 121(15):7175–7186, 2004.

[87] Y. F. Yen, Z. Wang, B. Xue, and B. Koplitz. Site propensities for hydrogen chloride and deuterium chloride formation in the reaction of chlorine atom with selectively-deuterated propanes. *Journal of Physical Chemistry*, 98(1):4–7, 1994.

[88] D. F. Varley and P. J. Dagdigian. Comparison of the dynamics of abstraction of primary vs. secondary hydrogens in the Cl + $CD_3CH_2CD_3$ reaction. *Chemical Physics Letters*, 255:393–400, 1996.

[89] D. F. Varley and P. J. Dagdigian. Product state resolved study of the Cl + $(CH_3)_3CD$ reaction: comparison of the dynamics of abstraction of primary versus tertiary hydrogens. *Journal of Physical Chemistry*, 100(11):4365–4374, 1996.

[90] S. J. Greaves, A. J. Orr-Ewing, and D. Troya. Classical trajectory study of the dynamics of the reaction of Cl atoms with ethane. *Journal of Physical Chemistry A*, 112(39):9387–9395, 2008.

[91] P. Andresen and A. C. Luntz. The chemical dynamics of the reactions of O(^{3}P) with saturated hydrocarbons. I. Experiment. *Journal of Chemical Physics*, 72(11):5842–5850, 1980.

[92] A. C. Luntz and P. Andresen. The chemical dynamics of the reactions of O(^{3}P) with saturated hydrocarbons. II. Theoretical model. *Journal of Chemical Physics*, 72(11):5851–5856, 1980.

[93] W. R. Simpson, A. J. Orr-Ewing, T. P. Rakitzis, S. A. Kandel, and R. N. Zare. Core extraction for measuring state-to-state differential cross sections of bimolecular reactions. *Journal of Chemical Physics*, 103(17):7299–7312, 1995.

[94] A. J. Orr-Ewing, W. R. Simpson, T. P. Rakitzis, S. A. Kandel, and R. N. Zare.

Scattering-angle resolved product rotational alignment for the reaction of Cl with vibrationally excited methane. *Journal of Chemical Physics*, 106(14):5961–5971, 1997.

[95] N. Choi, M. J. Pilling, P. W. Seakins, and L. Wang. Studies of site selective hydrogen atom abstractions by Cl atoms from isobutane and propane by laser flash photolysis/IR diode laser spectroscopy. *Physical Chemistry Chemical Physics*, 8:2172–2178, 2006.

[96] D. Sarzynski and B. Sztuba. Gas-phase reactions of Cl atoms with propane, n-butane, and isobutane. *International Journal of Chemical Kinetics*, 34(12):651–658, 2002.

[97] G. S. Tyndall, J. J. Orlando, T. J. Wallington, M. Dill, and E. W. Kaiser. Kinetics and mechanisms of the reactions of chlorine atoms with ethane, propane, and n-butane. *International Journal of Chemical Kinetics*, 29(1):43–55, 1997.

[98] T. P. Rakitzis, S. A. Kandel, T. Lev-On, and R. N. Zare. Differential cross section polarization moments: Location of the D-atom transfer in the transition-state region for the reactions Cl + C_2D_6 → DCl(v' = 0, J' = 1) + C_2D_5 and Cl + CD_4 → DCl(v' = 0, J' = 1) + CD_3. *Journal of Chemical Physics*, 107(22):9392–9405, 1997.

[99] R. A. Rose, S. J. Greaves, and A. J. Orr-Ewing. Velocity map imaging the dynamics of the reactions of Cl atoms with neopentane and tetramethylsilane. *Journal of Chemical Physics*, 132(24):244312, 2010.

[100] S. Yan, Y.-T. Wu, B. Zhang, X.-F. Yue, and Kopin. Do vibrational excitations of CHD_3 preferentially promote reactivity toward the chlorine atom? *Science*, 316:1723–1726, 2007.

[101] A. D. Estillore, L. M. Visger-Kiefer, T. A. Ghani, and A. G. Suits. Dynamics of H and D abstraction in the reaction of Cl atom with butane-1,1,1,4,4,4-d_6. *Physical Chemistry Chemical Physics*, 13:8433–8440, 2011.

[102] M. J. Frisch, G. W. Trucks, H. B. Schlegel, G. E. Scuseria, M. A. Robb, J. R. Cheeseman, G. Scalmani, V. Barone, B. Mennucci, G. A. Petersson, H. Nakatsuji, M. Caricato, X. Li, H. P. Hratchian, A. F. Izmaylov, J. Bloino, G. Zheng, J. L. Sonnenberg, M. Hada, M. Ehara, K. Toyota, R. Fukuda, J. Hasegawa, M. Ishida, T. Naka-

jima, Y. Honda, O. Kitao, H. Nakai, T. Vreven, J. A. Montgomery Jr., J. E. Peralta, F. Ogliaro, M. Bearpark, J. J. Heyd, E. Brothers, K. N. Kudinand V. N. Staroverov, R. Kobayashi, J. Normand, K. Raghavachari, A. Rendell, J. C. Burant, S. S. Iyengar, J. Tomasi, M. Cossi, N. Rega, J. M. Millam, M. Klene, J. E. Knox, J. B. Cross, V. Bakken, C. Adamo, J. Jaramillo, R. Gomperts, R. E. Stratmann, O. Yazyev, A. J. Austin, R. Cammi, C. Pomelli, J. Ochterski, R. L. Martin, K. Morokuma, V. G. Zakrzewski, G. A. Voth, P. Salvador, J. J. Dannenberg, S. Dapprich, A. D. Daniels, O. Farkas, J. B. Foresman, J. V. Ortiz, J. Cioslowski, and D. J. Fox. *GAUSSIAN 09 (Revision A.1)*. Gaussian, Inc., Wallington, CT, 2009.

[103] J. A. Montgomery Jr., M. J. Frisch, J. W. Ochterski, and G. A. Petersson. A complete basis set model chemistry. VI. Use of density functional geometries and frequencies. *Journal of Chemical Physics*, 110(6):2822–2827, 1999.

[104] J. A. Montgomery Jr., M. J. Frisch, J. W. Ochterski, and G. A. Petersson. A complete basis set model chemistry. VII. Use of the minimum population localization method. *Journal of Chemical Physics*, 112(15):6532–6542, 2000.

[105] A. D. Estillore, L. M. Visger, and A. G. Suits. Crossed-beam dc slice imaging of chlorine atom reactions with pentane isomers. *Journal of Chemical Physics*, 132(16):164313, 2010.

[106] A. D. Estillore, L. M. Visger, and A. G. Suits. Imaging the dynamics of chlorine atom reactions with alkenes. *Journal of Chemical Physics*, 133(7):074306, 2010.

[107] N. Herath, M. L. Hause, and A. G. Suits. The photodissociation dynamics of tetrachloroethylene. *Journal of Chemical Physics*, 134(16):164301, 2011.

[108] A. D. Estillore, L. M. Visger, R. I. Kaiser, and A. G. Suits. Crossed-beam imaging of the H abstraction channel in the reaction of CN with 1-pentene. *Journal of Physical Chemistry Letters*, 1(15):2417–2421, 2010.

[109] C. A. Picconatto, A. Srivastava, and J. J. Valentini. Reactions at suprathreshold energy: Evidence of a kinematic limit to the internal energy of the products. *Journal*

of Chemical Physics, 114(4):1663–1671, 2001.

[110] G. T. Evans, E. van Kleef, and S. Stolte. Chemical reaction dynamics: Combination of two models. *Journal of Chemical Physics*, 93(7):4874–4883, 1990.

[111] N. L. Allinger, J. T. Fermann, W. D. Allen, and H. F. Schaefer III. The torsional conformations of butane: Definitive energetics from ab initio methods. *Journal of Chemical Physics*, 106(12):5143–5150, 1997.

[112] A. Teslja and J. J. Valentini. State-to-state reaction dynamics: A selective review. *Journal of Chemical Physics*, 125(13):132304, 2006.

[113] J. J. Valentini. State-to-state chemical reaction dynamics in polyatomic systems: Case studies. *Annual Review of Physical Chemistry*, 52(1):15–39, 2001.

[114] R. S. Anderson, L. Huang, R. Iannone, and J. Rudolph. Laboratory measurements of the $^{12}C/^{13}C$ kinetic isotope effects in the gas-phase reactions of unsaturated hydrocarbons with Cl atoms at 298±3 K. *Journal of Atmospheric Chemistry*, 56:275–291, 2007.

[115] A. A. Ceacero-Vega, B. Ballesteros, J. Albaladejo, I. Bejan, and I. Barnes. Temperature dependence of the gas-phase reactions of Cl atoms with propene and 1-butene between 285<T<313 K. *Chemical Physics Letters*, 484(1–3):10–13, 2009.

[116] M. J. Ezell, W. Wang, A. A. Ezell, G. Soskin, and B. J. Finlayson-Pitts. Kinetics of reactions of chlorine atoms with a series of alkenes at 1 atm and 298 K: Structure and reactivity. *Physical Chemistry Chemical Physics*, 4:5813–5820, 2002.

[117] E. W. Kaiser and T. J. Wallington. Kinetics of the reactions of chlorine atoms with $C_2H_4(k_1)$ and C_2H_2 (k_2):A determination of $\delta H_{f,298}^{\circ}$ for C_2H_3. *Journal of Physical Chemistry*, 100(10):4111–4119, 1996.

[118] E. W. Kaiser and T. J. Wallington. Pressure dependence of the reaction Cl + C_3H_6. *Journal of Physical Chemistry*, 100(23):9788–9793, 1996.

[119] J. S. Pilgrim and C. A. Taatjes. Infrared absorption probing of the Cl + C_3H_6 reaction: Rate coefficients for HCl production between 290 and 800 K. *Journal of Physical*

Chemistry A, 101(32):5776–5782, 1997.

[120] J. S. Pilgrim and C. A. Taatjes. Infrared absorption probing of the Cl + C_2H_4 reaction: Direct measurement of Arrhenius parameters for hydrogen abstraction. *Journal of Physical Chemistry A*, 101(23):4172–4177, 1997.

[121] M. L. Ragains and B. J. Finlayson-Pitts. Kinetics and mechanism of the reaction of Cl atoms with 2-methyl-1,3-butadiene (isoprene) at 298 K. *Journal of Physical Chemistry A*, 101(8):1509–1517, 1997.

[122] J. Stutz, M. J. Ezell, and B. J. Finlayson-Pitts. Inverse kinetic isotope effect in the reaction of atomic chlorine with C_2H_4 and C_2D_4. *Journal of Physical Chemistry A*, 101(49):9187–9190, 1997.

[123] J. Stutz, M. J. Ezell, A. A. Ezell, and B. J. Finlayson-Pitts. Rate constants and kinetic isotope effects in the reactions of atomic chlorine with n-butane and simple alkenes at room temperature. *Journal of Physical Chemistry A*, 102(44):8510–8519, 1998.

[124] J. J. Sloan. On the dynamics of abstraction, insertion, and addition-elimination reactions in the gas phase. *Journal of Physical Chemistry*, 92(1):18–27, 1988.

[125] E. Arunan, R. Rengarajan, and D.W. Setser. Infrared chemiluminescence studies of the reactions of H atoms with CCl_3, CF_2Cl, and CH_2CH_2Cl radicals at 300 and 475 K: recombination-elimination vs. abstraction mechanisms. *Canadian Journal of Chemistry*, 72(3):568–576, 1994.

[126] C. A. Taatjes. Time-resolved infrared absorption measurements of product formation in Cl atom reactions with alkenes and alkynes. *International Reviews in Physical Chemistry*, 18(3):419–458, 1999.

[127] K. Liu. Recent advances in crossed-beam studies of bimolecular reactions. *Journal of Chemical Physics*, 125(13):132307, 2006.

[128] D. Townsend, W. Li, S. K. Lee, R. L. Gross, and A. G. Suits. Universal and state-resolved imaging of chemical dynamics. *Journal of Physical Chemistry A*, 109(39):8661–8674, 2005.

[129] A. I. Chichinin, K.-H. Gericke, S. Kauczok, and C. Maul. Imaging chemical reactions - 3D velocity mapping. *International Reviews in Physical Chemistry*, 28(4):607–680, 2009.

[130] P. Casavecchia, N. Balucani, and G. G. Volpi. Crossed-beam studies of reaction dynamics. *Annual Review of Physical Chemistry*, 50(1):347–376, 1999.

[131] Y. Matsumi, K. Izumi, V. Skorokhodov, M. Kawasaki, and N. Tanaka. Reaction and quenching of $Cl(^2P_j)$ atoms in collisions with methane and deuterated methanes. *Journal of Physical Chemistry A*, 101(7):1216–1221, 1997.

[132] W. B. Miller, S. A. Safron, and D. R. Herschbach. Exchange reactions of alkali atoms with alkali halides: A collision complex mechanism. *Discussions of the Faraday Society*, 44:108–122, 1967.

[133] A. M. Schmoltner, P. M. Chu, R. J. Brudzynski, and Y. T. Lee. Crossed molecular beam study of the reaction $O(^3P) + C_2H_4$. *Journal of Chemical Physics*, 91(11):6926–6936, 1989.

[134] A. M. Schmoltner, P. M. Chu, and Y. T. Lee. Crossed molecular beam study of the reaction $O(^3P) + C_2H_2$. *Journal of Chemical Physics*, 91(9):5365–5373, 1989.

[135] A. M. Schmoltner, S. Y. Huang, R. J. Brudzynski, P. M. Chu, and Y. T. Lee. Crossed molecular beam study of the reaction $O(^3P)$ + allene. *Journal of Chemical Physics*, 99(3):1644–1653, 1993.

[136] N. Balucani, O. Asvany, A. H. H. Chang, S. H. Lin, Y. T. Lee, R. I. Kaiser, H. F. Bettinger, P. v. R. Schleyer, and H. F. Schaefer III. Crossed beam reaction of cyano radicals with hydrocarbon molecules. I. Chemical dynamics of cyanobenzene (C_6H_5CN); and perdeutero cyanobenzene (C_6D_5CN); formation from reaction of CN with benzene (C_6H_6), and d_6-benzene (C_6D_6). *Journal of Chemical Physics*, 111(16):7457–7471, 1999.

[137] N. Balucani, O. Asvany, A. H. H. Chang, S. H. Lin, Y. T. Lee, R. I. Kaiser, H. F. Bettinger, P. v. R. Schleyer, and H. F. Schaefer III. Crossed beam reaction

of cyano radicals with hydrocarbon molecules. II. Chemical dynamics of 1-cyano-1-methylallene ($CNCH_3CCCH_2$); formation from reaction of CN with dimethylacetylene (CH_3CCCH_3). *Journal of Chemical Physics*, 111(16):7472–7479, 1999.

[138] N. Balucani, O. Asvany, A. H. H. Chang, S. H. Lin, Y. T. Lee, R. I. Kaiser, and Y. Osamura. Crossed beam reaction of cyano radicals with hydrocarbon molecules. III. Chemical dynamics of vinylcyanide (C_2H_3CN); formation from reaction of CN with ethylene, C_2H_4. *Journal of Chemical Physics*, 113(19):8643–8655, 2000.

[139] L. C. L. Huang, O. Asvany, A. H. H. Chang, N. Balucani, S. H. Lin, Y. T. Lee, R. I. Kaiser, and Y. Osamura. Crossed beam reaction of cyano radicals with hydrocarbon molecules. IV. Chemical dynamics of cyanoacetylene (HCCCN); formation from reaction of CN with acetylene, (C_2H_2). *Journal of Chemical Physics*, 113(19):8656–8666, 2000.

[140] G. A. Fisk, J. D. McDonald, and D. R. Herschbach. General discussion. *Discussions of the Faraday Society*, 44:228–229, 1967.

[141] P. Braña and J. A. Sordo. Theoretical approach to the mechanism of reactions between halogen atoms and unsaturated hydrocarbons: The Cl + propene reaction. *Journal of Computational Chemistry*, 24(16):2044–2062, 2003.

[142] S. Rudic, C. Murray, D. Ascenzi, H. Anderson, J. N. Harvey, and A. J. Orr-Ewing. The dynamics of formation of HCl products from the reaction of Cl atoms with methanol, ethanol, and dimethyl ether. *Journal of Chemical Physics*, 117(12):5692–5706, 2002.

[143] S. Rudic, C. Murray, J. N. Harvey, and A. J. Orr-Ewing. On-the-fly ab initio trajectory calculations of the dynamics of Cl atom reactions with methane, ethane and methanol. *Journal of Chemical Physics*, 120(1):186–198, 2004.

[144] H. A. Bechtel, J. P. Camden, and R. N. Zare. State-to-state dynamics of the Cl + $CH_3OH \rightarrow HCl + CH_2OH$ reaction. *Journal of Chemical Physics*, 120(9):4231–4239, 2004.

[145] C. Murray, A. J. Orr-Ewing, R. L. Toomes, and T. N. Kitsopoulos. Imaging the

quantum-state specific differential cross sections of HCl formed from reactions of chlorine atoms with methanol and dimethyl ether. *Journal of Chemical Physics*, 120(5):2230–2237, 2004.

[146] G. Hess. BP and DuPont Plan 'Biobutanol'. *Chemical and Engineering News*, 84:9, 2006.

[147] S.M. Sarathy, M.J. Thomson, C. Togb, P. Dagaut, F. Halter, and C. Mounaim-Rousselle. An experimental and kinetic modeling study of n-butanol combustion. *Combustion and Flame*, 156(4):852–864, 2009.

[148] P. S. Veloo, Y. L. Wang, F. N. Egolfopoulos, and C. K. Westbrook. A comparative experimental and computational study of methanol, ethanol, and n-butanol flames. *Combustion and Flame*, 157(10):1989–2004, 2010.

[149] S. Vranckx, K.A. Heufer, C. Lee, H. Olivier, L. Schill, W.A. Kopp, K. Leonhard, C.A. Taatjes, and R.X. Fernandes. Role of peroxy chemistry in the high-pressure ignition of n-butanol - Experiments and detailed kinetic modelling. *Combustion and Flame*, 158(8):1444–1455, 2011.

[150] M. R. Harper, K. M. Van Geem, S. P. Pyl, G. B. Marin, and W. H. Green. Comprehensive reaction mechanism for n-butanol pyrolysis and combustion. *Combustion and Flame*, 158(1):16–41, 2011.

[151] J. T. Moss, A. M. Berkowitz, M. A. Oehlschlaeger, J. Biet, V. Warth, P.-A. Glaude, and F. Battin-Leclerc. An experimental and kinetic modeling study of the oxidation of the four isomers of butanol. *Journal of Physical Chemistry A*, 112(43):10843–10855, 2008.

[152] G. Black, H.J. Curran, S. Pichon, J.M. Simmie, and V. Zhukov. Bio-butanol: Combustion properties and detailed chemical kinetic model. *Combustion and Flame*, 157(2):363–373, 2010.

[153] R. Grana, A. Frassoldati, T. Faravelli, U. Niemann, E. Ranzi, R. Seiser, R. Cattolica, and K. Seshadri. An experimental and kinetic modeling study of combustion of isomers

of butanol. *Combustion and Flame*, 157(11):2137–2154, 2010.

[154] P. Seal, E. Papajak, T. Yu, and D. G. Truhlar. Statistical thermodynamics of 1-butanol, 2-methyl-1-propanol, and butanal. *Journal of Chemical Physics*, 136(3):034306, 2012.

[155] X. Xu, E. Papajak, J. Zheng, and D. G. Truhlar. Multi-structural variational transition state theory: kinetics of the 1,5-hydrogen shift isomerization of the 1-butoxyl radical including all structures and torsional anharmonicity. *Physical Chemistry Chemical Physics*, 14:4204–4216, 2012.

[156] J. Zheng and D. G. Truhlar. Kinetics of hydrogen-transfer isomerizations of butoxyl radicals. *Physical Chemistry Chemical Physics*, 12:7782–7793, 2010.

[157] N. Qureshi and T. C. Ezeji. Butanol, 'a superior biofuel' production from agricultural residues (renewable biomass): Recent progress in technology. *Biofuels, Bioproducts and Biorefining*, 2(4):319–330, 2008.

[158] N. Qureshi, B. C. Saha, and M. A. Cotta. Butanol production from wheat straw by simultaneous saccharification and fermentation using *Clostridium beijerinckii*: Part II - Fed-batch fermentation. *Biomass and Bioenergy*, 32(2):176–183, 2008.

[159] N. Qureshi, B. C. Saha, B. Dien, R. E. Hector, and M. A. Cotta. Production of butanol (a biofuel) from agricultural residues: Part I - Use of barley straw hydrolysate. *Biomass and Bioenergy*, 34(4):559–565, 2010.

[160] N. Qureshi, B. C. Saha, R. E. Hector, S. R. Hughes, and M. A. Cotta. Butanol production from wheat straw by simultaneous saccharification and fermentation using *Clostridium beijerinckii*: Part I - Batch fermentation. *Biomass and Bioenergy*, 32(2):168–175, 2008.

[161] T. Yamanaka, M. Kawasaki, M. D. Hurley, T. J. Wallington, W. F. Schneider, and J. Bruce. Kinetics and mechanism of the gas phase reaction of chlorine atoms with i-propanol. *Physical Chemistry Chemical Physics*, 9:4211–4217, 2007.

[162] F. Taketani, K. Takahashi, Y. Matsumi, and T. J. Wallington. Kinetics of the reactions

of $Cl^*(^2P_{1/2})$ and $Cl(^2P_{3/2})$ atoms with CH_3OH, C_2H_5OH, n-C_3H_7OH, and i-C_3H_7OH at 295 K. *Journal of Physical Chemistry A*, 109(17):3935–3940, 2005.

[163] M. A. Crawford, Z. Li, H. A. Heuerman, and D. Kinscherff. A kinetic and product study of reaction of chlorine atom with CH_3CH_2OD. *International Journal of Chemical Kinetics*, 36(11):584–590, 2004.

[164] C. A. Taatjes, L. K. Christensen, M. D. Hurley, and T. J. Wallington. Absolute and site-specific abstraction rate coefficients for reactions of Cl with CH_3CH_2OH, CH_3CD_2OH, and CD_3CH_2OH between 295 and 600 K. *Journal of Physical Chemistry A*, 103(48):9805–9814, 1999.

[165] T. J. Wallington, L. M. Skewes, W. O. Siegl, C.-H. Wu, and S. M. Japar. Gas phase reaction of Cl atoms with a series of oxygenated organic species at 295 K. *International Journal of Chemical Kinetics*, 20(11):867–875, 1988.

[166] S. A. Cheema, K. A. Holbrook, G. A. Oldershaw, and R. W. Walker. Kinetics and mechanism associated with the reactions of hydroxyl radicals and of chlorine atoms with 1-propanol under near-tropospheric conditions between 273 and 343 K. *International Journal of Chemical Kinetics*, 34(2):110–121, 2002.

[167] Bernabe Ballesteros, Andres Garzon, Elena Jimenez, Alberto Notario, and Jose Albaladejo. Relative and absolute kinetic studies of 2-butanol and related alcohols with tropospheric Cl atoms. *Physical Chemistry Chemical Physics*, 9:1210–1218, 2007.

[168] A. Garzon, C. A. Cuevas, A. A. Ceacero, A. Notario, J. Albaladejo, and M. Fernandez-Gomez. Atmospheric reactions Cl + CH_3-$(CH_2)_n$-OH (n = 0-4): A kinetic and theoretical study. *Journal of Chemical Physics*, 125(10):104305, 2006.

[169] H. Wu, Y. Mu, X. Zhang, and G. Jiang. Relative rate constants for the reactions of hydroxyl radicals and chlorine atoms with a series of aliphatic alcohols. *International Journal of Chemical Kinetics*, 35(2):81–87, 2003.

[170] M. D. Hurley, T. J. Wallington, L. Laursen, M. S. Javadi, O. J. Nielsen, T. Yamanaka, and M. Kawasaki. Atmospheric chemistry of n-butanol: Kinetics, mechanisms, and

products of Cl atom and OH radical initiated oxidation in the presence and absence of NO_x. *Journal of Physical Chemistry A*, 113(25):7011–7020, 2009.

[171] F. Wicktor, A. Donati, H. Herrmann, and R. Zellner. Laser based spectroscopic and kinetic investigations of reactions of the Cl atom with oxygenated hydrocarbons in aqueous solution. *Physical Chemistry Chemical Physics*, 5:2562–2572, 2003.

[172] F. Filsinger, J. Küpper, G. Meijer, J.L. Hansen, J. Maurer, J.H. Nielsen, L. Holmegaard, and H. Stapelfeldt. Pure samples of individual conformers: The separation of stereoisomers of complex molecules using electric fields. *Angewandte Chemie International Edition*, 48(37):6900–6902, 2009.

[173] M. H. Kim, L. Shen, H. Tao, T. J. Martinez, and A. G. Suits. Conformationally controlled chemistry: Excited-state dynamics dictate ground-state reaction. *Science*, 315:1561–1565, 2007.

[174] Timothy S. Zwier. Conformers part company. *Nature Chemistry*, 1(9):687–688, 2009.

[175] Albert Stolow. Molecular conformations fielded. *Nature*, 461(7267):1063–1064, 2009.

[176] K. Ohno, H. Yoshida, H. Watanabe, T. Fujita, and H. Matsuura. Conformational study of 1-butanol by the combined use of vibrational spectroscopy and ab initio molecular orbital calculations. *Journal of Physical Chemistry*, 98(28):6924–6930, 1994.

[177] J. Moc, J. M. Simmie, and H. J. Curran. The elimination of water from a conformationally complex alcohol: A computational study of the gas phase dehydration of n-butanol. *Journal of Molecular Structure*, 928:149–157, 2009.

[178] R. D. Levine. *Molecular Reaction Dynamics*. Cambridge University Press, 2005.

[179] J. C. Polanyi. Dynamics of chemical reactions. *Discussions of the Faraday Society*, 44:293–307, 1967.

[180] A. C. Kollias, O. Couronne, and Jr. W. A. Lester. Quantum Monte Carlo study of the reaction: $Cl + CH_3OH \rightarrow CH_2OH + HCl$. *Journal of Chemical Physics*, 121(3):1357–1363, 2004.

[181] I. Glassman. *Combustion*. Academic, 1996.

[182] I. Cherchneff and A. E. Glassgold. The formation of carbon chain molecules in IRC +10216. *Astrophysical Journal Letters*, 419:L41, 1993.

[183] Ian M. Campbell. *Energy and the Atmosphere: A Physical-chemical Approach*. John Wiley and Sons Ltd, London, 1977.

[184] K. Fukuzawa, Y. Osamura, and H. F. Schaefer III. Are neutral-neutral reactions effective for the carbon-chain growth of cyanopolyynes and polyacetylenes in interstellar space? *Astrophysical Journal*, 505(1):278, 1998.

[185] F. Raulin, P. Coll, D. Coscia, M.C. Gazeau, R. Sternberg, P. Bruston, G. Israel, and D. Gautier. An exobiological view of Titan and the Cassini-Huygens mission. *Advances in Space Research*, 22(3):353–362, 1998.

[186] K. P. Huber and G. Herzberg. *Molecular Spectra and Molecular Structures IV: Constants of Diatomic Molecules*. Van Nostrand Reinhold, New York, 1979.

[187] I. R. Sims, J.-L. Queffelec, D. Travers, B. R. Rowe, L. B. Herbert, J. Karthauser, and I. W. M. Smith. Rate constants for the reactions of CN with hydrocarbons at low and ultra-low temperatures. *Chemical Physics Letters*, 211:461–468, 1993.

[188] R. J. Balla, K. H. Casleton, J. S. Adams, and L. Pasternack. Absolute rate constants for the reaction of cyanogen with methane, ethane, and propane from 292 to 1500 K using high-temperature photochemistry and diode laser absorption. *Journal of Physical Chemistry*, 95(22):8694–8701, 1991.

[189] I. R. Sims and I. W.M. Smith. Rate constants for the reactions CN(v = 0), CN(v = 1) + H_2, D_2 $\rightarrow$ HCN, DCN + H, D between 295 and 768 K, and comparisons with transition state theory calculations. *Chemical Physics Letters*, 149:565 – 571, 1988.

[190] Q. Sun, D. L. Yang, N. S. Wang, J. M. Bowman, and M. C. Lin. Experimental and reduced dimensionality quantum rate coefficients for $H_2(D_2)$ + CN $\rightarrow$ H(D)CN + H(D). *Journal of Chemical Physics*, 93(7):4730–4739, 1990.

[191] A. Szekely, R. K. Hanson, and C. T. Bowman. High-temperature determination of the rate coefficient for the reaction H_2 + CN $\rightarrow$ H + HCN. *International Journal of*

Chemical Kinetics, 15(9):915–923, 1983.

[192] A. F. Wagner and R. A. Bair. An ab initio determination of the rate constant for H_2 + CN → H + HCN. *International Journal of Chemical Kinetics*, 18(4):473–486, 1986.

[193] A. N. Brooks and D. C. Clary. Application of hyperspherical coordinates to four-atom reactive scattering: H_2 + CN → H + HCN. *Journal of Chemical Physics*, 92(7):4178–4190, 1990.

[194] L. R. Copeland, F. Mohammad, M. Zahedi, D. H. Volman, and W. M. Jackson. Rate constants for CN reactions with hydrocarbons and the product HCN vibrational populations: Examples of heavy-light-heavy abstraction reactions. *Journal of Chemical Physics*, 96:5817–5826, 1992.

[195] D. L. Yang, T. Yu, N. S. Wang, and M. C. Lin. Temperature dependence of cyanogen radical reactions with selected alkanes: CN reactivities towards primary, secondary and tertiary C-H bonds. *Chemical Physics*, 160(2):307–315, 1992.

[196] B. Atakan and J. Wolfrum. Kinetic studies of the reactions of CN radicals with alkanes in the temperature range between 294 and 1260 K. *Chemical Physics Letters*, 186(6):547–552, 1991.

[197] N. Sayah, X. Li, J. F. Caballero, and W. M. Jackson. Laser induced fluorescence studies of CN reactions with alkanes, alkenes and substituted aliphatic species. *Journal of Photochemistry and Photobiology A: Chemistry*, 45:177–194, 1988.

[198] L. Herbert, I. W. M. Smith, and R. D. Spencer-smith. Rate constants for the elementary reactions between CN radicals and CH_4, C_2H_6, C_2H_4, C_3H_6, and C_2H_2 in the range: $295 < T/K < 700$. *International Journal of Chemical Kinetics*, 24(9):791–802, 1992.

[199] D. A. Lichtin and M. C. Lin. Temperature dependence of the CN radical reactions with C_2H_2 and C_2H_4. *Chemical Physics*, 104(2):325–330, 1986.

[200] S. W. North, R. Fei, T. J. Sears, and G. E. Hall. CN radical reaction rate measurements by time-resolved FM spectroscopy. *International Journal of Chemical Kinetics*,

29(2):127–129, 1997.

[201] L. C. L. Huang, Y. T. Lee, and R. I. Kaiser. Crossed beam reaction of the cyanogen radical, CN, with acetylene, C_2H_2: Observation of cyanoacetylene, HCCCN. *Journal of Chemical Physics*, 110(15):7119–7122, 1999.

[202] L. C. L. Huang, N. Balucani, Y. T. Lee, R. I. Kaiser, and Y. Osamura. Crossed beam reaction of the cyano radical, CN, with methylacetylene, CH_3CCH: Observation of cyanopropyne, CH_3CCCN, and cyanoallene, $H_2CCCHCN$. *Journal of Chemical Physics*, 111(7):2857–2860, 1999.

[203] Y. Georgievskii and S. J. Klippenstein. Strange kinetics of the C_2H_6 + CN reaction explained. *Journal of Physical Chemistry A*, 111(19):3802–3811, 2007.

[204] D.-C. Che and K. Liu. A crossed-beam study of the reaction of CN + D_2. Is CN really a spectator bond? *Chemical Physics Letters*, 243:290–296, 1995.

[205] D.-C. Che and K. Liu. Reactive scattering of CN + D_2: The stereodynamics. *Chemical Physics*, 207:367–378, 1996.

[206] C. Huang, W. Li, R. Silva, and A. G. Suits. DC slice ion imaging of the ultraviolet photodissociation of BrCN. *Chemical Physics Letters*, 426:242–247, 2006.

[207] P. A. Willis, H. U. Stauffer, R. Z. Hinrichs, and H. F. Davis. Rotatable source crossed molecular beams apparatus with pulsed ultraviolet/vacuum ultraviolet photoionization detection. *Review of Scientific Instruments*, 70(6):2606–2614, 1999.

[208] E. S. Whitney, A. M. Zolot, A. B. McCoy, J. S. Francisco, and D. J. Nesbitt. Reactive scattering dynamics in atom + polyatomic systems: F + $C_2H_6 \rightarrow$ HF(v, J) + C_2H_5. *Journal of Chemical Physics*, 122(12):124310, 2005.

[209] A. Bottoni and G. Poggi. An *ab initio* study of hydrogen abstraction by fluorine, chlorine and bromine atoms from ethane and propane. *Journal of Molecular Structure: THEOCHEM*, 337(2):161–172, 1995.

[210] S. A. Kandel, T. P. Rakitzis, T. Lev-On, and R. N. Zare. Dynamics for the Cl + $C_2H_6 \rightarrow$ HCl + C_2H_5 reaction examined through state-specific angular distributions.

Journal of Chemical Physics, 105(17):7550–7559, 1996.

[211] D. Troya, R. Z. Pascual, D. J. Garton, T. K. Minton, and G. C. Schatz. Theoretical studies of the O(^{3}P) + ethane reaction. *Journal of Physical Chemistry A*, 107(37):7161–7169, 2003.

[212] D. J. Garton, T. K. Minton, D. Troya, R. Pascual, and G. C. Schatz. Hyperthermal reactions of O(^{3}P) with alkanes:Observations of novel reaction pathways in crossed-beams and theoretical studies. *Journal of Physical Chemistry A*, 107(23):4583–4587, 2003.

[213] F. Ausfelder and K. G. McKendrick. The dynamics of reactions of O(^{3}P) atoms with saturated hydrocarbons and related compounds. *Progress in Reaction Kinetics and Mechanism*, 25(4):299–370, 2000.

[214] G. M. Sweeney and K. G. McKendrick. Rotational and spin-orbit effects in the dynamics of O(^{3}P$_j$) + hydrocarbon reactions. II. Models for spin-orbit propensities. *Journal of Chemical Physics*, 106(22):9182–9189, 1997.

[215] B. Retail, R. A. Rose, J. K. Pearce, S. J. Greaves, and A. J. Orr-Ewing. The dynamics of reaction of Cl atoms with tetramethylsilane. *Physical Chemistry Chemical Physics*, 10:1675–1680, 2008.

[216] Arthur G. Suits. Titan: A Strangely Familiar World. *Journal of Physical Chemistry A*, 113(42):11097–11098, 2009.

[217] T.B. McCord, G.B. Hansen, B.J. Buratti, R.N. Clark, D.P. Cruikshank, E. D'Aversa, C.A. Griffith, E.K.H. Baines, R.H. Brown, C.M. Dalle Ore, G. Filacchione, V. Formisano, C.A. Hibbitts, R. Jaumann, J.I. Lunine, R.M. Nelson, and C. Sotin. Composition of Titan's surface from Cassini VIMS. *Planetary and Space Science*, 54(15):1524 – 1539, 2006.

[218] V. G. Kunde, A. C. Aikin, R. A. Hanel, D. E. Jennings, W. C. Maguire, and R. E. Samuelson. C_4H_2, HC_3N and C_2N_2 in Titan's atmosphere. *Nature*, 292(5825):686–688, 1981.

[219] D. Carty, V. Le Page, I. R. Sims, and I. W. M. Smith. Low temperature rate coefficients for the reactions of CN and C_2H radicals with allene and methyl acetylene. *Chemical Physics Letters*, 344:310–316, 2001.

[220] S. B. Morales, S. D. Le Picard, A. Canosa, and I. R. Sims. Experimental measurements of low temperature rate coefficients for neutral-neutral reactions of interest for atmospheric chemistry of Titan, Pluto and Triton: Reactions of the CN radical. *Faraday Discussions*, 147:155–171, 2010.

[221] S. W. North and G. E. Hall. Vector and scalar correlations in statistical dissociation: The photodissociation of NCCN at 193 nm. *Journal of Chemical Physics*, 106:60–76, 1997.

[222] K. L. Gannon, D. R. Glowacki, M. A. Blitz, K. J. Hughes, M. J. Pilling, and P. W. Seakins. H atom yields from the reactions of CN radicals with C_2H_2, C_2H_4, C_3H_6, trans-2-C_4H_8, and iso-C_4H_8. *Journal of Physical Chemistry A*, 111(29):6679–6692, 2007.

[223] A. J. Trevitt, F. Goulay, G. Meloni, D. L. Osborn, C. A. Taatjes, and S. R. Leone. Isomer-specific product detection of CN radical reactions with ethene and propene by tunable VUV photoionization mass spectrometry. *International Journal of Mass Spectrometry*, 280:113–118, 2009.

[224] X. Gu, F. Zhang, and R. I. Kaiser. Reaction dynamics on the formation of 1- and 3-cyanopropylene in the crossed beams reaction of ground-state cyano radicals (CN) with propylene (C_3H_6) and its deuterated isotopologues. *Journal of Physical Chemistry A*, 112(39):9607–9613, 2008.

[225] C. H. Huang, R. I. Kaiser, and A. H. H. Chang. Theoretical study on the reaction of ground state cyano radical with propylene in Titan's atmosphere. *Journal of Physical Chemistry A*, 113(45):12675–12685, 2009.

[226] L.-M. Lara, E. Lellouch, and V. Shematovich. Titan's atmospheric haze: The case for HCN incorporation. *Astronomy and Astrophysics*, 341:312–317, 1999.

[227] L. A. Capone, J. Dubach, S. S. Prasad, and R. C. Whitten. Galactic cosmic rays and N_2 dissociation on Titan. *Icarus*, 55:73–82, 1983.

ABSTRACT

PROBING THE DYNAMICS OF RADICAL REACTIONS WITH POLYATOMIC HYDROCARBONS BY CROSSED-BEAM DC SLICE IMAGING

by

ARMANDO D. ESTILLORE

August 2012

Advisor: Arthur G. Suits

Major: Chemistry (Physical)

Degree: Doctor of Philosophy

This work presents results of crossed molecular beam imaging studies on the reaction of radicals (Cl and CN) with polyatomic hydrocarbons of different functionalities such as pentane isomers, deuterated alkanes, alkenes, and alcohols. The reactively scattered alkyl radicals are probed as a function of collision energy using single photon ionization. The scattering results for pentane are quite similar for all reactants, suggesting that the nature of the abstraction site has surprisingly little influence on the dynamics studied at ∼5 and ∼9 kcal/mol. The angular distributions are broad with a backscattered peak at low collision energy and a sharp forward peak at high collision energy. The similarity of the angular distributions was observed in the Cl reactions with deuterated butane albeit studied at considerably high collision energy. The presence of conformers in this target molecule likely play a major role. The reduced translational energy distributions manifested distinct dynamics showing marked variation with collision energy in the backward direction and variation in the forward direction for primary versus secondary abstraction, respectively.

For alkenes, an isotropic component was observed in the angular distributions at low collision energy suggesting complex formation that survive for few rotational period, followed by HCl elimination. At increased collision energy, the distributions show a sharp forward peak superimposed on the isotropic component accounting for ∼13% of the product flux.

The forward translational energy distributions changed dramatically with collision energy. A sharp forward peak at ∼80% of the collision energy appears at higher energy, similar to that of pentane isomers.

The butanol isomers exhibit similar dynamics with that of saturated hydrocarbons although the HCl product distributions for these two systems are different. The angular distributions showed direct reaction with backscattering at low collision energy and enhanced forward scattering with respect to the alcohol beam with increased energy. This confirms that the well present in the potential energy surface is shallow to cause long-lived complexes to exist. The product translational energy distributions further support the similarity of these reactions. At high collision energy, a sharp peak of ∼80% of the collision energy is seen in the forward scattered products. The sideways-scattered product showed the lowest fraction of energy appearing in translation.

Hydrogen abstraction of CN radical with alkanes indicate direct reaction with the products largely backscattered and that most of the available energy (∼80% - 85%) goes into internal energy the recoiling products. In the 1-pentene system, the results demonstrate the presence of H-atom abstraction channel yielding a resonantly-stabilized C_5H_9 radical. The results have implications for hydrocarbon growth and nitrile incorporation in formation of haze particles on Saturn's moon, Titan.

AUTOBIOGRAPHICAL STATEMENT

ARMANDO D. ESTILLORE

Education:

Aug 2012 Ph.D., Chemistry (*anticipated*), Wayne State University.
Mar 2003 B.S., Chemistry, Mindanao State University-Iligan Institute of Technology.

Awards and Honors:

2012 Dan Trivich Memorial Award for Research in Physical Chemistry
2011 University Graduate Research Fellowship Dissertation Award
2010 Departmental Citation for Excellence in Teaching Service
2009 Graduate School Citation for Excellence in Teaching

Recent Publications:

1. A. D. Estillore, L. M. Visger-Kiefer, and A. G. Suits. "Reaction dynamics of Cl + butanol isomers by crossed-beam sliced ion imaging." *Faraday Discussions*, **157**, xxxx (2012). *In press*. DOI: 10.1039/C2FD20059G
2. A. D. Estillore, L. M. Visger-Kiefer, T. A. Ghani, and A. G. Suits. "Dynamics of H and D abstraction in the reaction of Cl atom with butane-1,1,1,4,4,4-d_6." *Physical Chemistry Chemical Physics*, **13**, 8433 (2011). DOI: 10.1039/c1cp20137a.
3. A. D. Estillore, L. M. Visger, and A. G. Suits. "Imaging the dynamics of chlorine atom reactions with alkenes." *Journal of Chemical Physics*, **133**, 074306 (2010). DOI: 10.1063/1.3473049.
4. A. D. Estillore, L. M. Visger, and A. G. Suits. "Crossed-beam dc slice imaging of chlorine atom reactions with pentane isomers." *Journal of Chemical Physics*, **132**, 164313 (2010). DOI: 10.1063/1.3414353.
5. A. D. Estillore, L. M. Visger, R. I. Kaiser, and A. G. Suits. "Crossed-Beam Imaging of the H Abstraction Channel in the Reaction of CN with 1-Pentene." *Journal of Physical Chemistry Letters*, **1**, 2417 (2010). DOI: 10.1021/jz100861t.
6. A. G. Suits, A. D. Estillore, and L. M. Visger. *Faraday Discussions*, **147**, 259 (2010). DOI: 10.1039/C005543N.
7. C. Huang, W. Li, A. D. Estillore, and A. G. Suits. "Dynamics of CN + alkane reactions by crossed-beam dc slice imaging." *Journal of Chemical Physics*, **129**, 074301 (2008). DOI: 10.1063/1.2968547.
8. C. Huang, A. D. Estillore, and A. G. Suits. "State-selected imaging of HCCO radical photodissociation dynamics." *Journal Chemical Physics*, **128**, 134301 (2008). DOI: 10.1063/1.2831788.
9. A. D. Estillore, C. Huang, and A. G. Suits. "New Doppler-free techniques for ion imaging studies." *ISRAPS Bulletin*, **20**, 4 (2008).
10. A. D. Estillore and A. G. Suits. "Probing the dynamics of chlorine atom reactions with polyatomic hydrocarbons by crossed-beam imaging." *Journal of Physical Chemistry A. In preparation* (2012).